FUNCTIONALIZED ALGINATE-GLUTATHIONE (GSH) HYDROGELS AS ANTIOXIDANT BIOMATERIALS FOR SKIN WOUND REPAIR

by

Danielle Abdul Nour

Thesis submitted to the University of Ottawa

in partial fulfillment of the requirements for the degree of

Master of Applied Science in Chemical Engineering

Department of Chemical and Biological Engineering

Faculty of Engineering

University of Ottawa

ABSTRACT

Skin serves as the body's primary barrier against pathogens, UV radiation, and mechanical damage. When blood flow is impaired or pressure is maintained, skin and underlying tissues can deteriorate, forming chronic wounds such as diabetic ulcers, pressure sores, and venous leg ulcers. These wounds remain trapped in a state of inflammation, where excess reactive oxygen species (ROS) and pro-inflammatory molecules disrupt normal healing processes. Hydrogels are widely used as wound dressings and can be enhanced with antioxidant components to reduce oxidative stress and help resolve the inflammatory phase of wound healing. In this study, alginate, a natural and biocompatible hydrogel polymer, was functionalized with glutathione (GSH), a natural antioxidant peptide of the human body responsible for reducing oxidative stress through ROS scavenging, via carbodiimide chemistry (EDC/NHS). The resulting conjugate is intended for the development of antioxidant dressings for the treatment of chronic wounds. The conjugate synthesis parameters ((EDC:GSH) molar ratio, pH, and reaction time) were optimized to maximize peptide content of the conjugates and thiol group availability for redox activity compared to a conventional carbodiimide chemistry method. Results showed that the (EDC:GSH) molar ratio and pH positively influenced GSH grafting, but negatively impacted reduced thiol group proportions, while reaction time had no significant effect. Optimal synthesis conditions were identified as: (EDC:GSH) = (4:1), pH = 5.0, reaction time = 2 hours. Chemical characterization of the conjugates using ^{1}H-NMR and quantitative analyses through BCA and Ellman assays demonstrated the successful conjugation of GSH to the alginate backbone through an amide linkage. The conjugates were able to scavenge 50% of H_2O_2 when dissolved in solution but seemed to have lost their scavenging capacity once crosslinked ionically into hydrogels. Nevertheless, alginate-GSH conjugates could show promise as an antioxidant dressing material to accelerate the healing of chronic skin wounds.

RÉSUMÉ

La peau constitue la première barrière du corps contre les pathogènes, les rayonnements UV et les blessures mécaniques. Lorsque la circulation sanguine est altérée ou que des pressions prolongées s'exercent, la peau et les tissus sous-jacents peuvent se dégrader, menant à des plaies chroniques telles que les ulcères diabétiques, les escarres et les ulcères veineux. Ces plaies demeurent dans un état inflammatoire persistant, caractérisé par un excès d'espèces réactives de l'oxygène (ERO) et de médiateurs pro-inflammatoires qui perturbent les processus de guérison tissulaire. Les hydrogels sont largement utilisés comme pansements et peuvent être enrichis en agents antioxydants afin de réduire le stress oxydatif et de rétablir un environnement propice à la guérison. Dans cette étude, l'alginate, un polymère naturel et biocompatible, a été fonctionnalisé avec le glutathion (GSH), un peptide antioxydant endogène, agissant comme capteur de ERO et contribue à diminuer le stress oxydatif du corps, par chimie carbodiimide (EDC/NHS). Le conjugué obtenu est destiné au développement de pansements antioxydants pour le traitement des plaies chroniques. Les paramètres de fonctionnalisation, le ratio molaire (EDC:GSH), le pH et le temps de réaction, ont été optimisés afin de maximiser la quantité de peptide attaché et la disponibilité des groupes thiols pour l'activité rédox, en comparaison avec une méthode classique de chimie carbodiimide. Les résultats montrent que le ratio molaire et le pH favorisent l'attachement du GSH, tandis que des niveaux plus élevés diminuent la proportion de thiols réduits, avec le temps de réaction qui n'a pas eu d'effet notable. Des conditions optimales de synthèse ont été identifiées : (EDC:GSH) = 4:1, pH = 5,0 et temps de réaction = 2 heures. La caractérisation chimique par RMN-^{1}H et par des analyses quantitatives (essais BCA et Ellman) confirment la formation d'une liaison amide entre l'alginate et le GSH. Les conjugués ont éliminé environ 50 % du H_2O_2 en solution, mais semblent perdre leur capacité redox après réticulation. Malgré cette limitation, les conjugués alginate-GSH présentent

un potentiel intéressant comme hydrogel antioxydant pour accélérer la cicatrisation des plaies cutanées chroniques.

ACKNOWLEDGEMENTS

I would like to extend a very warm thank you to my supervisor for his outstanding supervision, guidance, and mentorship throughout this thesis project, which continued through both my CO-OP internship and my honours thesis. I can say with certainty that I have grown significantly as a researcher, as a communicator, and as the best version of myself. Thank you for giving me the opportunity to try, fail, rise, and overcome, and most importantly, thank you for your steadiness and welcoming spirit through it all. You have had a profound impact on my life, something I will never forget.

I would also like to thank all my past and current colleagues for their collaboration and support, Luisa Metzler, Micheal Mulholland, Rayehe Giofrani, Olivia Steiner, Athena Prattas, Almaza Eileen Katia Karam, and Katherine Houlahan, with a special thank you to Sietske Barnes for providing training and assistance at the beginning of my research project. I also thank Dr. Betty Li for her excellent supervision and mentorship during my CO-OP placement in 3D bioprinting at the NRC. Another special thank you to my great teaching assistantship supervisors, Charbel Atallah and Johnny Matta, for making my teaching experience so rewarding. Finally, I extend a warm thank you to Professor Marc Dubé, Richard Dubé, and Margarita Garcia for sharing their knowledge and expertise while teaching the transformational leadership course as well as to Andrée-Anne Maranda and Pierre Bercy for their support in organizing a wellness event for university students. Lastly, I would like to express my deepest gratitude to my family, Nehmat Khairallah, Elie Abdul Nour, Dimitri Abdul Nour, Diane Abdul Nour, Khalil Khairallah, Nawal Hachem, Imad Khairallah, and all others; my friends, Chloé Monin, Bianni Bureau-Chabot, and Samantha Naous; and my partner, Nicolas Touma. You have always believed in my potential, and I cannot thank you enough for your constant support throughout the completion of this thesis.

TABLE OF CONTENTS

LIST OF TABLES

LIST OF FIGURES

LIST OF EQUATIONS

LIST OF ABBREVIATIONS

α1-PI	α1-protease inhibitor
AMPs	antimicrobial peptides
ANOVA	analysis of variance
BCA	bicinchoninic acid assay
bFGF	basic fibroblast growth factor
C5a	complement factor component 5a
$CaCl_2$	calcium chloride
cAMP	cyclic adenosine monophosphate
CD	cluster of differentiation
CD4+	cluster of differentiation 4 helper T cells
CD8+	cluster of differentiation 8 cytotoxic T cells
CO_2	carbon dioxide
$-COO^-$	carboxyl ion/carboxylate
-COOH	carboxylic acid
CXCL7	C-X-C motif chemokine ligand 7
CXCL8	C-X-C motif chemokine ligand 8
D_2O	deuterium oxide
DCC	dicyclohexyl carbodiimide
ddH_2O	double-distilled water
DOE	design of experiment
7-DHC	7-dehydrocholesterol
DMEM	dulbecco's modified eagle medium
DMSO	dimethyl sulfoxide
DNA	deoxyribonucleic acid
DPPH	2,2-diphenyl-1-picrylhydrazyl
DTNB	5,5′-dithiobis-(2-nitrobenzoic acid)
ECM	extracellular matrix
EDC/NHS	carbodiimide chemistry/coupling agents
EDTA	ethylenediaminetetraacetic acid
ERO	espèces reactives de l'oxygène
EDC	1-ethyl-3-(3-dimethylaminopropyl)carbodiimide hydrochloride
FBS	fetal bovine serum
FGF	fibroblast growth factor
GAGs	glycosaminoglycans
GCL	glutamate-cysteine ligase
GMP-140	granule membrane protein-140
GSH	glutathione
GST	glutathione s-transferase
HCl	hydrochloric acid
HI	heat inactivated
HIF-1α	hypoxia-inducible factor-1 alpha
HNE	hydroxyl-2-nonenal
^{1}H-NMR	proton nuclear magnetic resonance
H_2O_2	hydrogen peroxide
IGF-1	insulin-like growth factor-1

IL-1	interleukin-1
IL-1β	interleukin-1 beta
IL-8	interleukin-8
LCs	Langerhans cells
LOX	lectin-like oxidized low-density lipoprotein receptor
LRR-	leucine-rich repeat
MAPKs	mitogen-activated protein kinases
MDA	malondialdehyde
MES	4-morpholinoethanesulfonic acid
MHC I/II	major histocompatibility complex
MMPs	matrix metalloproteinases
MWCO	molecular weight cut-off
NAC	n-acetylcysteine
NaCl	sodium chloride
NADPH	nicotinamide adenine dinucleotide phosphate
NaOH	sodium hydroxide
NAP-2	neutrophil-activating peptide 2
NF-κB	nuclear factor kappa B
NHS	n-Hydroxysuccinimide
NIH3T3	NIH/Swiss mice embryonic cell line
NLRP3	NOD-, LRR- and pyrin domain-containing protein 3
NO	nitric oxide
NOD-	nucleotide-binding oligomerization domain
NOX	NADPH oxidase
O_2	oxygen
$\bullet O_2^{-2}$	peroxide
-OH	hydroxyl
•OH	hydroxyl radicals
OH^-	hydroxyl ion
PDGF	platelet derived growth factors
PEG	polyethylene glycol
PI3K	phosphatidylinositol 3-kinase
PRP	platelet rich plasma
PVA	polyvinyl alcohol
ROS	reactive oxygen species
SALT	skin-associated lymphoid tissues
-SH	thiol
TBO	triple resonance broadband observe
TCEP	Tris(2-carboxyethyl)phosphine hydrochloride
TGF-α	transforming growth factor alpha
TGF-β	transforming growth factor beta
TIMPs	tissue inhibitors of metalloproteinases
TNF-α	tumour necrosis factor-alpha
UV/UVB	ultraviolet
VEGF	vascular endothelial growth factor

STATEMENT OF CONTRIBUTION

The overall conception and design of the project was performed by Dr. Jean-Philippe St-Pierre, and the design of the experiments presented within this thesis was performed by Dr. Jean-Philippe St-Pierre and Danielle Abdul Nour. Preliminary work done on this thesis project was performed by Sietske Barnes and Siobhan Mcintyre.

All experiments presented within this thesis were conducted under the direct supervision of Jean-Philippe St-Pierre and by Danielle Abdul Nour. Sophia McKillop performed kindly all proton nuclear magnetic resonance (^{1}H-NMR) measurements as part of the alginate-GSH conjugate chemical characterization. All data analysis pertaining this project was performed by Danielle Abdul Nour.

This thesis was written by Danielle Abdul Nour, where Dr. Jean-Philippe St-Pierre greatly contributed to the thesis reviewing and editing. Athena Prattas assisted with the document formatting.

CHAPTER 1: INTRODUCTION

1.1 Rationale

The skin is the biggest organ of the human body, providing a continuous protective layer with a surface area of approximately 1.5 to 2.0 square meters. Indeed, this organ plays critical roles as it serves as the primary barrier against pathogen infiltration, UV radiation, and mechanical injuries. However, due to causes such as mechanical force (e.g.: scrapes, shear, bites), thermal or chemical exposure causing burns, biological factors (infections, diseases such as diabetes) or intrinsic skin fragility (aging, poor blood circulation, dehydration), the skin can rupture leading to the formation of a wound, preventing the skin from performing its protective function. Acute wounds can heal through intrinsic mechanisms involving four phases: homeostasis, inflammation, proliferation and remodelling. However, the disruption of one or more of these phases due to causes such as poor blood perfusion or ischemia at a localized body area, or diseases such as diabetes, preventing oxygen and other nutrients from reaching the wound, could result in significantly slowed or arrested healing processes. When a wound fails to progress through normal healing cascades, the wound becomes chronic. Chronic wounds can be characterized by persistent infection, excessive neutrophil infiltration, and cell senescence or dysregulation. Critically, chronic wounds are characterized by the presence of high oxidative stress and inflammation, as they are unable to transition from the inflammation phase to the proliferation phase. Several treatments of chronic skin wounds are present on the market and include medication (antibiotics, analgesics, anti-inflammatory drugs, and growth factors), compression therapy using bandages or stockings, revascularization procedures such as angioplasty or stenting, offloading devices such as specialized footwear, cushions or orthotic inserts, glycemic control strategies (lifestyle modifications, oral

antidiabetic medications, or insulin therapy) as well as dressings, that are already widely commercialized for wound moistening and protection to guide its healing. However, these treatments fail in addressing the high oxidative stress and inflammation that is localized at the wound site. Hydrogels have shown great promise as dressings materials to support the processes of wound healing because of their biocompatibility and tunable properties, as well as their ability to retain moisture and provide a hydrated environment to healing wounds through their porous structure and the hydrophilic nature of their polymeric constituents. These can also be modified for controlled drug release, or to introduce specific bioactivities that can help restore the normal wound healing process, including for oxidative stress mitigation. Alginate, a polysaccharide extracted from brown algae is an interesting base polymer for the fabrication of hydrogels for this application because of its biocompatibility, non-toxicity, and the presence of active hydroxyl and carboxylic groups on its backbone that can be modified covalently with peptides to confer bioactivity. One such peptide is glutathione (GSH), an important natural tripeptide produced in the human body from three amino acids, glutamate, cysteine, and glycine, with its synthesis regulated by the action of the glutamate-cysteine ligase (GCL), the glutathione synthetase and the glutathione s-transferase (GST). This molecule is fundamental for neutralizing free radicals, such as reactive oxygen species (ROS), through its free thiol group present on its cysteine.

1.2 Thesis Objectives

The work presented in this thesis aims to demonstrate the synthesis of an alginate-GSH conjugate through carbodiimide chemistry that could be integrated into biomaterials to interface with chronic skin wounds in order to reduce local oxidative stress and induce tissue repair. The work elaborated in this thesis focusses on the following three objectives:

1. Optimization of the synthesis conditions for GSH conjugation to alginate using carbodiimide chemistry.
2. Characterization of the GSH-alginate conjugate confirming the functionalization.
3. Investigation of the ability of the conjugate to scavenge ROS in solution and following hydrogel formation.

1.3 Thesis Organization

This thesis is divided into five chapters. Chapter 2 will provide an extensive review of the literature pertaining with the skin's physiology, treatments for chronic wounds, as well as the progress done to date on the synthesis of antioxidant hydrogels for chronic skin wound healing. Chapter 3 will detail all relevant methods employed to carry out this project. Chapter 4 will present the results from this work and will include a discussion that includes a comparison with trends found in the literature. Finally, Chapter 5 will state the main conclusions drawn from the results of this study and will highlight future avenues for refinement of the resulting biomaterials' performance.

CHAPTER 2: LITERATURE REVIEW

2.1 Skin and wound healing processes

The skin is the largest organ of the human body. The skin's structure comprises an intricate architecture that serves as the body's initial barrier against pathogens, ultraviolet (UV) light, chemicals, and mechanical injuries. This organ also contributes to regulating temperature and the amount of water released from the body[1]. It is comprised of three main layers: the epidermis, the dermis and the hypodermis, also called the subcutis (Figure 2.1) [1,2].

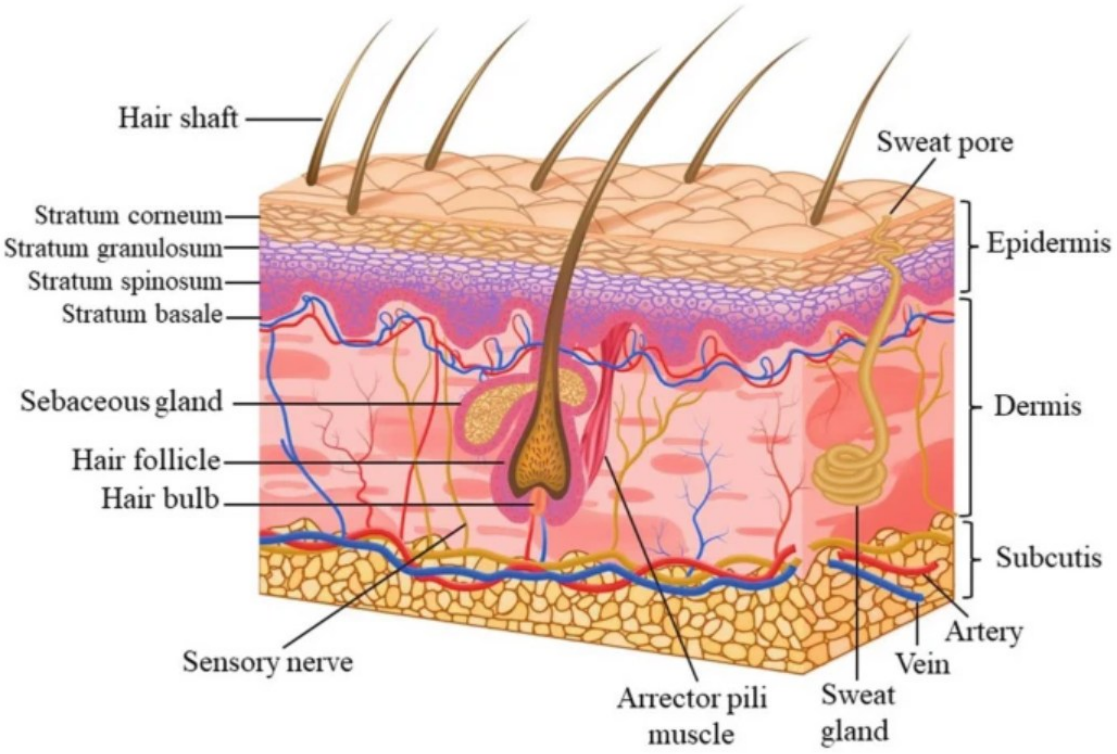

Figure 2. 1. Schematic illustration of the skin structure and its components. The skin structure is divided into three layers: i) the epidermis, composed of several strata (stratum corneum, stratum lucidum, stratum granulosum, stratum spinosum, and stratum basale) ii) the dermis, consisting of connective tissue, blood vessels, nerve endings, hair follicles, and sweat glands iii) and the subcutis (hypodermis), composed mainly of connective tissue and fat stored in adipocytes. Schematic reproduced with permission from Prohic (2024)[2].

2.1.1 The skin's structure and functions

The epidermis, the skin's outermost layer, is composed of several strata and various cell types crucial for its function. From the most superficial to the deepest, the epidermal layers are the *stratum corneum, stratum lucidum, stratum granulosum, stratum spinosum, and stratum basale*[1,2]. They differ in their cell structure, function, and degree of maturity, with the deeper layers composed of stem cells exhibiting high mitotic activity, which progressively transition into flattened, dead cells specialized for protection as the skin surface is reached[1]. The epidermis comprises primarily keratinocytes, with a smaller density of melanocytes, Langerhans and Merkel cells. Keratinocytes originate from the basal layer of the epidermis while their differentiation is regulated through a calcium concentration gradient from the basal layer to the *stratum corneum*, leading to epidermal maturation and barrier formation[3]. This epidermal water barrier formation is ensured through the production of lipids and keratin from keratinocytes. Finally, when exposed to UVB light, keratinocytes can mediate the production of subcutaneous vitamin D_3 and participate in its activation[4–6]. Melanocytes are found interspersed between cells of the *stratum basale* and are derived from neural crest cells[7]. They are responsible for synthesizing melanin, a biopolymer, through the conversion of tyrosine to dihydroxyphenylalanine by the enzyme tyrosinase, giving to the skin its natural pigmentation. UVB light stimulates melanin secretion, protecting against further UV radiation exposure [1]. Langerhans cells (LCs) are dendritic cells that represent the first line of immune defense in the skin[8]. They are derived from CD34-positive bone marrow stem cells and reside in *stratum spinosum*. LCs express major histocompatibility complex (MHC) I and MHC II molecules, allowing them to present antigens to CD8+ and CD4+ T cells[9]. They are part of the mononuclear phagocytic system as they are able to uptake antigens found in the skin and mediate their transport to the lymph nodes[1], where they are destroyed. Merkel cells are oval-shaped modified epidermal cells found in the *stratum basale*, directly above the basement membrane.

These cells serve as mechanoreceptors for sustained light touch sensations and texture perception. They are found in the palms, soles, and oral and genital mucosa, with the highest concentration in the fingertips, lips and hair follicles. The cell membranes of Merkel cells interact with free nerve endings in the skin, allowing them to transduce touch and transmit it to the nervous system [1,10].

The dermis is located underneath the epidermis and is also separated into two layers: the superficial papillary dermis, a thin layer of connective tissue where capillaries, elastic and reticular fibers, as well as collagen are found; and the deeper reticular dermis, consisting of denser connective tissue accompanied by fibroblasts, responsible for extracellular matrix (ECM) production comprising of elastin and collagen. These structural proteins confer the skin's elasticity and tensile strength and structural support, respectively. Mast cells which are immune response mediators[11] as well as macrophages are also contained in the deeper reticular dermis. They are sensitive to antigens and play a role in skin homeostasis maintenance[12]. This section of the skin embeds larger blood and lymphatic vessels, as well as hair follicles along with smooth muscles, sweat glands and nerve endings[2]. Functions of the dermis include providing nutrients and support to the epidermis and elasticity to the skin while participating in sensory and thermoregulation functions[13].

The third and deepest layer of the skin is the hypodermis, also referred to as subcutis. This layer consists mainly of connective tissue and fat stored in adipocytes. This layer also contains nerves and blood vessels. This adipose tissue serves in temperature insulation, absorbs mechanical shock and stores the energy of the body[2].

The skin has multiple general functions. It is primarily protective as it acts as a barrier against various external threats. Specifically, the skin shields the body from excessive water loss or absorption, invasion by microorganisms, mechanical and chemical trauma, and UV light damage[1].

The skin plays a crucial role in both adaptive and innate immunity through its specialized immune network referred to as skin-associated lymphoid tissues (SALT), composed of LCs, keratinocytes, and T-cells for immune surveillance and pathogen defense[14]. The skin also releases various peptides that possess antibacterial and antifungal properties[15]. SALT is a significant component of the immune system as even minor skin breaks can lead to infection. The skin also plays a vital role in maintaining body temperature, through three phenomena: (i) blood vessel vascular changes where dilatation is done to release heat, and constriction for heat conservation; (ii) through the action of small muscles at the base of hair follicles that contract, raising hairs while trapping a thin layer of warm air near the skin; (iii) and through water balance, where sweat glands produce sweat that evaporates from the skin's surface, a process that consumes heat, cooling the body down as its temperature rises[16]. Furthermore, the skin manages the rate of water evaporation and absorption[1]. Indeed, lipids contained in the *stratum corneum* prevent water evaporation through the formation of an organized waterproof "mortar" between skin cells, composed of ceramides, cholesterol, and free fatty acids, restricting movement of water molecules out of the body[17]. In addition, the skin produces an essential body hormone, vitamin D_3, by converting 7-dehydrocholesterol (7-DHC) under UVB light and is transported through the dermal capillary system to the hole body to support bone health and calcium metabolism, the body's immune functions, muscle movement and nerve signaling[18]. Other skin's exocrine functions include skin and hair protection and lubrication through sebum coating, secreted by the sebaceous glands[1,19]. Finally, the skin is equipped with several skin receptors and nerve endings allowing our interaction with the environment such as Meissner receptors, responsible for light touch detection alongside the action of Merkel cells; Pacinian corpuscles perceiving deep pressure and vibrational changes; Ruffini endings that detect deep pressure and stretching of the skin's collagen fibers; and free nerve endings that stretch to the epidermis, responsible for responding to pain, light touch, and

temperature variations[20]. The skin's sensory roles are essential for an individual's movement and protection[1]. When the skin is subjected to harsh environments, it can rupture leading to the formation of an open wound, preventing the skin from performing properly its protective and sensory functions.

2.1.2 Acute skin wounds and the four stages of wound healing

Skin wounds can be classified into two main categories: acute and chronic wounds. The origin of acute wounds can be characterized by sudden traumatic or surgical events. Instances of acute wounds include abrasions, superficial scraping of the skin from friction, lacerations that correspond to irregular tears caused by blunt trauma, incisions caused by clean sharp cuts, punctures forming narrow and deep wounds from nails or needles, penetrating wounds caused by an object that enters the body, possibly damaging deeper tissues, and burns from thermal, chemical, electrical or radiation exposure to the skin[21]. Acute wounds are typically followed by normal intrinsic repair processes, resulting in wound closure and durable healing in a predictable timeframe of four to six weeks[22,23]. This is done through several molecular events leading in a gain in structural integrity, involving four distinct phases: hemostasis, inflammation, proliferation and remodeling (Figure 2.2)[24,25].

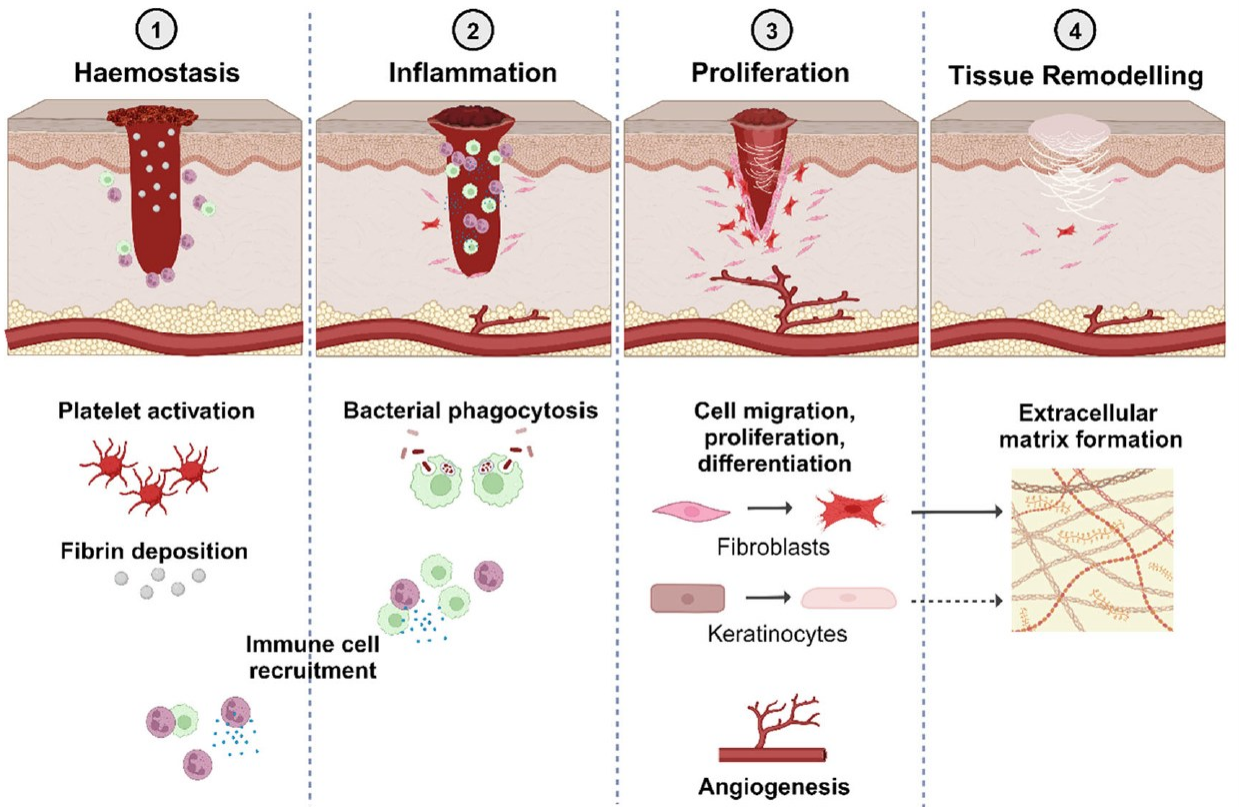

Figure 2. The four stages of wound healing. Acute wounds repair through four stages: 1) haemostasis (hemostasis), leading to blood clot formation through platelet activation and fibrin deposition; 2) inflammation, serving in cleaning the wound with the gathering of immune cells and pathogen phagocytosis; 3) proliferation, where granulation tissue is formed through fibroblasts and keratinocytes differentiation, proliferation, and migration, and through angiogenesis and ECM deposition; 4) and remodeling, where the ECM rearranges forming final scar tissue. This schematic was reproduced from the open access publication of Hunt et al.'s (2024)[25].

Once the wound is formed, hemostasis begins, where bleeding from the wound is interrupted by the formation of a blood clot at the wound surface. This phenomena happens through blood flow restriction, and the action of platelets, the primary cellular mediators of this phase, which are activated by their contact with extracellular matrix (ECM) components such as collagen type I[26], as well as signals from other resident cells[24]. Coagulation is initiated through the secretion of proteins such as fibronectin, collagen, and glycoproteins, and factors such as von Willebrand factor, that attach to platelets receptors. The release of granules among other molecules such as pro-

coagulants, prothrombin, thrombospondin, growth factors and cyclic adenosine monophosphate (cAMP) is also promoted, activating platelet aggregation. This cascade results in fibrin strands formation, leading to the fabrication of a blood clot[24,27]. Inactive clotting enzyme proteases activate once bounded to the platelet's membranes, gathering more proteases, accelerating the clotting cascade[26]. Blood clots prevent bacteria or other pathogens from infiltrating the wound, while insuring supply of cytokines and growth factors from activated platelets for immune cell recruitment[24], initiating the repair process. Indeed, through degranulation processes (blood clot degradation)[22], a cytokine and growth factor "cocktail", including platelet derived growth factors (PDGF), transforming growth factor alpha and beta (TGF-α, TGF-β), basic fibroblast growth factor (bFGF), insulin-like growth factor-1 (IGF-1), and vascular endothelial growth factor (VEGF), is released into the wound area. These species monitor the recruitment of immune and repair cells, where neutrophils and monocytes are recruited by PDGF and TGF-β, initiating the inflammatory response[26,28]; endothelial cells are activated by VEGF, TGF-α and bFGF to initiate blood vessel reconstruction (angiogenesis); and fibroblasts are recruited by PDGF, leading them to migrate to the wound site and insure collagen and glycosaminoglycans (GAGs) production for tissue reconstruction. Homeostasis is a critical phase, allowing the commencement of the tissue repair process, and can last from minutes to hours in healthy wounds[24].

The inflammatory phase begins once bleeding is controlled and serves in cleaning the wound. Vasoconstriction decreases to allow vasodilatation and higher capillary permeability, done through the release of vasoactive substances from damaged endothelial, platelets and Mast cells[26,29] such as histamine, prostaglandins, complement factor component 5a (C5a) and thrombin[22]. This process allows for plasma and bloodborne cells to leak into the wound, resulting in swelling (edema), redness (erythema) and drainage (exudate). This process also permits the transportation of cells involved in the repair process to the wound site, and for the removal of damaged cells,

pathogens, and bacteria from the wound area[22,24]. Specifically, the cytokines (e.g.: interleukin-1 (IL-1) and tumour necrosis factor-alpha (TNF-α))[30], growth factors and chemokines produced by the α-granules of platelets (e.g.: CXCL7(NAP-2), CXCL8 (IL-8), etc.)[31,32] and by damaged cells attract leukocytes (neutrophils, macrophages, lymphocytes) to the wound bed, via margination and diapedesis, processes characterized by binding the endothelial cells forming the capillary linings through the leukocytes' integrins, and their migration to the wound bed, respectively[22]. Neutrophils mediate the first line of phagocytosis by binding to damaged tissue, bacteria or molecules and engulf the latter for destruction through the action of intracellular enzymes and free oxygen radicals. They also mediate the release of growth factors to attract additional leukocytes to the area. Macrophages replace neutrophils, continuing phagocytosis processes, while releasing high amounts of potent growth factors (PDGF, TGF-β, TGF-α, IGF-1, and FGF)[26], stimulating angiogenesis, fibroblast migration and proliferation, keratinocytes' migration as well as connective tissue synthesis. Finally, T lymphocytes act in secreting additional wound-healing cytokines and by destroying viral organisms and foreign cells[22,24]. The inflammation phase occurs within 24 hours after injury and can last up to two weeks during the healing of normal wounds[26].

The proliferation phase consists in new skin tissue formation, where the wound surface is covered with new connective tissue and epithelium through three key processes: connective tissue synthesis, involving matrix deposition and collagen synthesis, neoangiogenesis, at the source of granulation tissue formation, followed by epithelialization[22,26]. Granulation tissue formation occurs simultaneously with neoangiogenesis, resulting in newly formed capillary loops and synthesized connective tissue proteins (ECM) such as collagen type III, filling the wound defect[22]. Specifically, early granulation tissue is composed of unstructured collagen and high levels of fibronectin and laminin. It also contains proteoglycans such as hyaluronic acid, that serve in protecting cells against free-radical and proteolytic damage, while contributing to the viscoelastic

properties of the tissue[22]. Neoangiogenesis is stimulated by the action of growth factors produced by injured endothelial cells, macrophages, fibroblasts and keratinocytes (e.g.: VEGF, bFGF, PDGF) which attract stem progenitor stem cells, ensuring their differentiation into endothelial cells, and stimulating them to proliferate and migrate, resulting in blood vessel formation. The new blood vessels permit oxygen and nutrients delivery to the wound bed, aiding in further angiogenesis and guiding repair processes. At the same time, fibroblasts migrate into the wound bed from surrounding tissues[23], through upregulation of their integrin binding sites from PDGF and TGF-β[22,26], where they proliferate and mediate collagen synthesis and release into the wound bed. This phase also involves contraction by the action of myofibroblasts responsible of gripping the wound edges and pulling them together, reducing the wound size to facilitate healing[22,23,26]. In healthy stages of wound healing, granulation tissue is pink or red and uneven in texture. Finally, keratinocytes resurface the injury through the process of epithelialization, involving lateral and vertical migration, and differentiation, which gradually reestablishes epidermal thickness and function[22,23,26].

The last phase of wound healing involves remodeling, through which the granulation tissue matures and strengthens through the re-organization of collagen fibers, resulting in the final scar tissue[22,27]. Specifically, the matrix is gradually converted to a mature and relatively acellular scar, a process that involves replacement of the type III collagen with type I collagen, with elastin degradation, giving the scar tissue a stiffer property compared to granulation tissue[22]. This task is accomplished through synthesis and degradation of the ECM (excess collagen)[23] from fibroblasts and matrix metalloproteinases (MMPs) (e.g.: collagenases, gelatinases and stromelysins) along with certain serine proteases (neutrophil elastase), respectively[22,26,27]. The destructive action from the proteolytic enzymes is regulated by enzyme inhibitors, produced by cells in the wound bed. Inhibitors of the MMPs are the tissue inhibitors of metalloproteinases (TIMPs), with α1-protease

inhibitor (α1-PI) and α2 macroglobulin inhibitors of serine proteases[26]. The new collagen deposited gains in order by aligning parallel to the wound's stress line[22], while their covalent cross-linking is increased by the lysyl oxidase enzyme, secreted by fibroblasts[26]. This provides the wound with higher tensile strength[22]. Wound contraction also peaks during this healing stage[23], that can last 12 months or more[22,23]. Other changes in the tissue involve reduction in the number of capillaries through aggregation into larger vessels and a decrease in proteoglycans, GAGs, water, cell density along with their metabolic activity[26].

2.1.3 The role of reactive oxygen species in normal wound healing processes

Reactive oxygen species (ROS) are molecules acting as derivatives of oxygen (O_2), that are highly reactive as per their added electron conferred by their reduced form[30,33], including superoxide (O^{2-}), hydroxyl radicals (•OH) and ions (OH^-), peroxide ($•O_2^{-2}$), and hydrogen peroxide (H_2O_2)[33]. They are produced primarily by neutrophils and macrophages, and from damaged tissues through mechanisms involving nicotinamide adenine dinucleotide phosphate (NADPH) oxidase enzymes (NOX)[34]. They are also released through mitochondrial respiration[25]. They act as secondary messenger-signaling molecules, influencing cell cycles and cell-mediated defense responses and have crucial roles in wound healing processes[25]. Indeed, they mediate vasodilatation and vasoconstriction processes and local cell signaling in hemostasis for blood clot formation[30,33]; attract blood vessel-bound neutrophils and monocytes to the wound site for protection against pathogens and participate in bacteria and fungi phagocytosis and destruction[30,33]; and intervene in cell division and migration of keratinocytes and endothelial cells for angiogenesis, and fibroblasts for collagen formation[33]. Hydrogen peroxide (H_2O_2) for instance, at low concentrations ($< 50\mu M$), serves as a signaling molecule activating chemotactic redox-sensitive nuclear factor kappa B (NF-κB), which enhances pro-inflammatory cytokines and antimicrobial peptides expression[35] and

induces kinases activation (e.g.: mitogen-activated protein kinases (MAPKs) and phosphatidylinositol 3-kinase (PI3K)), controlling endothelial cell proliferation, migration and tube formation processes at the root of angiogenesis[36]. Higher H_2O_2 concentrations (> 100 μM) exert direct antimicrobial activity through •OH production, compromising bacterial viability and facilitating their clearance from the wound environment [30,37]. Another ROS, nitric oxide (NO), primarily released from macrophages, plays a crucial role in host defense as per its antimicrobial properties, that allows the molecule to diffuse into bacterial cells and modify bacterial proteins through S-nitrosylation[38]. It also inactivates enzymes involved in metabolic and replication pathways.

2.2 Chronic skin wounds and current treatments

2.2.1 Chronic skin wounds

The second category of skin wounds are referred to as chronic skin wounds. These types of wounds fail to proceed normally through all phases of wound healing, leading to a prolonged healing period (above 6 weeks)[23] or failure to establish a durable wound closure[22]. They include pressure and vascular ulcers, along with neuropathic wounds and are characterized by continuous unresolving inflammation (increased number of neutrophils, macrophages, and lymphocytes, and high levels of pro-inflammatory cytokines, such as TNF-α, IL-1 and IL-6)[26], persistent infection, necrosis[24], cellular senescence, a deficiency of growth-factor receptor sites, the absence of initial bleeding needed to trigger fibrin formation and growth-factor release, and elevated levels of proteases [22,26]. The causes leading to the manifestation of chronic skin wounds include arterial or venous insufficiency, repetitive insults to the skin tissue and predominant and persistent inflammation[39] that may be combined or worsened by present bacterial infection. Other systemic causes are diseases such as diabetes, from uncontrolled blood sugar levels suppressing the body's

inflammatory response while being more prone to microvascular diseases, malnutrition causing decreased albumin levels[22,39,40] specifically from lack of vitamins and minerals, aging, certain pharmaceuticals such as chemotherapeutics (e.g.: hydroxyurea) and steroids[40], genetics, and nicotine consumption[39]. Impediments to healing, such as ischemia, necrotic tissue, heavy bacterial loads, and high levels of proinflammatory MMPs prolong the inflammatory phase by continuing to recruit macrophages and neutrophils into the wound bed, and cause ongoing destruction of the ECM[22,41]. In addition, high levels of inflammatory proteases[26] combined with lower levels of growth factors leave the cells in the quiescent G_0 phase, preventing fibroblasts and keratinocytes from proliferating[22]. These cells also exhibit reduced motility, possibly due to ECM abnormalities, as well as reduced numbers of growth factor receptor sites, at the source of their senescent phenotype[42].

2.2.2 Oxidative stress

Excessive levels of ROS are measured in chronic wounds. This can lead to oxidative stress, one of the main factors leading to chronic skin wounds. Oxidative stress is defined as a redox imbalance, from the decrease of antioxidant enzyme activity[34,43] and, in cells, through aging mitochondria, increasing ROS levels and accelerating organelle and cell senescence[34]. Oxidative stress can lead to lipid peroxidation, a process involving oxidative degradation of lipids from ROS, causing a vicious cycle increasing production of free radicals and lipid peroxides, causing significant damage to cellular membranes[34,44]. Products of these phenomena include malondialdehyde (MDA), 4-hydroxyl-2-nonenal (HNE) and isoprostane, which serve as markers for local and systemic oxidative damage[43]. ROS can also cause significant DNA damage through base modifications and cleavage[34], DNA-protein cross-links, and double-strand breaks, driving genomic instability, mutations and delayed wound healing[43]. Excessive ROS release leads to NF-κB activation, which

propagates inflammation, upregulates IL-1 and IL-8, and TNF-α resulting in a positive feedback loop for inflammatory stagnation, minimal granulation tissue formation, and persistent activation of ROS-generating leukocytes, characteristic of chronic wounds[43]. H_2O_2 induces endothelial cell expression of granule membrane protein-140 (GMP-140), maintaining leukocyte adhesion and inflammation[43]. ROSs also activate Nucleotide-binding Oligomerization Domain (NOD-), Leucine-Rich Repeat (LRR-) and pyrin domain-containing protein 3 (NLRP3) inflammasome in macrophages, leading to the release of IL-1β, further amplifying inflammation while stalling the healing process[43]. Furthermore, high ROS levels disrupt angiogenesis and ECM formation through inhibition of prolyl hydroxylase domain proteins, leading to the "over-stabilisation" of hypoxia-inducible factor-1 alpha (HIF-1α) and resulting in vascular leakage[43,45]. Oxidative damage impairs keratinocyte proliferation and migration, crucial for re-epithelialisation. Harmful ECM damage is also a consequence of NF-κB and TNF-α activation, amplifying the secretion of MMPs (e.g.: MMP-1 and MMP-3 from fibroblasts; and MMP-2 and MMP-9 from macrophages). If oxidative stress is left unaddressed, dysregulated wound healing processes can lead to fibrosis through fibroblast differentiation into myofibroblasts from TGF-β overexpression, producing excessive amounts of collagen, fibronectin, and other ECM components[43]. This process is amplified through inhibition of apoptosis in myofibroblasts, suppression of the activity of MMP with TIMP, all from the action of TGF-β. Finally, oxidative stress promotes the activation of p38 MAPK pathway, which increases the activity of lectin-like oxidized low-density lipoprotein receptor (LOX), leading to abnormal collagen cross-linking during the remodeling phase and the development of keloids and hypertrophic scars[43].

2.2.3 Current treatments of chronic skin wounds

Current approaches to accelerate healing of chronic skin wounds involve addressing underlying causes such as poor blood perfusion and infection or treating diseases such as diabetes. First, chronic wounds are cleaned regularly using saline solutions[46] thereby removing slough, debris, necrotic tissue, and bacteria, that represent barriers to healing, to reduce the risk of infection and to enhance the wound environment for tissue repair. Debridement, the process with which dead or inflamed tissue is removed from the wound area through surgical, or autolytic and enzymatic mechanisms, is also used for the same purpose[46–48]. Strategies improving blood perfusion towards the wound area include the use of compression stockings and compression bandages, negative pressure wound therapy[46] and revascularization procedures such as angioplasty or stenting, usually for ischemic injuries. Hyperbaric oxygen therapy is also used, increasing blood oxygen concentration, improving the blood supply to the wound area, promoting wound healing processes through increased fibroblast proliferation, immune function, and angiogenesis stimulation[46,47]. As diabetic patients are prone to developing chronic skin wounds, glycemic control strategies, including lifestyle modifications, oral antidiabetic medications or insulin therapy, can be used to mitigate pathological effects of chronic skin wounds and aid in their healing.

Wound dressings (e.g.: films, gauze, hydrogel and hydrocolloid dressings, dressings containing silver or alginates and foam dressings) are also present on the market and applied over wounds to keep them moist and/or remove excess fluid, to prevent and mitigate infections and to relieve pain[46–48]. In addition, platelet rich plasma (PRP) therapy, where the patients' blood is processed to increase its plasma concentration, can be applied to the wound area in gel form, to supply it with key growth factors and guide skin wound repair[46]. In cases where the wound is too large leading to difficulties with achieving closure, skin autografts, allografts or even xenografts

can be placed onto the wound area. Collagen products have been used on recalcitrant chronic ulcers (derived from multiple sources, including bovine and porcine collagen) to facilitate attraction of critical cell types to wound healing, while depleting negative effectors such as free radicals and proteases[47]. Finally, antibiotics, drainage techniques and blue light therapy[48] are used for infection management combined with anti-inflammatory drugs for pain management[46]. However, all these strategies encounter limitations in re-guiding homeostatic wound healing processes, especially as they fail in addressing the localized and important oxidative stress and inflammation present at the wound site, representing the main motivation of this study.

2.3 Hydrogels for wound healing

2.3.1 Key properties of hydrogels for wound healing applications

Hydrogels are three-dimensional porous structures formed through covalent or non-covalent crosslinking[49] networks of hydrophilic polymers. Through this crosslinking, interactions between the polymers and surrounding water molecules promote swelling, leading to the formation of a hydrated network with a water content typically exceeding 90%[50]. Polymers that exhibit behaviors conducive to the formation of hydrogels can be natural (e.g., chitosan, gelatin, alginate, hyaluronic acid, agar, etc.), synthetic (e.g., polyethylene glycol (PEG), polyvinyl alcohol (PVA), poly(N-isopropylacrylamide), polyvinyl pyrrolidone, polyethylene oxide, etc.)[50], or hybrids[51]. Hydrogels have demonstrated great promise as biomaterials that can interface with chronic skin wounds to ensure faster healing, precisely in the form of dressings, because of their intrinsic properties[49–53]. These include (i) a high biocompatibility, which can be defined as inducing minimal adverse effects or immune response activation while interfacing with open wounds, (ii) appropriate mechanical properties (e.g.: strength and flexibility) preferably matching that of native skin tissue, with appropriate adhesion[50], insuring wound protection from load and movement around the wound

area with painless removal, (iii) and tunable porosity allowing nutrients and oxygen flow as well as exudates and debris removal, accelerating healing[49,51,52]. Furthermore, their high moisture retention capabilities provide a hydrated environment to wounds ideal for faster healing, favoring processes such as epithelialization and angiogenesis while reducing scarring probabilities[52] and pain sensations[49].

Hydrogels can also be easily modified for controlled drug release[49,51,52] or to be conferred with biological activities that can help reinstate normal wound healing processes. Indeed, they can gain antimicrobial or anti-inflammatory properties through incorporation of antimicrobial agents (e.g.: antimicrobial peptides (AMPs) and metal ions) and growth factors, mitigating effects of underlying infection and high inflammation, re-establishing homeostasis leading to acceleration in wound contraction and healing[49,50]. The same way and specifically for this study, hydrogels can be modified to lower oxidative stress at a chronic wound site, facilitating healing[49].

2.3.2 Antioxidant bioactive hydrogels for oxidative stress mitigation

Providing antioxidant cues to hydrogels as a potential therapeutic for reinstating normal wound healing processes of chronic wounds has been explored by many. Indeed, advancements in this strategy for wound healing started with the use of curcumin, a polyphenol found in turmeric, N-acetylcysteine (NAC), a precursor of glutathione (GSH), an endogenous antioxidant able to scavenge free radicals, and quercetin, a flavonoid found in fruits and vegetables. These antioxidant molecules are able to reduce inflammation and increase GSH levels in the body, respectively[54,55]. Antioxidants can be categorized as hydrophilic (e.g.: ascorbic acid (vitamin C), melatonin, GSH), hydrophobic (e.g.: alpha-tocopherol (vitamin E), ubiquinone (Coenzyme Q10), carotenoids) or amphiphilic (alpha-lipoic acid, flavonoids and other polyphenols)[56]. Hydrophilic antioxidants tend to react with oxidants in the cell cytoplasm and in the blood plasma, whereas hydrophobic

antioxidants are responsible for protecting cell membranes from lipid peroxidation[57]. Antioxidants also serve in the extracellular environment. They are critical at maintaining a balanced redox state, especially in fluid compartments including blood plasma, interstitial fluid, and epithelial lining fluid[58]. They are essential for preventing protein oxidation and lipid peroxidation by eliminating ROS prior to cell membrane damage[58–60], especially considering the higher oxidative space outside of cells.

Multiple studies involving the combination of antioxidants with hydrogels for skin wound healing have been conducted. Indeed, a study done by Ravi et al. (2023) involved the fabrication of a gellan-g-poly(ethylene glycol) methacrylate matrix loaded with ascorbic acid through diffusion filling, encouraging higher collagen synthesis and the reduction of oxidative stress and inflammation in a HaCaT cell model[61]. Another study from Qian et al. (2021) used a graphene oxide-collagen scaffold mixed with NAC on NIH3T3 fibroblast cultures. The material was able to resist the oxidative stress environment in culture and lead to angiogenesis, ECM production and epithelialization promotion[62]. In addition, Zhang et al. (2023) synthesized a hyaluronic acid-g-lipoic acid conjugate able to eliminate excessive ROS at the wound site in diabetic mice models while up-regulating the secretion of reparative growth factors[63]. Finally, Shefa et al. (2020) fabricated an oxidized cellulose nanofiber-polyvinyl alcohol hydrogel system incorporated with curcumin through solubilization, which showed significant wound contraction after 2 weeks in skin excisional wound rat models, through ROS and lipid peroxides scavenging[64]. These studies, among many others, demonstrate the potential of combining antioxidants into hydrogels for their delivery into non-healing wound sites to stimulate repair processes. In the same way, this thesis will discuss the synthesis of a novel biomaterial, using GSH, an abundant antioxidant with both intracellular and extracellular ROS scavenging capabilities, covalently attached to alginate, a

biocompatible and non-toxic hydrogel. This biomaterial is intended to interface with chronic wounds and support natural repair processes by guiding tissue regeneration.

2.4 Alginate's conjugation with glutathione for skin wound repair

2.4.1 Properties of sodium alginate

Alginate is a polysaccharide extracted from brown algae (*Phaeophyceae*) or secreted from bacteria (*Pseudomonas* or *Azotobacter*). Its backbone contains 1,4-linked β-D-mannuronic acid (M) and 1,4-linked α-L-guluronic acid (G) with regions containing one or the other unit, or in an alternate sequence[50]. Alginate can be of low, medium, or high viscosity, or of low or high molecular weight depending on polymer chain lengths. It displays several advantageous properties regarding skin wound healing. It is hydrophilic, soluble in water, and can form hydrogels due to GG blocks interactions when in contact with polyvalent cations (divalent: Ca^{2+}, Ba^{2+}, Sr^{2+}, Cd^{2+}, Co^{2+}, Cu^{2+}, Mn^{2+}, Ni^{2+}, Pb^{2+}, and Zn^{2+} and trivalent: La^{3+}, Pr^{3+}, Nd^{3+}, Eu^{3+}, and Tb^{3+})[65], forming a network referred to as the "egg-box model"[50]. Alginate demonstrates high biocompatibility, tunable biodegradability, viscosity and mechanical properties, and adequate porosity for particle and molecular diffusion. The M/G monomer ratio of alginate plays a role in the mechanical properties (stiffness versus elasticity) of the ionically crosslinked hydrogels, where higher G blocks leads to an increase in stiffness[66]. When crosslinked with Zn^{2+} or Ag^{+}[67], alginate can provide antibacterial properties[68]. Alginate is able to aid normal inflammatory cascades promoting macrophages activation and interleukin-6 (IL-6) and tumor necrosis factor α (TNF-α) production by monocytes, thereby quickening chronic wound healing[50]. Dry alginate dressings can absorb wound exudates, resulting in the formation of a gel, which subsequently releases water for wound hydration while providing painless and safe dressing removals[50]. Furthermore, alginate has innate antioxidant properties as it can scavenge ROS through direct electron donation from its structural -OH and

carboxyl (-COO^-) groups, while acting as a metal ion chelator[69]. Its antioxidant activity is increased as its molecular weight reduces[70]. Finally, alginate possesses active -COOH groups on its backbone that can be modified covalently with other bioactive molecules such as antioxidant peptides for oxidative stress mitigation.

2.4.2 Glutathione

Glutathione (GSH) is a natural tripeptide, composed of glutamate, cysteine, and glycine amino acids, and is present in every cell of the human body[56]. It can neutralize ROS and free radicals amounts present in the body. Its antioxidant capacity in cells is paramount as its function has been linked to various physiological processes, including wound healing. GSH deficiency increases the potential for development of oxidative stress-related diseases, such as neurodegenerative disorders and liver damage[71]. The mechanisms by which GSH plays its antioxidant role include through direct free radical (e.g.: superoxide and hydroxyl radicals) scavenging and neutralization, acting as an electron donor[72–74], through the regeneration of other antioxidants such as vitamin C and E[72–74], and through detoxification of harmful substances and metabolic products with its ability to bind to toxins, making them more water-soluble to facilitate their removal out of the body, mediated by the enzyme glutathione s-transferase (GST)[73,74]. For instance, GSH can scavenge H_2O_2 through the action of glutathione peroxidase (GPx), oxidizing GSH to glutathione disulfide (GSSG) while releasing water (H_2O) molecules[75,76]. This reaction can also occur spontaneously without the enzyme, although at a slower rate[77]. From its functions, GSH has potential in aiding the healing of chronic skin wounds.

2.4.3 Carbodiimide chemistry for alginate functionalization with peptides

Carbodiimide chemistry is a well-established functionalization method broadly used to functionalize alginate with other bioactive peptides[78–82]. Carbodiimides are defined as zero-length

crosslinking agents, with the general formula RN=C=NR, that activate -COO^- groups for coupling with primary amine-containing compounds, facilitating the formation of amide or phosphoramidate linkages. Some carbodiimides are water-soluble, ideal for biological conjugations and others water-insoluble, more suited for synthesis reactions involving organic compounds[83]. Popular carbodiimides include 1-ethyl-3-(-3-dimethylaminopropyl) carbodiimide hydrochloride (EDC), a water-soluble compound used for aqueous conjugation reactions, and dicyclohexyl carbodiimide (DCC), for non-organic synthesis methods[84]. EDC undergoes conjugation through reaction with -COOH to form an active O-acylisourea intermediate, that undergoes nucleophilic attack from primary amino groups, leading to the formation an amide bond. An EDC by-product is released in the reaction mixture as a soluble urea derivative[84]. EDC coupling is most efficient in acidic conditions (pH = 4.5) and is usually performed in 4-morpholinoethanesulfonic acid (MES) buffers[84], with other phosphate and neutral buffers providing lower efficiency, although still being chemically compatible[84]. However, the O-acylisourea intermediate is unstable in aqueous solutions, leading to its hydrolysis, accompanied by the regeneration of -COOH and the release of an N-unsubstituted urea, if no amine reaction occurs[84]. For this matter, N-hydroxysuccinimide (NHS) is often used alongside EDC, stabilizing the O-acylisourea intermediate through the formation an NHS ester. This allows for reaction occurrence at physiological conditions[84], ideal for fabricating conjugates for biomedical applications.

2.5 Research hypothesis and objective

Current treatments for chronic skin wounds fail to locally address the high oxidative stress at the wound site. Interestingly, exploratory studies demonstrate that antioxidant hydrogels can interface with chronic skin wounds to restore angiogenesis, ECM production and epithelialization through the delivery of antioxidant molecules. As such, it was of interest to combine covalently alginate, a

natural, biocompatible, non-toxic and intrinsically antioxidant hydrogel, with GSH, an antioxidant and naturally occurring tripeptide in the human body able to mediate redox reactions and decrease oxidative stress levels. Covalent bonding between alginate and GSH is possible through -COOH groups present on the alginate backbone and GSH's primary amine present on its main chain, through carbodiimide (EDC/NHS) chemistry. Covalent bonding is done to provide prolonged activity and to ensure potential regeneration of GSH from their oxidized to their reduced form from the wound environment. This alginate-GSH conjugate could demonstrate high potential for mitigating pathologies of chronic skin wounds and encourage skin tissue repair.

In this thesis, we aim to synthesize an alginate-GSH conjugate by means of carbodiimide chemistry and optimize the synthesis conditions to maximize conjugation and thiol group presentation for redox activity. We also aim to chemically characterize the conjugate to confirm covalent modifications onto the alginate backbone and investigate its ability to scavenge ROS in solution and in the form of a hydrogel.

CHAPTER 3 : MATERIALS AND METHODS

3.1 Synthesis of alginate-glutathione conjugates

3.1.1 Conventional carbodiimide-based conjugation of peptides to alginate

A 1% (w/v) sodium alginate (Protanal LF10/60, MW=89 000 g/mol) solution was prepared in 0.1 MES (Sigma-Aldrich) and 0.3 M sodium chloride (NaCl) buffer. The solution was vortexed and incubated at 37 °C until fully dissolved (approximately 1 hour). The pH was adjusted to 6.0 using 1 M sodium hydroxide (NaOH) solution. NHS (Sigma Aldrich) was added first to the alginate solution to a final concentration of [NHS]=0.326 mg/ml, and the mixture was stirred at 200 rpm for 5 minutes at room temperature. Then, EDC (Sigma Aldrich) was added to the reaction mixture at a final concentration of [EDC]=1.086 mg/ml (1:1 molar ratio with 10% of the active monomers composing the alginate backbone; (NHS:EDC) molar ratio=1:2) and stirred for 45 minutes in the same conditions as previously. Finally, a solution of reduced GSH (Sigma Aldrich) was added dropwise to the reaction mixture at a 1:1 molar ratio with EDC and was left to stir at 200 rpm for 16 hours. The mixture was then dialysed for two days against 500 mL of double-distilled water (ddH_2O, 8 water changes total) using cellulose-membrane dialysis (molecular weight cut-off (MWCO): 12,000-16,000) and freeze-dried for 48 hours. All samples were stored in the dark at room temperature. Controls were prepared (i) without the addition of the coupling agents (EDC/NHS), (ii) without the addition of the GSH, and (iii) comprising alginate only.

Modifications to this initial protocol were also investigated to increase GSH grafting onto the alginate backbone (DOE #1). Specifically, the (NHS:GSH) and the (EDC:GSH) molar ratios as well as the reaction pH were varied in the following ranges: (EDC:GSH) = [+: (1.2: 1); 0: (1.1: 1); -: (1: 1)]; (NHS:GSH) = [+: (0.75: 1); 0: (0.55: 1); -: (0.35: 1)]; and pH = [+: pH = 7.0; 0: pH = 6.0;

-: pH = 5.0], where all other manipulations remained identical to the initial protocol, including purification, drying steps and storage conditions. GSH content was measured using the BCA assay (*section 3.2.1*). The highest GSH quantification was observed at the following conditions (optimal conditions): (EDC:GSH) = (1.2:1); (NHS:GSH) = (0.35:1); pH=7.0; in comparison to the original (initial) conditions: (EDC:GSH) = (1.1:1); (NHS:GSH) = (0.55:1); pH=6.0. The functionalization efficiency (η) for all trials was calculated using the below formula:

$$\eta\ (\%) = \left(\frac{[GSH]_{measured} - [GSH]_{free}}{[GSH]_{Total}}\right) \times 100 \qquad \text{Equation 1}$$

Where $[GSH]_{measured}$ and $[GSH]_{free}$ are the measured and free GSH concentration taken from a functionalized alginate sample and a blend of alginate with GSH (negative control of reaction) respectively, both subjected to the same synthesis conditions, with $[GSH]_{Total}$ being the theoretical concentration to reach 10% of the functionalized monomers.

Select reactions were performed using the optimal synthesis conditions stated above to functionalize 5% of alginate's active monomers, with a slower GSH addition (1 ml/hour) using a programmed syringe pump, and with GSSG, respectively, in which the thiol group content ([-SH]) was measured using the Ellman's assay (*section 3.2.2*).

3.1.2 TCEP reduction of GSH and GSSG alginate conjugates

The alginate-GSH conjugate (5% functionalization) was reduced using Tris(2-carboxyethyl)phosphine hydrochloride (TCEP; Sigma Aldrich) in ddH_2O using final reaction mixture concentrations of 1% (w/v) alginate-GSH and 5 mM TCEP. Reaction mixtures were agitated at 80 rpm for 1 hour at 37 °C on a lab rocker. Following reduction, samples were purified by dialysis (ddH_2O changes every 30 minutes) with stirring at 100 rpm and subsequently

freeze-dried, maintaining the same conditions described in *section 3.1.1*, each step lasting 24 hours. An identical reduction procedure was performed using alginate-GSSG conjugates (5% functionalization), prepared at 1% (w/v) alginate-GSSG with 26.0 mM TCEP. Samples were agitated at 80 rpm for 30 minutes at room temperature and purified using the same dialysis method as above, but with the following water-change schedule over 48 hours: twice every 30 minutes, twice every hour and once every 2 hours. After purification, samples were frozen as previously described and freeze-dried for 48 hours. The same corresponding controls described in *section 3.1.1* were prepared for both reactions, including some with and without TCEP. All samples were measured for thiol group content using the Ellman's assay (*section 3.2.2*).

3.1.3 Thiol group loss assessment - GSH incubation in MES and ddH_2O

To gain insight into the effects of the different components of the carbodiimide reaction mixture on the loss of GSH thiol groups, GSH was added at a concentration of 5.15 mM (representing the concentration needed for a 10% functionalization of alginate monomers in a 1% (w/v) solution) in two buffers: (i) 0.1 M MES with 0.3 M NaCl, and (ii) ddH_2O in absence of alginate, and with or without the EDC and NHS coupling agents (initial: [NHS]=0.326 mg/ml & [EDC]=1.086 mg/ml; optimal: [NHS]= 0.207 mg/ml & [EDC]= 1.18 mg/ml). The solutions were subjected to both the initial and optimal reaction conditions as described in *section 3.1.1* and stirred at 200 rpm for 16 hours at room temperature before their thiol group content was measured the same way as previously.

3.1.4 GSH functionalization to alginate based on Ullah Shah et al. (2016) methodology

Based on the observation that thiol groups in reduced form are lost under conventional reaction conditions, an alternative reaction procedure based on the work from Ullah Shah et al (2016)[85] was investigated. Briefly, sodium alginate was dissolved in ddH_2O at a concentration of 1% (w/v),

to which EDC was added at a final concentration of 50 mM (targeting 100% of alginate's active monomers). The reaction mixture was mixed for 45 minutes at room temperature, after which GSH was added at a (2:1) = (sodium alginate:GSH) mass ratio and the pH was adjusted to 4.0. The solution was stirred for 2 hours at 200 rpm at room temperature using a magnetic stir plate. The pH of the solution was then adjusted to 6.0 and stirred for another hour. Resulting samples were then dialysed for 20 hours at room temperature using cellulose-membrane dialysis (MWCO: 12,000-16,000), while conducting four 500 mL dialysate changes: one time with 1 mM hydrochloric acid (HCl) (left for 1 hour), two times with 1 mM HCl and containing 1% (w/v) NaCl (overnight, then for 2-3 hours), and one last time with 1 mM HCl (for the remainder of the 20 hours). Selected reactions were also performed with the addition of NHS prior to EDC, at a (1:1) molar ratio with EDC. Controls were prepared (i) without the addition of the coupling agents (EDC/NHS), (ii) without the addition of the GSH, and (iii) comprising alginate only. The samples were then collected and freeze-dried for 48 hours before being characterized. All samples in dry form were stored in a desiccator at room temperature. The functionalization efficiency on the conjugated samples was calculated using the equation 2 from this report, with $[GSH]_{Total}$ (mM) being the amount of GSH added in the reaction mixture, corresponding to a (alginate: GSH) mass ratio of (2:1).

3.1.5 Optimization of the synthesis conditions from Ullah Shah et al. (2016)

Using the reaction conditions details in *section 3.1.4.* as a starting point, a 2-level factorial design (DOE #2) was conducted to optimize the grafting of GSH onto alginate and the preservation of thiol groups necessary for ROS scavenging by varying three parameters: (i) the (EDC:GSH) molar ratio [+: (3: 1); 0: (2.25: 1); -: (1.5: 1)]; (ii) the pH [+: pH = 8.0; 0: pH = 6.0; -: pH = 4.0], and (iii) the reaction time [+: t = 8 hours; 0: t = 5 hours; -: t = 2 hours]. Of note, the pH was only tuned once

after the addition of GSH. Subsequently, a second 2-level factorial design (DOE #3) of this method was performed to further attempt to increase the GSH content of conjugates while maintaining elevated levels of thiol groups in reduced form. This DOE was further evaluated for the effect of the following two parameters: (i) the (EDC:GSH) molar ratio [+: (4: 1); 0: (3: 1); -: (2: 1)] and (ii) the pH [+: pH = 5.0; 0: pH = 4.0; -: pH =3.0]. Four replicates of the centre point were performed in both DOEs for pure and standard error estimations.

3.1.6 Design of experiments (DOE) – Statistical analysis

All statistical analysis relevant to DOEs were performed using an RStudio code (R version 4.3.1). Three-way analysis of variance (ANOVA) (DOE #1 for conventional synthesis protocol, DOE #2, Ullah Shah et al.'s methodology) and a two-way ANOVA (DOE #3, Ullah Shah et al.'s methodology) along with first-order linear regression modeling of the parameters fitted to each individual response (DOE#1: [GSH] (mM); DOE #2 and DOE #3: [GSH] (mM), %[-SH]/[GSH detected], %[-SH]/[GSH added]), including main and interaction effects, were used to evaluate factor effects and interactions. The standard error associated with each regression coefficient was calculated from the residual mean square error (MSE) and the structure of the design matrix. Statistical significance was assessed at the confidence levels provided by the following p-values: *$p < 0.05$; **$p < 0.01$; and ***$p < 0.001$. Curvature assessments were also performed indicating nonlinearity for each first-order linear regression model, using a significance level of the p-Center < 0.05. Normality of residuals were assessed through visual inspection of Q-Q plots. Experimental error estimation was generated from the replicated center points (n=4), from which a mean and standard deviation was calculated to quantify replicability.

3.2 Characterization of the conjugates

3.2.1 BCA assay for peptide (GSH) quantification

The BCA assay (Thermofisher Scientific) was used to estimate the peptide (GSH) content of solutions according to a modified version of supplier instructions. Briefly, samples and controls were prepared at a concentration of 1% (w/v) in ddH_2O and vortexed until completely dissolved. GSH standards were prepared in ddH_2O. The kit master mix was prepared following instructions from the assay kit protocol. Aliquots of 25 µL of each standard and samples were pipetted, in triplicates, in a transparent 96-well plate to which 200 µL of the master mix was added per well. The plate was incubated for 30 minutes at 37°C with agitation before the absorbance of each well was measured using a spectrophotometer (BioTek) at a wavelength of $562\ nm$.

3.2.2 Ellman's assay

An Ellman's assay was used to estimate the free thiol (-SH) content of samples[86]. Briefly, samples and controls were prepared at a concentration of 1% (w/v) in ddH_2O and vortexed until completely dissolved. An assay buffer composed of 0.1 M sodium phosphate (Sigma Aldrich) and 1mM ethylenediaminetetraacetic acid (EDTA; Fisher Scientific) in ddH_2O was prepared, and its pH was adjusted to 8.0 using 2 M NaOH solution. A 10 mM solution of 5,5′-dithiobis-(2-nitrobenzoic acid) (DTNB; Thermofisher Scientific) and Cysteine-HCl (Sigma Aldrich) standards ranging from 0.25 mM to 1.5 mM were prepared in the assay buffer. Aliquots of 100 µL of each standard and sample were mixed with 1 ml of the assay buffer and 20 µL of 10 mM DTNB solution. The reaction mixtures were vortexed and incubated for 15 minutes at room temperature. Aliquots of 200 µL of each reaction solution were pipetted into a transparent 96-well plate, and the absorbance of each well was measured using a spectrophotometer (BioTek) at a wavelength of $412\ nm$.

3.2.3 Hydrogen peroxide (H_2O_2) assay

The H_2O_2 remaining in sample solutions were quantified using an H_2O_2 assay kit (Sigma Aldrich) according to supplier instructions. Briefly, 50 µL aliquots of red peroxidase substrate were prepared by resuspension of 1 vial with 250 µL of Dimethyl sulfoxide (DMSO). The same manipulation was conducted for preparing 200 µL aliquots of the Horseradish Peroxidase (20 units/mL) by mixing 1 vial with 1 ml of assay buffer. H_2O_2 standards ranging from 1.5225 to 12.5 µM were prepared in ddH_2O. The master mix solution was prepared following the kit instruction. Briefly, a sufficient volume of master mix solution was prepared proportionally to the following recipe (5 ml total volume basis): 50 µL red peroxidase substrate stock, 200 µL 20 units/ml peroxidase stock completed with 4.75 ml of assay buffer. Aliquots of 50 µL of each standard and sample were pipetted in triplicates into a black bottom 96-well plate and mixed with 50 µL of the master mix solution. The plate was incubated for 15 minutes at room temperature in the dark, and the fluorescence signal of each well was measured using a spectrophotometer (BioTek) at excitation and emission wavelengths of $540\ nm$ and $590\ nm$, respectively.

The scavenging efficiency was calculated using the formula below:

$$\%H_2O_2\ Scavenging = \left(\frac{[H_2O_2]_{Total} - [H_2O_2]_{Remaining}}{[H_2O_2]_{Total}}\right) \times 100 \qquad \text{Equation 2}$$

Where $[H_2O_2]_{Total}$ and $[H_2O_2]_{Remaining}$ are the theoretical total concentration of H_2O_2 (500 µM) and the H_2O_2 concentration measured in the sample, respectively.

3.2.4 ^{1}H-NMR spectroscopy

The alginate-GSH conjugate (FUNC 10%), as well as a blend (ALG+GSH) and alginate alone (ALG), both processed according to the same conditions of synthesis and purification, and pure

glutathione (GSH), were dissolved in deuterium oxide (D_2O) at a concentration of 2% (w/v) and characterized chemically using proton nuclear magnetic resonance (^{1}H-NMR) with the Bruker AVANCE II 400 MHz spectrometer (operating frequency for protons of 400 MHz), equipped with a triple resonance broadband observe (TBO) iProbe. The MestReNova 14.2.1 software was used to process the ^{1}H-NMR spectra. The spectra were obtained by averaging 32 independent scans taken at 25 °C with a 2 minutes 51 seconds acquisition time.

3.2.5 Characterization of GSH and free thiol groups retention in alginate gels post-crosslinking

4% (w/v) solutions of alginate-GSH conjugate (synthesized according to the protocol detailed in *section 3.1.4* with the following synthesis conditions: (EDC:GSH) = (4:1); pH=5.0; reaction time = 2 hours) were prepared in ddH_2O and crosslinked into 10 µL beads by dropwise addition in 100 mM Calcium Chloride ($CaCl_2$; ACS) solution and incubated at room temperature for 30-40 minutes. The beads were collected in a 100 µm cell strainer, washed three times with 10 ml of ddH_2O, lightly dabbed with a Kim wipe for water removal, placed in a 1.5 ml microtube, and weighed. The beads were tested for their GSH and -SH content post-degradation using the BCA and Ellman's assays detailed above, respectively, where bead degradation was allowed from carbonate and sodium phosphate present in the BCA and Ellman's assay buffers, respectively. Results were corrected to a total 100 µL alginate solution baseline (10 µL/bead x 10 = 100 µL alginate solution) assuming proportionality, addressing variability in microbead fabrication between samples. Samples without (EDC/NHS), without GSH, and with alginate alone, synthesized in the same conditions, were also prepared.

3.2.6 Evaluation of H_2O_2 scavenging capacity of alginate-GSH conjugates

Solutions of 8% (w/v) alginate-GSH conjugate, synthesized according to *section 3.1.4.* (synthesis conditions: (EDC:GSH) = (4:1), pH= 5.0, 2-hour reaction time) were prepared in ddH_2O. Each

solution was mixed at a 1:1 volume ratio with a 1 mM H_2O_2 solution prepared in ddH_2O, yielding in final reaction mixture concentrations of 4% (w/v) conjugate and 500 µM H_2O_2. After mixing, samples were incubated for 24 hours at room temperature in the dark, and the remaining H_2O_2 content was quantified using the H_2O_2 assay described in *section 3.2.3*.

3.2.7 DPPH assay to quantify the antioxidant capacity of alginate-GSH conjugate gels

The antioxidant capacity of alginate-GSH conjugate hydrogel beads was measured using the 2,2-diphenyl-1-picrylhydrazyl (DPPH) assay[87,88]. Briefly, 10 beads prepared as described in *section 3.2.5* were mixed with 750 µL of 100 µM DPPH (Sigma Aldrich) solution, prepared in pure methanol. The microtubes were sealed with parafilm and incubated for two hours at room temperature in the dark to allow scavenging. The samples were then measured for remaining DPPH content by injecting 200 µL per well of each sample, in triplicates, in a transparent 96-well plate. The absorbance of each well was measured using a spectrophotometer (BioTek) at a wavelength of $517\ nm$. A blank of reaction (100 µM DPPH solution alone) was also prepared and measured.

The scavenging efficiency was calculated using the following formula:

$$\%\ DPPH\ Scavenging = \left(\frac{A_{Blank} - A_{Sample}}{A_{Blank}}\right) \times 100 \qquad \text{Equation 3}$$

Where A_{Blank} and A_{Sample} are the absorbances of the blank and the sample, respectively.

3.3 Establishment of a cellular model of cell death following exposure to H_2O_2

3.3.1 NIH3T3 cell culture

Immortalized NIH3T3 fibroblast cells were cryopreserved in Dulbecco's Modified Eagle Medium containing 4.5 g glucose/L (DMEM-4.5; Corning) with 10% Heat Inactivated (HI) fetal bovine serum (FBS; VWR) and 10% DMSO at a cell concentration of 2×10^6 cells/mL and previously

passaged 42 times. The cells were thawed in a 37°C water bath and injected into a T182.5 flask containing 24 ml of culture media composed of DMEM-4.5 supplemented with 10% HI FBS and 100 units/mL penicillin, 100 units/mL streptomycin, and 250 ng/mL amphotericin B (1X antibiotic-antimycotic; Gibco). The cells were allowed to adhere to the flask and maintained in a cell incubator at 37°C, 5% carbon dioxide (CO_2), and 95% humidity. Media changes were done three times a week until cells reached the desired confluency (80-90%).

3.3.2 H_2O_2 exposition on cells – cytotoxicity study

At 80-90% confluency, NIH3T3 cells were washed three time with DMEM-4.5 and detached using 3 ml of 1X trypsin (Trypsin-EDTA (0.25%), phenol red; Fisher Scientific) pre-incubated at 37°C. The flask was incubated for 2-3 minutes in a cell incubator at 37°C, 5% CO_2, and 95% humidity, after which 1 mL of HI FBS and 6 mL of DMEM-4.5 media were added for trypsin deactivation. The cells were collected in a 50 ml Falcon tube and washed three times in DMEM-4.5. Cells were then counted with a hemocytometer under an light microscope and resuspended in culture media at a final cell concentration of 60,000 cells/mL, seeded into a 24-well plate (1 mL per well), and allowed to adhere for 24 hours in a cell incubator adjusted at 37°C, 5% CO_2, and 95% humidity. After 24 hours, the media from each well was replaced with 1mL of culture medium supplemented with H_2O_2 at concentrations ranging from 25 to 750 µM. The plate was incubated for 24 hours at 37°C, 5% CO_2, and 95% humidity, whereafter, cytotoxicity was tested on the cultures using the alamarBlue assay (Fischer Scientific).

3.3.3 alamarBlue Assay

The number of viable cells in each well was estimated indirectly by evaluation of their metabolic activity using the alamarBlue assay. Briefly, the media from the each well comprising NIH3T3 cells exposed to H_2O_2 (as well as controls cultured in absence of H_2O_2) was withdrawn and replaced

with 1mL of a 10% alamarBlue Cell Viability Reagent prepared in culture media and incubated for 4 hours in a cell incubator at 37°C, 5% CO_2, and 95% humidity. Empty wells that did not contain cells were also prepared with the 10% alamarBlue Cell Viability Reagent, acting as blanks. Following incubation, the medium from each well was well mixed and a 100 µL aliquot was added to a black bottom 96-well plate, in triplicates, and the fluorescence signal of each well was measured using a spectrophotometer (BioTek) at excitation and emission wavelengths of $560\ nm$ and $590\ nm$, respectively.

3.4 Statistical Analysis

Besides DOEs, thiol group redemption attempts (GSH's slow addition, GSSG functionalization and TCEP reduction), all other experiments were replicated at least 3 times ($n \geq 3$), with conjugates produced via independent reactions, where all data is presented as averages ± standard deviation. The statistical analysis on the data was performed using a Single factor or a two-factor ANOVA with replication along with standard Tukey's Honestly Significant Difference (HSD) for even sample sizes, and a two-factor ANOVA with regression with a post hoc Tukey's Kramer HSD, for unequal sample sizes. These analyses were performed using the XRealStatsx add-in on the Microsoft Excel software (version 2604 Build 16.0.19929.20086 64-bit). The p-values used for analysis were $*p < 0.05$; $**p < 0.01$; and $***p < 0.001$.

CHAPTER 4: RESULTS AND DISCUSSION

4.1 Investigation of a conventional carbodiimide reaction for alginate functionalization with GSH peptide

The work presented in this thesis followed efforts by a previous student in the group to functionalize sodium alginate with the short antioxidant peptide glutathione (GSH) by means of carbodiimide chemistry, a widely studied technique for alginate coupling with peptides[89–92]. This chemistry involves the reaction of EDC with the -COOH group on the β-D-mannuronic acid (M) and α-L-guluronic acid (G) monomers forming the alginate backbone and subsequently with the primary amine present at the N-terminus of a peptide. This reaction forms a highly active O-acylisourea intermediate and is most efficient in acidic aqueous solutions (pH = 4.5)[93]. NHS stabilizes the intermediate through the formation of an NHS ester, allowing more efficient coupling reactions at neutral pH. The reaction is typically performed in MES-based buffers and conducted at a near neutral pH to support the synthesis of materials for biological applications, as well as the amidation reaction that typically occurs at a pH between 7.0 to 9.0[93]. Initial efforts by the previous student had resulted in alginate-GSH conjugates with a minimal H_2O_2 scavenging capacity.

In a first attempt to address this limitation, efforts to increase the scavenging capacity of conjugates were focussed on optimizing the synthesis conditions to achieve higher GSH grafting onto the alginate backbone. Three key parameters were identified that could have a potential effect on amidation between alginate and GSH: (i) the (EDC:GSH) and (ii) (NHS:GSH) molar ratios, as well as (iii) the pH of the reaction mixture. These factors were used in the construction of a first design of experiment (DOE #1) using a complete 2-level factorial design including four centre

points for a total of 12 samples. The levels chosen for each factor were the following: (EDC:GSH) ratio = [+: (1.2: 1), 0: (1.1: 1), -: (1.0: 1)]; (NHS:GSH) ratio = [+: (0.75: 1), 0: (0.55: 1), -: (0.35: 1)]; and pH = [+: pH= 7.0, 0: pH= 6.0, -: pH= 5.0]. The concentration of GSH ([GSH] mM) in each sample post dialysis and lyophilization (reflecting GSH grafting), was quantified using the BCA assay on 1% (w/v) functionalized alginate solutions prepared in ddH_2O. Results for each trial are tabulated in Supplementary Table 1.

A three-way ANOVA of the results showed that the (EDC:GSH) molar ratio ($p < 0.05$), as well as the pH ($p < 0.01$) have significant and positive effects on GSH retention in functionalized samples (Supplementary Table 2, Figure 4.1), while the (NHS:GSH) molar ratio did not show a statistically significant effect on the measured response. These results reflect expected outcomes, as higher amounts of EDC in reaction solutions as well as a higher pH could facilitate and promote a higher rate of amidation (more alginate monomers bound with GSH's primary amine). Indeed, elevated amounts of EDC or in excess to the peptide could lead to higher amounts of activated -COOH groups on the alginate backbone, inducing more available binding sites for the nucleophilic attack of GSH's primary amine on the NHS ester, leading to higher amidation rates. Furthermore, it is reported that a reaction pH between 7.0 and 9.0[93] favors the formation of an amide bond. As the highest pH explored in this experimental design is 7.0, it is expected to see an increase in GSH concentrations in conjugate solutions as we are approaching amidation optimal conditions. Of note, a Q-Q plot for this DOE (Supplementary Figure 1) shows slight deviations of the percentiles against the normality model at the plot extremes, but considering the sample size and the balanced design, the assumption of normality was deemed acceptable.

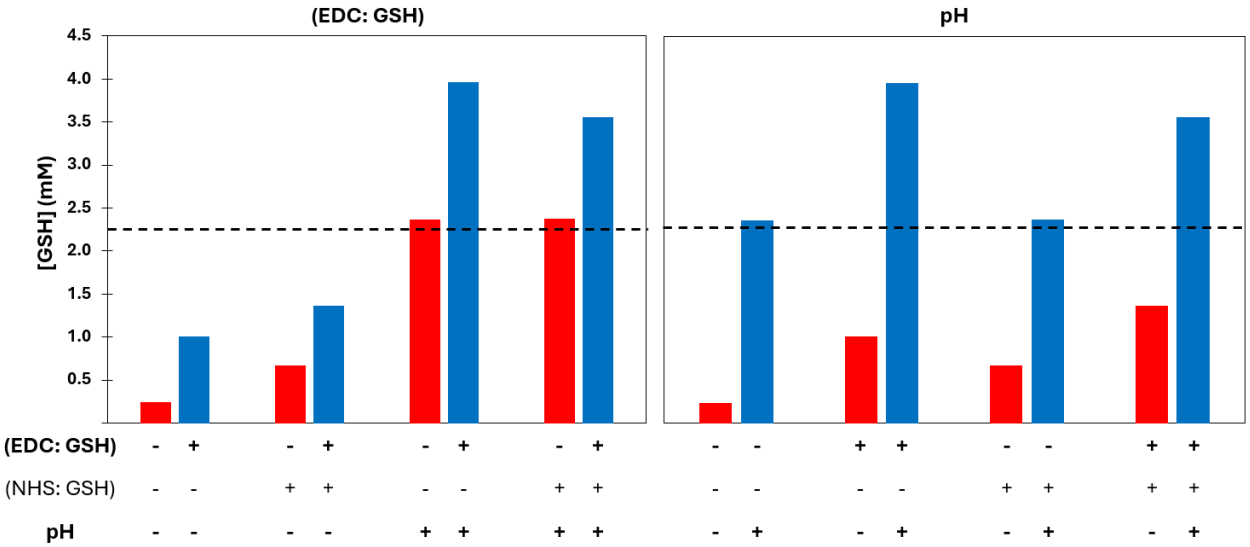

Figure 4.1. DOE #1 – Response plot showing the effect of (EDC:GSH) molar ratio and pH on GSH grafting onto alginate ([GSH] (mM)). GSH concentration ([GSH] (mM)) responses in 1% (w/v) conjugate solutions, resulting from positive (+) and negative (-) level variations of (EDC:GSH) molar ratio and pH, are represented in blue and red, respectively. The black dashed line represents the mean on the middle points ([GSH] = 2.25 ± 0.33 mM). All parameters of interest have been bolded.

Further analysis of the DOE data is presented in Table 4.1. The determination of the values and statistical significance of each coefficient suggests that a linear model can predict the concentration of GSH (mM) in 1% (w/v) alginate-GSH conjugate solutions post functionalization at specific synthesis conditions of (EDC:GSH) between [1.2-1:1] and pH between [5.0-7.0]:

$$[GSH](mM) = 2.05 + 0.532X_1 + 1.12X_2 \qquad \text{Equation 4}$$

Where $2.05\ mM$ represents the grand mean estimation of the response, with X_1 and X_2 being the effect parameters of (EDC:GSH) and pH, respectively. The model demonstrated an adequate fit (adjusted $R^2 = 0.88$), indicating that changes in the GSH concentrations measured in alginate-GSH conjugate samples are caused mainly by changes in the (EDC:GSH) molar ratio and the reaction pH, rather than that of other known or unknown factors. Furthermore, curvature tests on the center points suggest no apparent curvature in the model (p-Center > 0.05, Supplementary Table 3), suggesting further that the response can be explained with the above linear model. Finally, the

standard deviation for the replicates of the center point (sd = 0.334) indicates the presence of moderate experimental variability, especially on lower [GSH] (mM) response ranges. The conditions that resulted in the highest GSH concentration in a 1% (m/v) functionalized alginate solution (3.96 mM) and consequently the highest functionalization efficiency (η = 78.8%) are: (EDC:GSH) = (1.2:1); (NHS:GSH) = (0.35:1); pH=7.0.

Table 4.1. Regression model results – Optimization of a conventional alginate functionalization method with GSH. Levels of significance: $p < 0.05$ (*); $p < 0.01$ (**); $p < 0.001$ (***).

Coefficients	Factors	Estimate	Standard Error	t-value	p-value
β_0	Intercept	2.05	0.110	18.552	4.97×10^{-5}***
β_1	(EDC:GSH)	0.532	0.135	3.937	0.0170*
β_2	(NHS:GSH)	0.0495	0.135	0.367	0.732
β_3	pH	1.12	0.135	8.307	0.00115**
β_4	(EDC:GSH) x (NHS:GSH)	-0.0607	0.135	-0.450	0.676
β_5	(EDC:GSH) x pH	0.165	0.135	1.220	0.289
β_6	(NHS:GSH) x pH	-0.149	0.135	-1.100	0.333
β_7	(EDC:GSH) x (NHS:GSH) x pH	-0.0429	0.135	-0.318	0.767
Residual Error (df = 4)		0.382			
Multiple R-squared		0.956			
Adjusted R-squared (R^2)		0.88			
F-statistic (df = 7 & 4)		12.52			
p-value		0.0139*			

However, conventional ways of functionalizing alginate resulted in major thiol group losses on the alginate conjugate, with calculated thiol group proportions normalized to the GSH added in solution of 0.1% to 0.4%. This low thiol group availability left the conjugate inactive and unable to perform its role as an antioxidant hydrogel for skin wound healing. The remainder of this work will discuss attempts to overcome this challenge.

4.2 Investigation of the effect of components of the carbodiimide reaction on free thiol groups on the GSH peptide

To better understand the factors affecting the presence of free thiols in the carbodiimide reaction, free GSH was incubated in two different buffering systems (0.1 M MES with 0.3 M NaCl and ddH_2O), with and without EDC/NHS, subjected to two different conditions, the initial condition: (EDC:GSH) = (1.1:1), (NHS:GSH) = (0.55:1), pH = 6.0, and the optimal condition as identified in section 4.1: (EDC:GSH) = (1.2:1), (NHS: GSH) = (0.35:1), pH=7.0. The concentration of free thiol groups remaining in solution after a 16-hour incubation at room temperature were quantified in each sample using the Ellman's assay. The results are presented in Figure 4.2.

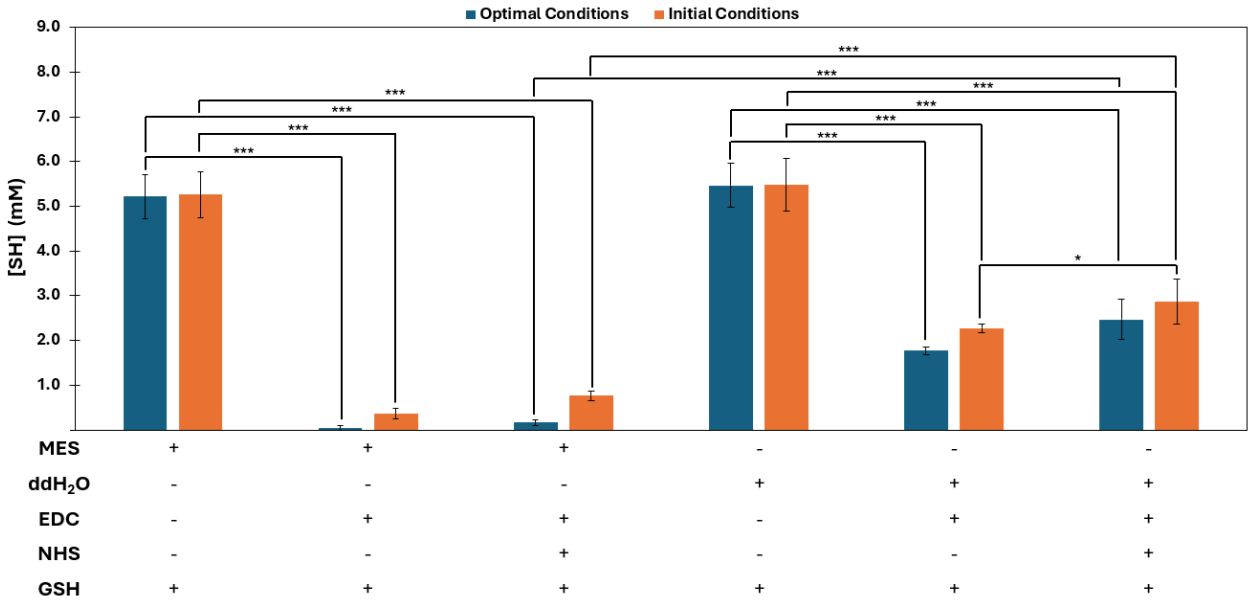

Figure 4. 2. Free thiol group stability of GSH in different reaction formulations and conditions. Thiol group concentration (mM) in each 5.15 mM GSH solution formulation was measured using the Ellman's assay. (+) and (-) indicate addition or omission of the components. Error bars represent the standard deviation on the mean. Statistical significance levels are indicated as follows: $p < 0.05$ (*), $p < 0.01$ (**), $p < 0.001$ (***).

Results show a significant loss of free thiols in solution following the addition of EDC. This may be explained by the fact that EDC can participate in secondary reactions with the sulfhydryl

group on GSH as it represents a competing nucleophile with -COOH. This unintended reaction may occur more readily in this specific experiment because of the absence of alginate with its -COOH groups in the solution. This side reaction would lead to the depletion of free thiol groups in solution. The addition of NHS to EDC resulted in a significant protective effect on free thiol groups ($p < 0.05$) in the ddH_2O buffering system, when subjected to initial rather than optimal incubation conditions, but the effect was not significant for other incubation conditions. The reason why this significant difference is not seen in the ddH_2O buffering system optimal conditions as opposed to initial could be justified by the slight increase of coupling agents' proportions and pH leading to higher EDC activation and -COOH deprotonation on GSH (as alginate is absent), increasing NHS ester concentrations. This effect could be added to the higher proportions of sulfhydryl groups deprotonated, increasing the number of reactive species in solution, giving more opportunities for thiolate groups to react, making the protective effect of NHS negligeable at "optimal" incubation conditions [94]. However, as results under the optimal conditions are substantially similar to those of the initial conditions for all other buffering formulations, the "protective effect of NHS" can be deemed to be the same between initial and optimal conditions when using the ddH_2O buffering system. In addition, NHS also showed negligeable protective effects on free thiol groups in the MES buffering system, no matter the incubation condition employed. The protective effects of NHS observed in water may result from the unbuffered system conferred by ddH_2O. Indeed, as EDC hydrolyzes and decomposes, the pH of the solution is expected to drift towards more acidic levels, leaving higher protonated thiol group proportions on GSH molecules[95]. Furthermore, at a lower pH, the O-acylisourea intermediate is expected to become more short-lived and prone to hydrolysis, potentially favoring the formation of a GSH-derived NHS ester via the γ-glutamyl -COOH group to stabilize the highly unstable intermediate[93,95]. This complex may then become more selective for coupling reactions through primary amines than through protonated thiol groups.

The MES buffering system, on the other hand, tends to stabilize the pH despite the hydrolysis of EDC[96], increasing the amount of thiolate ions in comparison to intact sulfhydryl groups, which may react through GSH-GSH crosslinking and thioester intermediates formation from EDC by-products (e.g.: N-substituted urea and N-acylurea)[95,97], among other re-arranged products.

Importantly, while free thiol concentration appeared comparably maintained when incubated in MES buffer or ddH_2O in absence of the coupling agents, their addition leads to a substantially more pronounced loss of free thiol in MES than in ddH_2O. This result suggests that carrying out the alginate-GSH conjugation reaction in ddH_2O instead of MES buffer could provide an avenue for the preservation of an increased percentage of GSH in reduced form. This is critical in order to preserve the antioxidant activity of GSH in the conjugate. It should also be noted that no contribution of the different synthesis conditions, including variations in pH and coupling agent proportions between the initial and optimal synthesis conditions, were observed on the concentration of free thiol groups measured in solution at the end of the incubation.

4.3 Modifications to the conventional carbodiimide method of alginate functionalization to protect the thiol group on GSH

As per the results in section 4.2, it was speculated that the sulfhydryl group of GSH tends to deprotonate and enter side reactions with the action of EDC/NHS, forming side products, especially at higher pH. Another issue that may be hindering thiol group availability in the reaction mixtures, especially at near neutral pH (6.0-7.0), is GSH oxidation, forming glutathione disulfide (GSSG). Indeed, GSSG formation is accelerated or favored in aqueous solutions at higher pH, allowing thiolate formation, in the presence of dissolved O_2, in the presence of metal ions (Cu^{2+}, Fe^{3+} or Mn^{2+}) (from water, buffer, glassware or reactants), or from ROS formation when the reaction is

exposed to light [98,99]. To recover sulfhydryl groups or to prevent the formation of disulfide bonds between them, a few remedy attempts were conducted.

The first attempt consisted in adding a solution containing the appropriate amount of GSH to the reaction mixture [5% functionalized monomers, (GSH:active monomers) = (1:1)] at a slower rate of 1 ml per hour, using a programmed syringe pump. This was intended to reduce GSH proportions present in solution at any given time during the reaction, thereby decreasing the probability that GSH molecules react with each other through the formation of disulfide bonds. As can be seen in Figure 4.3, preliminary results for this strategy did not show a substantial increase in thiol group recovery when the GSH solution is added at a rate of 1 ml per hour (termed "SLOW") in comparison to standard extrusion addition consisting of GSH addition all at once (termed "FAST"). Indeed, the sulfhydryl group proportion detected in the sample from the total amount of GSH added ([GSH] = 2.58 mM) in the reaction mixture for SLOW and FAST additions are 0.276% and 0.345%, respectively, which represents a tremendously small amount of preserved thiol groups. This result may be explained by the fact that pH of the reaction mixture is high (pH = 7.0), favoring NHS ester activation and thiolate formation[94], encouraging their covalent interaction, as well as GSH oxidation into GSSG, that is, at least for the addition rate investigated. The slight decrease in preserved thiol proportions in the slow addition rate of GSH conjugate in comparison to the fast addition rate conjugate could be due to oxidation of GSH in solution prior to its addition into the reaction mixture, considering its residence time in the syringe.

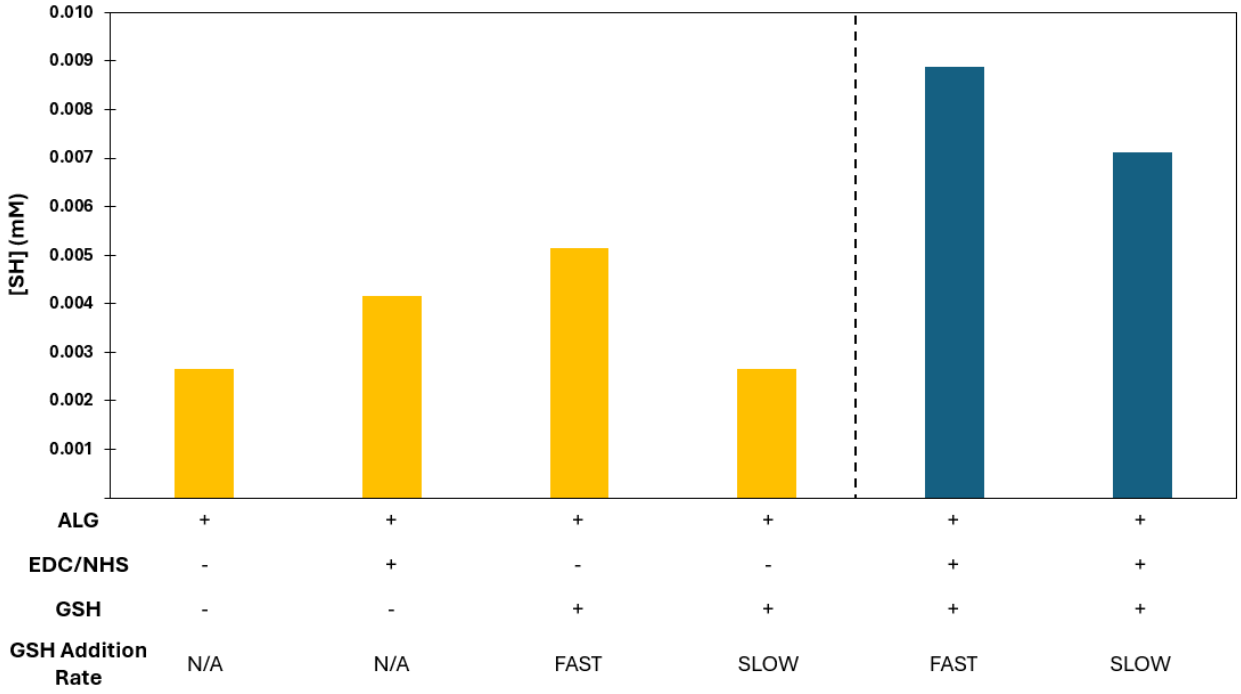

Figure 4. 3. Free thiol group content in alginate-GSH conjugates following slow addition of GSH. The thiol group concentration (mM) in 1% (w/v) conjugate solutions were measured using the Ellman's assay. The black dashed line separates negative controls of reaction (yellow) from the test samples (dark teal). The appropriate GSH quantity was either added to the reaction mixture "FAST" (regular extrusion) or "SLOW" (at a controlled rate of 1 ml/hour using a programmed syringe pump). (+) and (-) indicate addition or omission of the components. Experiment repeated only once.

Given that the addition of GSH at a slower rate did not have a substantial impact on free thiol group preservation in the conjugate, we tested the effect of incubating the conjugate with the reducing agent TCEP, as a strategy to reduce any GSH molecule bound to alginate and recover free thiol groups. Indeed, TCEP acts as a nucleophile, attacking one sulfur atom in the disulfide bond and breaks it into a thioalkoxyphosphonium cation and a free thiol/cysteine ($R\text{-}S^-$), that can be protonated by surrounding water molecules[100] to form a stable sulfhydryl group. Results show no apparent change in free thiol group proportions in the functionalized sample that was reacted with TCEP in comparison with the control incubated in absence of TCEP (Figure 4.4). This could be explained by the fact that most sulfhydryl groups from GSH were not lost in the form of disulfide

bonds during the carbodiimide reaction. Instead, it is likely that the loss of free thiol groups from the GSH in conjugates is the result of secondary reactions between EDC and these thiol groups. For example, thioethers (R-C(O)-SR) could be formed by acylation of thiolate groups with activated -COOH[101] from EDC's action, or "over-oxidized sulfurs" (RSO_2H or RSO_3H) could be formed, which are especially likely because of the prolonged oxidative conditions that the samples

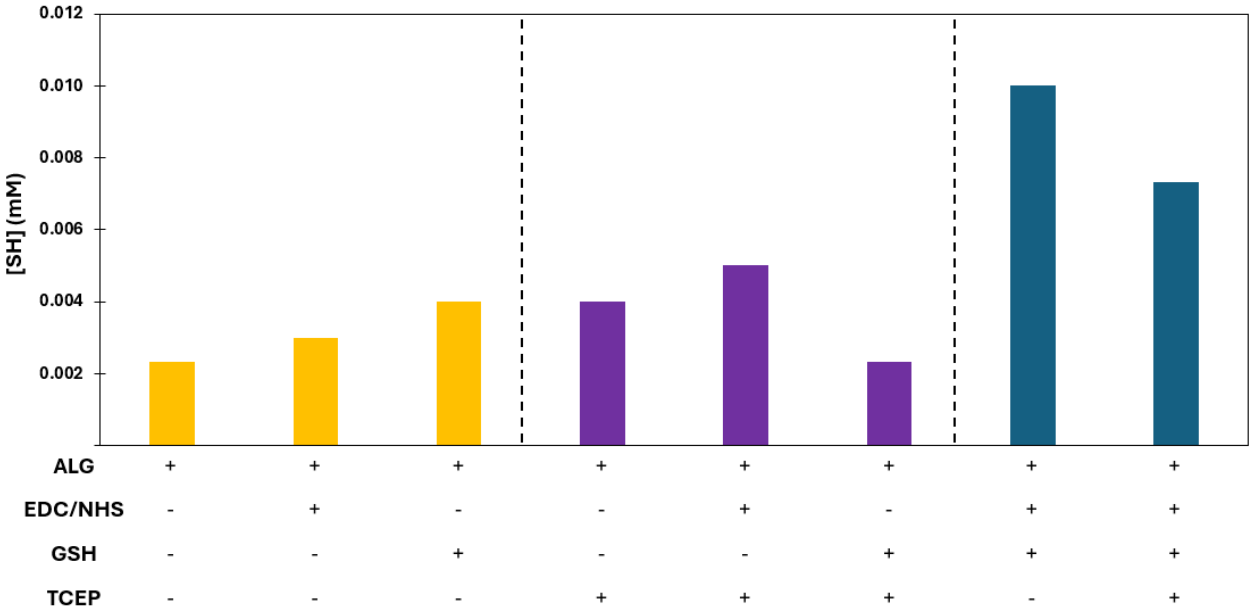

Figure 4. 4. Free thiol group content in alginate-GSH conjugates following TCEP addition post-functionalization. Thiol group concentration (mM) in 1% (w/v) conjugate solution were measured using the Ellman's assay. The black dashed lines separate negative controls of reaction, with (yellow) and without (purple) TCEP, from the test samples (dark teal). (+) and (-) indicate addition or omission of the components. Experiment repeated only once.

were subjected to during the reaction and purification steps. TCEP would not react with these chemical species and therefore not aid in thiol group regeneration. Finally, there is also a possibility that after reduced thiols were regenerated from the action of TCEP, most groups reverted into their oxidized form (GSSG), as the samples stay exposed to dissolved and ambient oxygen for a prolonged period, post-reaction during the dialysis (over 48 hours). However, this effect has not been observed by others who have used TCEP successfully to reduce GSSG[102,103].

Next, we functionalized alginate with GSSG, as a strategy for protecting the thiol groups with disulfide bonds during functionalization reaction and therefore to minimize their interaction with surrounding nucleophiles, after which, the conjugates were incubated with TCEP to break the disulfide bonds on the GSSG attached to alginate and obtain sulfhydryl groups. Results from this attempt show an interaction between TCEP and the Ellman's assay, most likely due to an insufficient purification during the dialysis step (Figure 4.5).

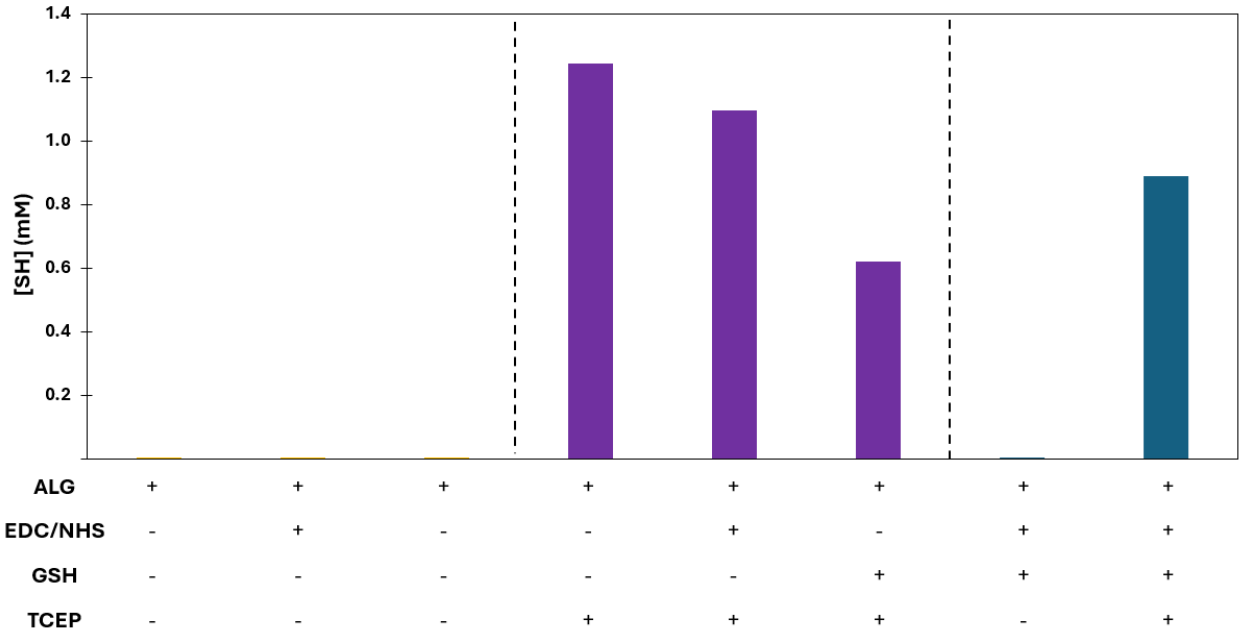

Figure 4. 5. Free thiol group content in alginate- GSSG conjugates following TCEP addition post-functionalization. Thiol group concentration (mM) in 1% (w/v) conjugate solution were measured using the Ellman's assay. The black dashed lines separate negative controls of reaction, with (yellow) and without (purple) TCEP, from the test samples (dark teal). (+) and (-) indicate addition or omission of the components. Experiment repeated only once.

4.4 Investigation of a carbodiimide reaction for alginate functionalization with GSH peptide based on the work by Ullah Shah, et al.

Following the unsuccessful attempts to preserve the thiol groups using the conventional carbodiimide reaction conditions, it became evident that the synthesis conditions needed to be revisited to ensure both effective glutathione binding to the alginate backbone and sufficient free

thiol preservation, to allow this conjugate to perform its antioxidant function effectively. A procedure by Ullah Shah et al. (2016)[85] was identified as a starting point. In comparison to the conventional functionalization method used in our work to this point, the method by Ullah Shah et al.'s uses lower reaction times (up to 3 hours in comparison to 16 hours), includes pH adjustments during synthesis, while maintaining the reaction mixture acidic (between pH = 4.0 to 6.0), uses higher GSH and EDC quantities with a (2:1) mass ratio of (alginate:GSH) and a (3:1) molar ratio of (EDC:GSH), without the use of NHS, and critically conducts the reaction in a ddH_2O buffering system instead of one composed of MES and NaCl. Finally, the dialysis used for purification was understood to last for approximately 20 hours in comparison to the 48 hours used in our previous efforts, with samples purified against acidic dialysate solutions (first dialysate change with 1mM HCl, twice with 1mM HCl containing 1% (w/v) NaCl, and once more against 1mM HCl). Considering that longer reaction times and higher pH could promote side reactions and GSH oxidation into GSSG, as well as our results suggested that more free thiol was preserved following incubation with EDC in water than MES buffer (section 4.2), these new conditions represented a promising direction for thiol group protection. Furthermore, an increased excess in EDC could compensate for the lower pH used, as amidation is favored at higher pH levels. Because the work reported in Ullah Shah et al. had not expanded on the efficiency of this reaction, we first replicated this protocol in house and measured the GSH and free thiol groups in resulting conjugates (Figure 4.6). The effect of NHS addition was also considered for this study, as a trend toward higher thiol group preservation had been observed in ddH_2O samples that contained NHS in comparison with the ones that did not (section 4.2).

Results from Figure 4.6 show significantly higher GSH content ($p < 0.01$) in samples with EDC only, in comparison to the ones where NHS is added ($[GSH]_{FUNC} = 4.73\, mM$;

$[GSH]_{FUNC+NHS} = 2.45\ mM$), but with a significantly lower thiol group content ($[-SH]_{FUNC} = 0.118\ mM$; $[-SH]_{FUNC+NHS} = 0.491\ mM$). This result supports our observations thus far in relation to the "protective effect of NHS", where amide bonding is favored in the given conditions, over other side reactions that could result in the loss of sulfhydryl groups. While functionalization

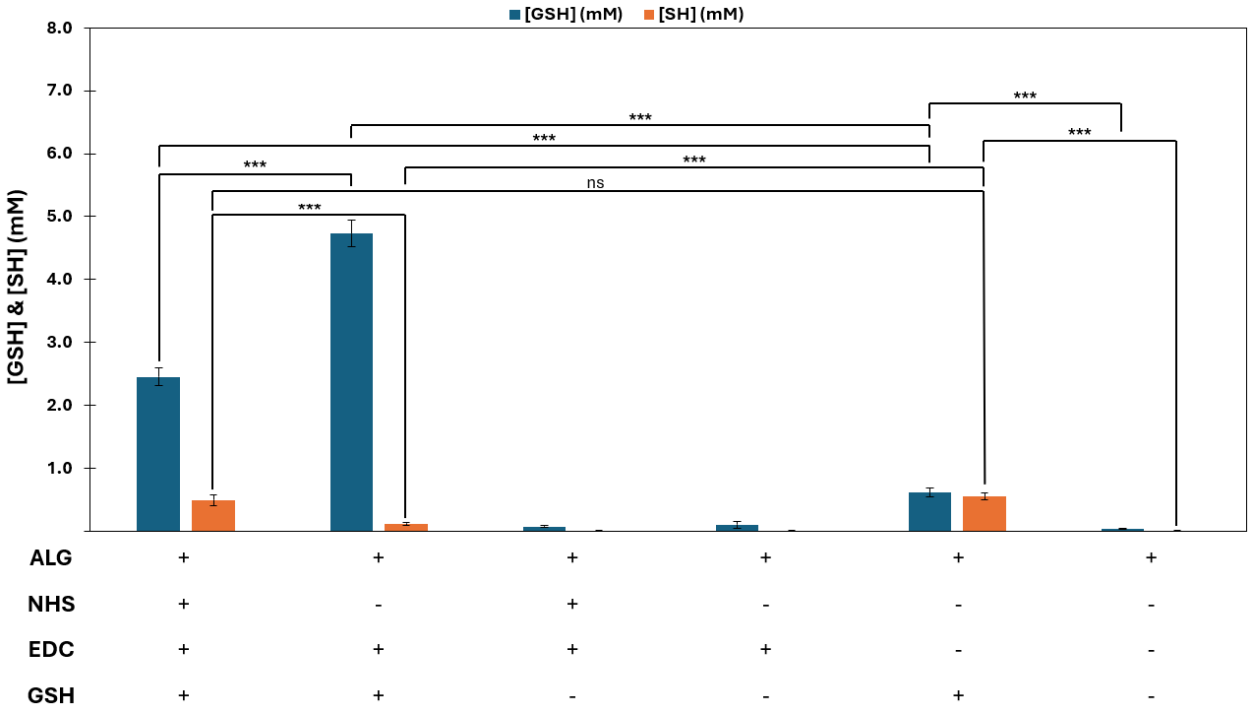

Figure 4. 6. GSH and thiol group content (mM) in functionalized alginate with GSH using Ullah Shah and al.'s protocol. Concentrations of GSH (dark teal) and thiol groups (orange) (mM) in 1% (w/v) alginate-GSH conjugate solutions were quantified using the BCA assay and Ellman's assay, respectively. (+) and (-) indicate addition or omission of the components. Error bars represent the standard deviation on the mean. Statistical significance levels are indicated as follows: $p < 0.05$ (*), $p < 0.01$ (**), $p < 0.001$ (***).

efficiency seems lower with the addition of NHS ($\eta_{FUNC} = 25.3 \pm 1.5\%$; $\eta_{FUNC+NHS} = 11.3 \pm 1.1\%$), the increased amount of free thiol groups retained normalized to the GSH amount detected of the sample represents a reasonable trade-off to ensure the conjugate's bioactivity ($20.1 \pm 4.1\%$); in comparison to roughly 0.343% for 5% functionalized alginate using optimal conventional synthesis conditions. This procedure also resulted in elevated thiol group preservation

normalized to the amount of GSH added in the reaction solution ($3.02 \pm 0.51\%$), in comparison to the one of conventional methods (0.345%).

Furthermore, the new purification method, while considering a shorter dialysis period, seems to be efficient at removing free GSH molecules when calculating removed GSH portions from the blend control (GSH added to alginate alone) $\left(\left[\frac{[GSH]_{Added}-[GSH]_{remaining}}{[GSH]_{Added}}\right] \times 100 = 96.2 \pm 0.5\%\right)$. However, this result needs to be interpreted with caution, as GSH could interact with other components of the reaction mixture which can influence GSH retention in conjugated materials after purification. Nonetheless, this new approach seems to have a higher capacity at protecting thiol groups, while ensuring some alginate conjugation with GSH.

4.5 Ullah Shah et al.'s functionalization procedure optimization

4.5.1 1st Design of experiment using Ullah Shah et al.'s methodology (DOE #2)

To build on these promising results, we set out to optimize the synthesis conditions for two main objectives: (i) to maximize GSH grafting, and (ii) to maximize thiol group availability and therefore achieve ROS scavenging. A new design of experiment using a two-level three parameters factorial design including four center points was executed, taking Ullah Shah et al.'s protocol as a baseline for selected conditions. The parameters selected for this study were the (EDC:GSH) molar ratio, the pH, as well as the reaction time. The levels chosen for this design were (EDC:GSH) molar ratios of +: (3: 1), 0: (2.25: 1), -: (1.5: 1), pH levels of +: 8.0; 0: 6.0 -: 4.0, and reaction times of +: 8 hours, 0: 5 hours, -: 2 hours. The response variables of interest were the concentration of GSH (mM) measured in 1% (w/v) alginate-GSH conjugate samples prepared in ddH_2O, and the concentration of free thiol (mM) available for scavenging, normalized over two baselines: (i) the amount of GSH detected in the sample (indicating what proportion of the GSH bound presented free thiols available for scavenging), and (ii) the amount of GSH added in the reaction mixture

(representing the proportion of the free thiols added to the reaction mixture that was preserved at the end of the full process). Results of all trials are tabulated in Supplementary Table 4.

4.5.1.1 GSH grafting optimization

A three-way ANOVA analysis of the GSH grafting results from this DOE shows similar trends as those observed in section 4.1 with the conventional reaction conditions. Indeed, the (EDC:GSH) molar ratio ($p < 0.01$) as well as the pH ($p < 0.01$) have significant and positive effects on GSH grafting to alginate, while the reaction time ($p > 0.05$) did not demonstrate an effect on the response (Supplementary Table 5, Figure 4.7).

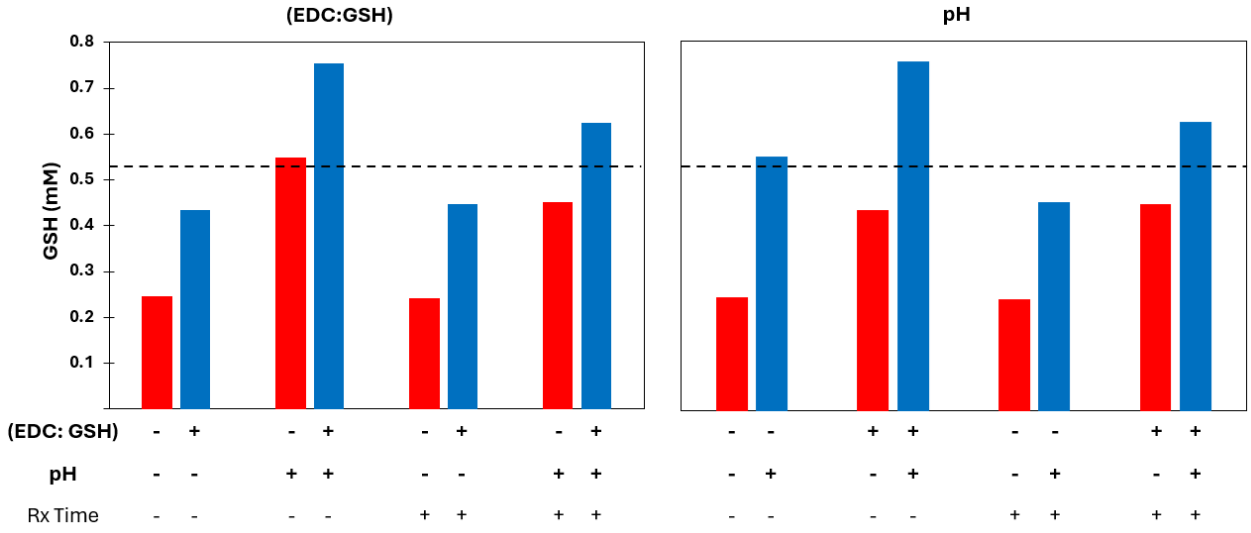

Figure 4. 7. DOE #2 – Response plot showing the effect of (EDC:GSH) molar ratio and pH on GSH grafting ([GSH] (mM)). GSH concentration ([GSH] (mM)) responses in 1% (w/v) conjugate solutions, resulting from positive (+) and negative (-) level variations of (EDC: GSH) molar ratio and pH, are represented in blue and red, respectively. The black dashed line represents the mean on the middle points ([GSH] = 0.535 ± 0.028 mM). All parameters of interest are shown in bolded characters.

These parameter effects on GSH retention are in accordance with theoretical outcomes as explained previously (section 4.1) and are more pronounced given the wider ranges evaluated for each parameter. The absence of effect from varying the reaction time on GSH grafting was unexpected but could potentially be explained by multiple reasons. First, the O-acylisourea intermediate

formed by the action of EDC is usually short lived in aqueous solutions, meaning that they can hydrolyze quickly, resulting in a shorter reaction window[93]. Once the intermediate is hydrolyzed, no further reaction can occur, regardless of the reaction time. Some studies have also shown that kinetics of the carbodiimide crosslinking reaction is highly influenced by reactant concentration as well as pH, as the reaction tends to progress until reactants decay, where time does not represent a limiting factor [10], at least, for the time range chosen for this study. Indeed, the possibility remains that a shorter reaction-time interval could have revealed a significant effect; however, additional experimentation is required to substantiate this.

The regression model analysis presented in Table 4.2 suggests a linear model predicting the concentration of GSH (mM) in alginate solutions post functionalization at a (EDC:GSH) molar ratio and a pH ranging between 1.5:1 and 3:1 and 4.0 and 8.0, respectively:

$$[GSH](mM) = 0.490 + 0.0966X_1 + 0.127X_2 \qquad \text{Equation 5}$$

Table 4. 2. Regression model results – DOE #2 – GSH grafting optimization using Ullah Shah and al.'s alginate functionalization method with GSH. Level of significance: $p < 0.05$ (*); $p < 0.01$ (**); $p < 0.001$ (***).

Coefficients	Factors	Estimate	Standard Error	t-value	p-value
β_0	Intercept	0.490	0.0172	28.570	8.93×10^{-6}***
β_1	(EDC:GSH)	0.0966	0.0210	4.593	0.0101*
β_2	pH	0.127	0.0210	6.023	0.00383**
β_3	Time	-0.0274	0.0210	-1.305	0.262
β_4	(EDC:GSH) x pH	-0.00162	0.0210	-0.077	0.942
β_5	(EDC:GSH) x Time	-0.00175	0.0210	-0.083	0.938
β_6	pH x Time	-0.0298	0.0210	-1.418	0.229
β_7	(EDC:GSH) x pH x Time	-0.00611	0.0210	-0.291	0.786
Residual Error (df = 4)		0.0595			
Multiple R-squared		0.939			
Adjusted R-squared (R^2)		0.831			
F-statistic (df = 7 & 4)		8.74			
p-value		0.0267*			

The model demonstrates an adequate fit (adjusted $R^2 = 0.831$). However, curvature tests done on the center points suggest the presence of curvature in the model (p-Center < 0.05, Supplementary Table 6), meaning that conclusions from response predictions using the model from equation 3 may be somewhat unreliable. However, theoretical evidence can be sufficient in supporting positive and significant effects of (EDC:GSH) molar ratio and pH on peptide linkage to alginate through amidation reactions. Finally, standard deviation on the center points (sd = 0.028) indicate low experimental variability which supports the replicability of the design. Finally, a Q-Q plot of this design (Supplementary Figure 2) seems to show similar trends as the first optimization attempt, proving the normal distribution of the data set.

4.5.1.2 Thiol group preservation normalized to GSH grafted

A three-way ANOVA analysis of results shows significant negative effects of (EDC:GSH) molar ratio ($p < 0.05$), pH ($p < 0.01$), as well as an interaction between these two factors ($p < 0.05$), on thiol group proportions relative to the GSH bound onto the alginate backbone (Supplementary Table 7, Figure 4.8). These results are in accordance with what was demonstrated previously (section 4.2) as higher EDC proportions and higher pH as well as both effects combined, make the reaction mixture more prone to side reactions while increasing the chance of thiol group deprotonation. These results are in accordance with what was demonstrated previously (section 4.2) as higher EDC proportions and higher pH as well as both effects combined, make the reaction mixture more prone to side reactions while increasing the chance of thiol group deprotonation.

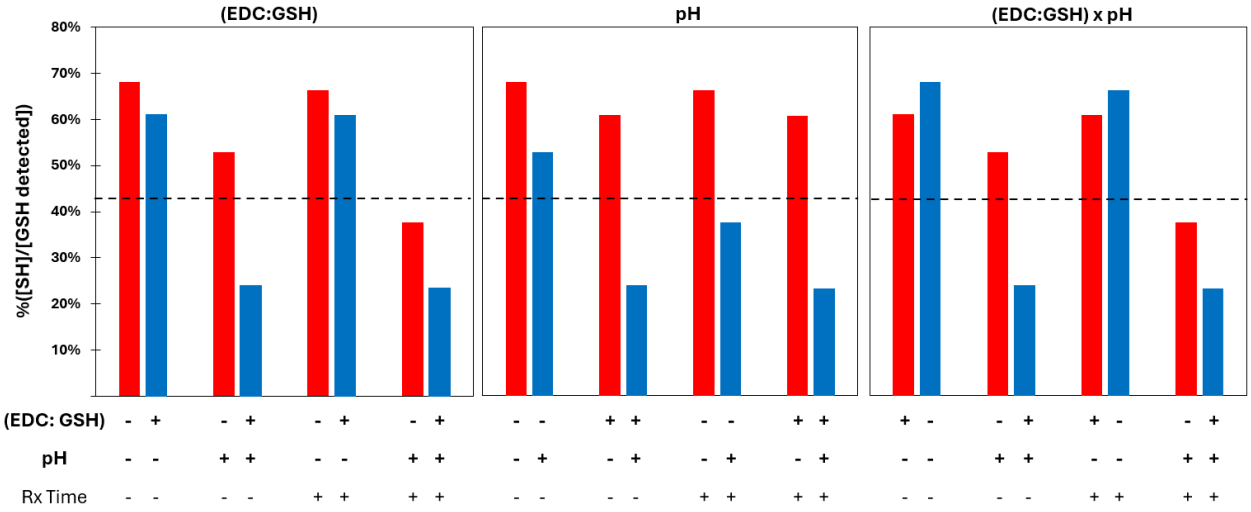

Figure 4. 8 - DOE #2 – Response plot showing the effect of (EDC:GSH) molar ratio, pH and (EDC:GSH) x pH on thiol group proportions ([-SH]/ [GSH grafted]). Thiol group proportions were calculated from GSH and thiol groups concentrations (mM) measured in 1% (w/v) alginate-GSH conjugate solutions. Positive (+) and negative (-) variations of the (EDC: GSH) molar ratio, pH and their interaction on [-SH]/ [GSH grafted] are represented in blue and red, respectively. The black dashed line represents the mean on the middle points (%([-SH]/ [GSH grafted]) = 43.4 ± 3.4%). All parameters of interest are shown in bolded characters.

The regression model (Figure 4.3) predicting the ratio of thiol group concentrations over the GSH concentration detected (grafted) in the sample in terms of (EDC:GSH) molar ratio ($p < 0.05$) and pH ($p < 0.01$) can be displayed using the equation below:

$$\left[\frac{[-SH](mM)}{[GSH\ grafted](mM)}\right] = 0.473 - 0.0696X_1 - 0.148X_2 \qquad \text{Equation 6}$$

However, the regression model analysis on this response suggests that the interaction between (EDC:GSH) molar ratio and pH ($p > 0.05$) shows an insignificant effect on thiol group proportions, meaning that this interaction alone has negligeable effect on the response. This is a frequent occurrence in design of experiment models, considering that it is a combined effect for two parameters, with multiple level testing with the presence of multicollinearity, where predictors can overlap in the variance they explain and can lead to inflation in the corresponding standard error. Nonetheless, the regression model displays an adjusted $R^2 = 0.860$ with a p-value on the center

Table 4. 3. Regression model results – DOE #2 – % ([SH active]/ [GSH grafted]) optimization using Ullah Shah and al.'s alginate functionalization method with GSH. Statistical significance levels are indicated as follows: $p < 0.05$ (*), $p < 0.01$ (**), $p < 0.001$ (***).

Coefficients	Factors	Estimate	Standard Error	t-value	p-value
β_0	Intercept	0.473	0.0163	29.042	8.37×10^{-6}***
β_1	(EDC:GSH)	-0.0696	0.0199	-3.491	0.0251*
β_2	pH	-0.148	0.0199	-7.425	0.00176**
β_3	Time	-0.0222	0.0199	-1.114	0.328
β_4	(EDC:GSH) x pH	-0.0384	0.0199	-1.923	0.127
β_5	(EDC:GSH) x Time	0.0202	0.0199	1.015	0.368
β_6	pH x Time	-0.0172	0.0199	-0.864	0.436
β_7	(EDC:GSH) x pH x Time	0.0161	0.0199	0.808	0.464
Residual Error (df = 4)		0.0564			
Multiple R-squared		0.949			
Adjusted R-squared (R^2)		0.860			
F-statistic (df = 7 & 4)		10.67			
p-value		0.0187*			

points above 0.05 (Supplementary Table 8), displaying an adequate linear fit with absence of curvature, respectively, supporting the plausibility of conclusions that can be drawn from this model. Finally, the standard deviation on the center points (sd = 0.0339) indicates low experimental variability and shows an adequate normal distribution (Supplementary Figure 3).

4.5.1.3 Thiol group preservation normalized to GSH added to reaction mixture

The same analysis as detailed in sections 4.5.1.1 and 4.5.1.2 was repeated for the proportions of free thiol groups measured in each sample over the amount of GSH added to achieve 10% functionalization of alginate monomers. Results from the three-way ANOVA test show that only the interaction between the (EDC:GSH) molar ratio and the pH has a significant and negative impact on free thiol group content ($p < 0.05$) (Supplementary Table 9, Figure 4.9).

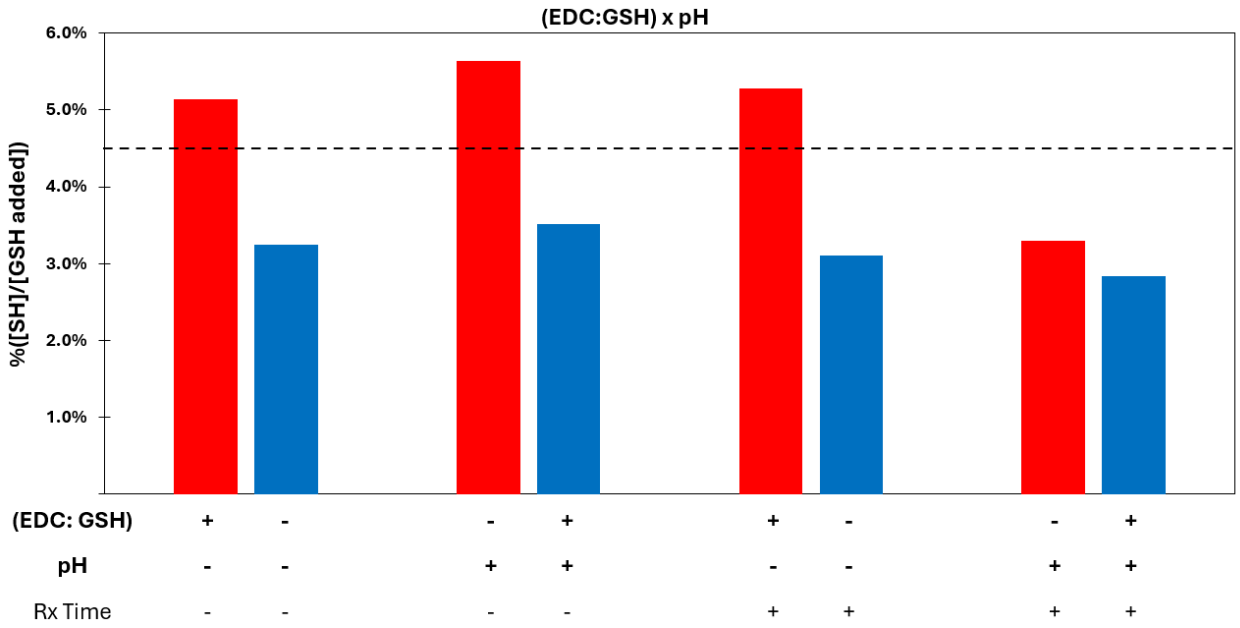

Figure 4. 9. DOE #2 – Response plot showing the effect of (EDC:GSH) x pH on thiol group proportions ([-SH]/ [GSH added]). Thiol group proportions were calculated from measured thiol groups and added GSH concentrations (mM) in 1% (w/v) alginate-GSH conjugate solutions. Positive (+) and negative (-) variations of the interaction between the (EDC: GSH) molar ratio and pH on [-SH]/ [GSH added] are represented in blue and red, respectively. The black dashed line represents the mean on the middle points (%([-SH]/ [GSH added]) = 4.50 ± 0.38%). All parameters of interest are shown in bolded characters.

In addition, the regression model analysis (Table 4.4) shows that only the coefficient corresponding to the combined effects resulted from (EDC:GSH) molar ratio and pH changes explain the variability in the results, and not the same parameters independently. This model is expressed such as:

$$\left[\frac{[-SH](mM)}{[GSH\ added](mM)}\right] = 0.0417 - 0.00831X_4 \qquad \text{Equation 7}$$

Table 4. 4. Regression model results – DOE #2 – %([SH active]/ [GSH added]) optimization using Ullah Shah and al.'s alginate functionalization method with GSH. Statistical significance levels are indicated as follows: $p < 0.05$ (*), $p < 0.01$ (**), $p < 0.001$ (***).

Coefficients	Factors	Estimate	Standard Error	t-value	p-value
β_0	Intercept	0.0417	0.00151	27.710	1.01×10^{-5}***
β_1	(EDC:GSH)	0.00184	0.00184	0.998	0.375
β_2	pH	-0.00186	0.00184	-1.011	0.369
β_3	Time	-0.00377	0.00184	-2.042	0.111
β_4	(EDC:GSH) x pH	-0.00831	0.00184	-4.506	0.0108*
β_5	(EDC:GSH) x Time	0.00243	0.00184	1.319	0.258
β_6	pH x Time	-0.00379	0.00184	-2.055	0.109
β_7	(EDC:GSH) x pH x Time	0.00172	0.00184	0.931	0.405
Residual Error (df = 4)		0.00522			
Multiple R-squared		0.893			
Adjusted R-squared (R^2)		0.705			
F-statistic (df = 7 & 4)		4.76			
p-value		0.0753			

This result was anticipated given the reaction's low efficiency bringing to light other parameters outside the reaction perimeter, such as the purification and drying process, and atmospheric conditions, on thiol group availability, rather than the effect from the parameters chosen for the design. This could be an explanation for the absence of effect from the (EDC:GSH) molar ratio and pH independently, but a perceivable effect once both are changed simultaneously. This fact can also be seen in the adjusted $R^2 = 0.705$ for this model, showing that approximately 30% of the model predictions are explained by variables that are outside of the design parameters. Finally, and consistent with most of the responses investigated, curvature tests and standard deviation on the center points (sd = 0.00380) suggest no apparent curvature in the model (p-Center > 0.05, Supplementary Table 10), as well as low experimental variability, which supports the model's

plausibility and replicability, respectively. Adequate normal distribution is also seen from Supplementary Figure 4.

4.5.2 2nd Design of experiment using Ullah Shah et al.'s methodology (DOE #3)

Knowing that the (EDC:GSH) molar ratio and the reaction pH have a positive effect on GSH grafting, but a negative effect on the preservation of free thiol groups, with the reaction time having no significant effect on any of those responses, it was decided to conduct a second design of experiment using a two-level and two parameters factorial design with four zero points for pure error quantification, to further refine our understanding of the observed effects. Here, we varied the (EDC:GSH) molar ratio at a higher range than in the first design of experiment to increase GSH grafting, while protecting free thiol groups from oxidation and potential side reactions, with the following values selected: +: (4: 1), 0: (3: 1), -: (2: 1). The pH however was varied at a lower range than in the first design of experiment to protect thiol groups from thiolate formation and the potential of any side reaction occurrence with the following values selected: +: 5.0, 0: 4.0, -:3.0. The reaction time was fixed at 2 hours, and the samples were subjected to the same measurements as in DOE #2. Supplementary Table 11 shows the response for each trial relative to this second attempt at optimization.

4.5.2.1 GSH grafting optimization

A three-way ANOVA test was conducted, looking specifically at the effects of the parameters on GSH concentrations in functionalized samples (Supplementary Figure 12). Results show no apparent effect of either (EDC:GSH) molar ratios or pH on GSH concentrations in functionalized samples ($p > 0.05$). However, the regression model analysis suggests a moderate positive individual contribution of (EDC:GSH) molar ratio on GSH grafting ($p < 0.05$, Table 4.5).

Table 4. 5. Regression model results – DOE #3 – GSH grafting optimization using Ullah Shah and al.'s alginate functionalization method with GSH. Statistical significance levels are indicated as follows: $p < 0.05$ (*), $p < 0.01$ (**), $p < 0.001$ (***).

Coefficients	Factors	Estimate	Standard Error	t-value	p-value
β_0	Intercept	0.371	0.0111	33.590	4.69×10^{-6}***
β_1	(EDC:GSH)	0.0675	0.0156	4.317	0.0125*
β_2	pH	0.0430	0.0156	2.751	0.0513
β_3	(EDC:GSH) x pH	0.0363	0.0156	2.319	0.0813
Residual Error (df = 4)		0.0313			
Multiple R-squared		0.888			
Adjusted R-squared (R^2)		0.803			
F-statistic (df = 3 & 4)		10.53			
p-value		0.0228*			

This result was expected as only low rates of amidation can occur at the range of pH chosen for this study, leading to the absence of effect from pH on GSH grafting and the observation of a positive effect from (EDC:GSH) alone on the response, with this same effect lost once this parameter is weighed on the response overall. This observation is supported by an adequate model fitting (adjusted $R^2 = 0.803$) with the absence of curvature ($p > 0.05$, Supplementary Table 13). Finally, the standard deviation on the center points (sd = 0.0348) suggest low experimental variability, which supports the model's replicability. A normal distribution of the data is also observed for this design (Supplementary Figure 5).

4.5.2.2 Thiol group preservation normalized to GSH grafted

The same analysis as above was conducted looking at the effect of (EDC:GSH) molar ratio and pH on free thiol content normalized to the GSH bound to alginate. Results show that parameter variability has no significant effect on this measure ($p > 0.05$, Supplementary Table 14). The same result is observed from the linear regression model analysis (Table 4.6).

Table 4. 6. Regression model results – DOE #3 – % ([SH active]/ [GSH grafted]) optimization using Ullah Shah and al.'s alginate functionalization method with GSH. Statistical significance levels are indicated as follows: $p < 0.05$ (*), $p < 0.01$ (**), $p < 0.001$ (***).

Coefficients	Factors	Estimate	Standard Error	t-value	p-value
β_0	Intercept	0.597	0.0249	23.975	$1.8x10^{-5}$***
β_1	(EDC:GSH)	-0.0972	0.0352	-2.757	0.051
β_2	pH	-0.0500	0.0352	-1.419	0.229
β_3	(EDC:GSH) x pH	-0.00864	0.0352	-0.245	0.818
Residual Error (df = 4)		0.0705			
Multiple R-squared		0.708			
Adjusted R-squared (R^2)		0.488			
F-statistic (df = 3 & 4)		3.23			
p-value		0.144			

These results are in accordance with what expectations as thiol groups should remain protonated in an acidic milieu (pH = 3 to 5). The pH range investigated is relatively far from the functional group's pKa that is between 8.6 to 9[104–107]. This could also explain the attenuated effect of (EDC:GSH) molar ratio from the reaction conditions. However, conclusions cannot be drawn from this model as per its inadequate fit (adjusted $R^2 = 0.488$; $p < 0.144$) showing that the parameters' variability cannot properly explain variations in the free thiol present in conjugates normalized to the GSH bound. Nonetheless, these results are still in accordance with what can be expected, considering that the parameter ranges chosen that do not properly encourage amidation reactions, and that the theoretical outcomes relative to the insignificant thiol group deprotonation from the GSH molecule when employing lower pH conditions. Somewhat adequate normality can be visualized in the Supplementary Figure 6.

4.5.2.3 Thiol group preservation normalized to GSH added to reaction mixture

Results from the three-way ANOVA (Supplementary Table 16) show a significant and positive effect from the (EDC:GSH) molar ratio alone and the interaction between (EDC:GSH) and pH on

the free thiol content of conjugates as normalized to the amount of GSH added at the start of the reaction. However, the regression model indicates that no parameter or interaction influence this measure. Particularly, the regression model displays a negative and small adjusted R-squared (R^2 = -0.0654), suggesting that the parameters at the level chosen tend to "over-fit" the model (Table 4.7).

Table 4. 7. Regression model results – DOE #3 – % ([SH active]/ [GSH added]) optimization using Ullah Shah and al.'s alginate functionalization method with GSH. Statistical significance levels are indicated as follows: $p < 0.05$ (*), $p < 0.01$ (**), $p < 0.001$ (***).

Coefficients	Factors	Estimate	Standard Error	t-value	p-value
β_0	Intercept	0.0421	0.00111	37.823	2.92×10^{-6}***
β_1	(EDC:GSH)	0.000664	0.00157	0.422	0.695
β_2	pH	0.000770	0.00157	0.489	0.650
β_3	(EDC:GSH) x pH	0.00231	0.00157	1.467	0.216
Residual Error (df = 4)		0.00315			
Multiple R-squared		0.391			
Adjusted R-squared (R^2)		-0.0654			
F-statistic (df = 3 & 4)		0.857			
p-value		0.5318			

It is possible that, under the conditions chosen for this second design of experiment, other factors associated with the purification and freeze drying steps, as well as ambient conditions (temperature and pressure), may play a bigger a role on thiol group retention in functionalized samples than the contribution of (EDC:GSH) and pH, that end up appearing as noise in the response. Despite these results, standard deviation on the mid-points is low compared to the mean (sd = 0.00133), showing low experimental variability, ensuring replicability of the experiment. Normality is also somewhat ensured from the Q-Q plot of the data (Supplementary Figure 7).

From all rounds of optimization, trial 4 in this last design of experiment (DOE #3) [(EDC:GSH) = (4:1), pH = 5.0, reaction time = 2 hours] was selected as the final optimized biomaterial as it showed higher ends of GSH and thiol content ([GSH] (mM) = 0.524, [-SH] (mM) = 0.247) in comparison to other trials. This material will be used for all further experiments discussed in this thesis.

4.6 Characterization of alginate-GSH conjugate

4.6.1 Quantitative characterization of GSH and free thiol content in conjugates

As a first step, we characterized the GSH and free thiol contents of conjugates produced according to our optimized synthesis conditions, compared to that in controls including alginate alone, alginate with EDC/NHS and alginate with GSH (blend). All controls were subjected to the exact same process required for the synthesis of conjugates. As shown in Figure 4.10, alginate-GSH conjugates contained an average peptide concentration of $0.585\ mM$, in contrast with the alginate and GSH blend which contained an average peptide concentration of $0.320\ mM$. This difference was statistically significant ($p < 0.001$) and indicated that a higher GSH retention is observed in the conjugate after purification in comparison to the blend, suggesting GSH grafting to the alginate backbone. Furthermore, the purification efficiency of the functionalization process, meaning the amount of free GSH removed from the sample using dialysis normalized to the amount added in the reaction mixture, calculated the same way as in section 4.4, in the conditions chosen, is in

average equal to $95.3 \pm 1.1\%$, similar to the one obtained from reproducing the exact functionalization method of Ullah Shah and al.'s ($96.2 \pm 0.5\%$).

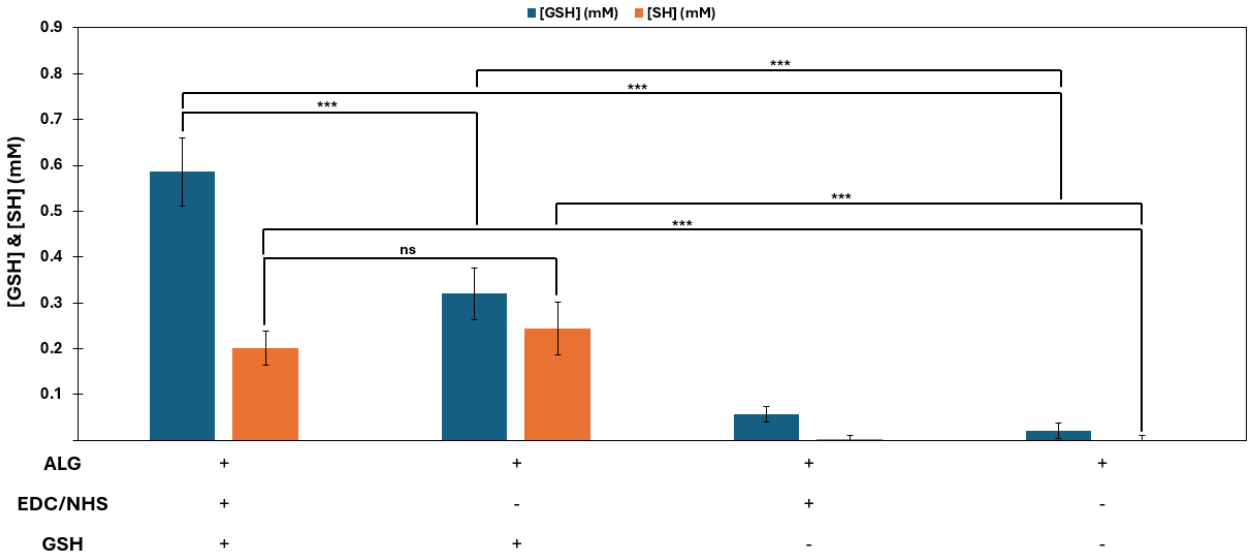

Figure 4. 10. Quantitative analysis of GSH and free thiol group concentrations in alginate-GSH conjugates. Concentrations of GSH (dark teal) and thiol groups (mM) (orange) in 1% (w/v) alginate-GSH conjugate solutions were quantified using the BCA assay and Ellman's assay, respectively. (+) and (-) indicate addition or omission of the components. Error bars represent the standard deviation on the mean. Statistical significance levels are indicated as follows: $p < 0.05$ (*), $p < 0.01$ (**), $p < 0.001$ (***).

However, even with this high and maintained purification efficiency, there is still a non-negligeable amount of GSH that was measured in the blend in comparison to the alginate-GSH conjugate, to which, a change in the purification parameter (i.e.: increased time) might represent a double edge sword. Indeed, an increased purification duration could lead to higher amounts of GSH removed, but at the cost of free thiols loss, leading to lower ROS scavenging capabilities by the conjugate.

Furthermore, the functionalization efficiency for this process is lower ($\eta_{FUNC\ 10\%} = 5.15 \pm 1.03\%$), in comparison to the intact Ullah Shah's methodology ($\eta_{FUNC+NHS} = 11.3 \pm 1.1\%$), probably due to higher GSH quantities employed for reaction (16.28 mM in Ullah Shah's protocol

compared to 5.15 mM added the optimized procedure developed in this study), targeting a higher monomer amount for conjugation reactions. In addition, the slightly higher pH utilized in the Ullah Shah method (pH = 6.0) as opposed to the one employed in this optimized procedure (pH = 5.0) could encourage higher amidation reaction occurrences.

The free thiol concentrations of the conjugate and blend were statistically comparable, such that a larger GSH proportion found in the blend remained in reduced form, allowing for higher free thiol presentation, in comparison to that observed in the conjugate. As was demonstrated with the incubation of GSH in solution (section 4.2), an interaction between EDC molecules and the GSH sulfhydryl groups is suspected, which could contribute to the observed decrease in the percentage of GSH presenting free thiol group in the conjugates. This also brings to light that the comparable levels of thiol groups between the alginate-GSH conjugate and the blend is the result of the low functionalization efficiency achieved using the optimal synthesis conditions, instead of a purification issue. Nevertheless, the conjugate is still able to provide adequate free thiol group retention representing $34.5 \pm 4.2\%$ of the GSH presumably bound to the alginate, and substantially higher than the level reported in the study by Ullah Shah et al. $(20.1 \pm 4.1\%)$. This justifies the interest in continuing with the optimized set of conditions for further experiments.

4.6.2 ^{1}H-NMR

Once GSH and -SH concentrations have been measured in alginate-GSH conjugates, it was necessary to confirm bonding of GSH onto the alginate backbone through the formation of an amide bond between the GSH's primary amine present on its main chain, and the -COOH groups present on the β-D-mannuronic acid (M) and α-L-guluronic acid (G) monomers forming the alginate backbone. To achieve this objective, 10% functionalized alginate (FUNC 10%), with two negative controls of reaction (blend with alginate and GSH [ALG + GSH] and alginate alone

[ALG]) and pure GSH, were dissolved in deuterium oxide (D_2O) at a concentration of 2% (w/v) and subjected to proton nuclear magnetic resonance spectroscopy (^{1}H-NMR, Figure 4.11).

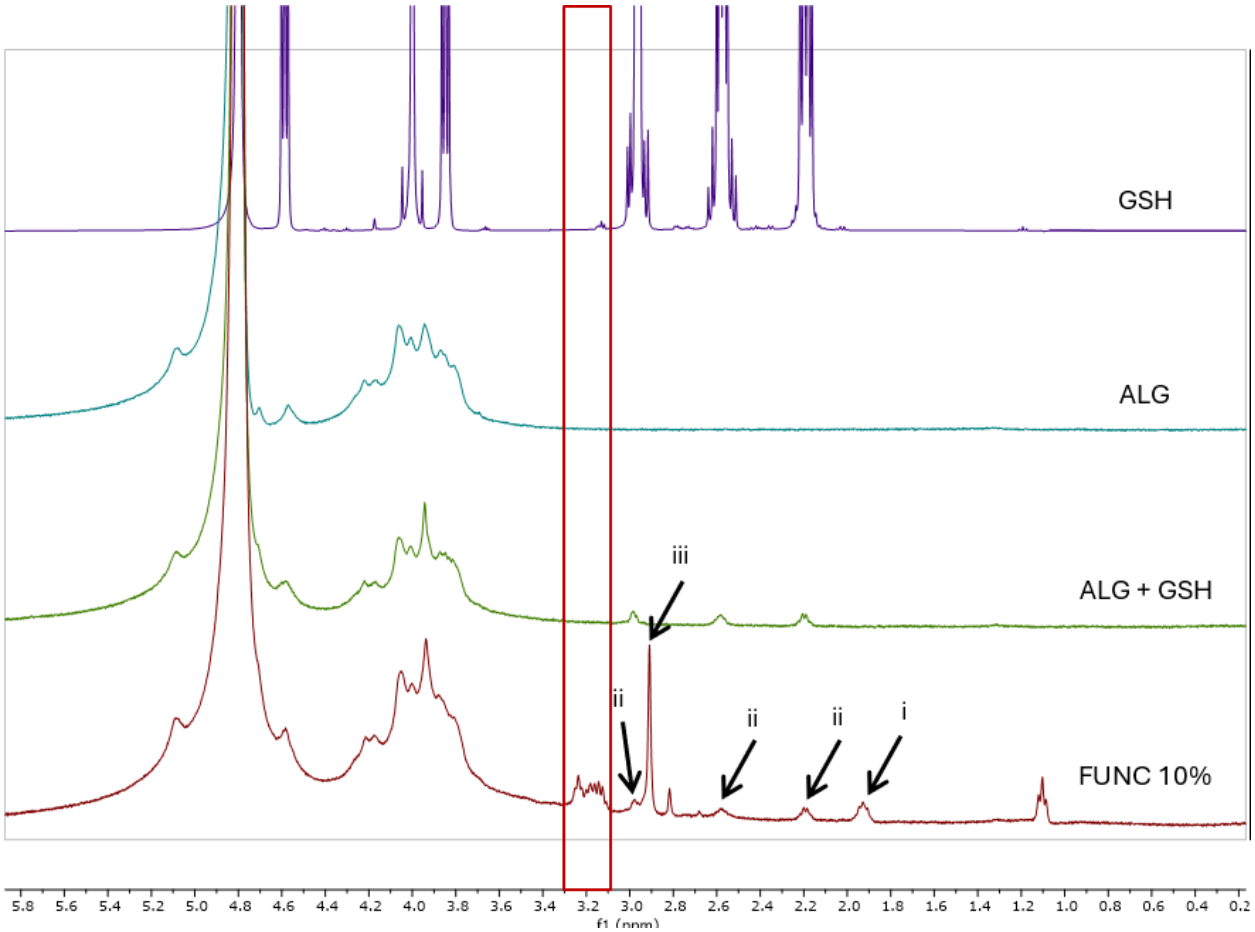

Figure 4. 11. ^{1}H-NMR of alginate-GSH conjugates in comparison with a blend of alginate and GSH, alginate alone and pure GSH. ^{1}H-NMR spectrums of functionalized alginate (FUNC 10%) as well as the relevant negative controls: alginate blend with GSH (ALG + GSH), and alginate alone (ALG) as well as pure glutathione (GSH). Peaks: (i) 1.93 ppm: polymer-bound Glu side-chain CH_2 from GSH; (ii) 2.19 ppm: Glu-βCH_2; 2.58 ppm: Glu-ϒCH_2; and 2.96 ppm: Cys β-CH_2; (iii) 2.9 ppm: free GSH or EDC traces. The red boxed area highlights GSH CH/CH_2 protons in a new environment, suggesting amide linkage of GSH to alginate.

The alginate-GSH, in comparison with the blend and alginate alone, show unique broad signals: one at 1.93 ppm (i) that could represent the polymer-bound Glu side-chain CH_2 of GSH; and another between 3.1 and 3.3 ppm (red boxed region), that shows the CH/CH_2 protons of GSH in a

new environment created by covalent attachment, most likely through an amide linkage of the peptide onto the alginate backbone. Equivalent patterns were observed in alginate functionalized with the peptides RGD and PDEA through EDC/NHS chemistry resulting in amide bond formation [108],[90]. Furthermore, characteristic peaks of glutathione (GSH)[109,110] are present in alginate-GSH and in the blend (ii): the glutamate side chain (Glu-βCH_2, peak around 2.19 ppm), the two methylene protons located on the gamma carbon of the Glutamate (Glu-ϒCH_2, peak around 2.58 ppm) and the Cys β-CH_2 (peak around 2.96 ppm). The α-CH and Gly CH_2 peaks between 3.6 and 4.6 ppm are overlapping with peaks the ring protons of β-D-mannuronic (M) and α-L-guluronic (G) units present in alginate. Of note, a sharp peak (iii) appears at 2.9 ppm. This observation may indicate several outcomes. The first one is the presence of free GSH within the conjugate, most likely due to residual unbound GSH remaining after purification, as suggested by the sharpness of the signal and its proximity to the characteristic Cys β-CH_2 peak at 2.96 ppm. However, this peak is absent in the blend. One explanation is that the alginate-GSH mixture contains reaction by-products, altered ionic strength, and distinct microenvironments arising from the addition of EDC/NHS, which may promote interactions between free GSH and the modified polymer or lead to the formation of micro-aggregates[111]. Such interactions could also account for the more difficult removal of GSH from the functionalized sample compared with the blend, particularly when using cellulose-membrane dialysis, which relies solely on concentration gradients for purification. A second likeliest explanation is the presence of remaining O-acylisourea traces, formed through the covalent interaction of EDC with alginate -COOH groups[112]. However, more testing is required to confirm this result, notably through the addition of one more spectrum of the alginate blend with EDC/NHS subjected to the same conditions of synthesis and purification as the conjugate. Nonetheless, these results seem to suggest that GSH is found in the conjugate, with a proportion of it at least bound to the alginate backbone.

4.6.3 Evaluation of the retention of GSH and free thiols in alginate hydrogels

To better support ^{1}H-NMR results, another quantitative experiment was conducted to evaluate if the presence of GSH and free thiols was maintained in conjugates following ionic crosslinking. This was done in direct comparison to all relevant controls. Because the buffers used for the quantification assays contain chelating agents (carbonate in BCA assay buffer and sodium phosphate in the Ellman's assay buffer), hydrogels dissolve in solution, allowing quantification. Crosslinking the alginate provides an opportunity for the free GSH from all samples to be released through diffusion and be washed off before quantification. As such, the majority of the GSH remaining in the functionalized sample should correspond to the ones attached to the alginate backbone, as secondary proof of conjugation. Results of GSH and thiol group concentration (mM) quantification following this procedure is shown in Figure 4.12. A significant difference in GSH proportions in the alginate-GSH conjugate as opposed to the blend between alginate and GSH is present after one crosslinking & degradation cycle, indicating that the amount retained in the conjugate must be mostly attached. Furthermore, peptide levels measured in the blend sample are comparable to those measured for the alginate alone representing background signal, suggesting that one hydrogel crosslinking cycle is sufficient in removing most of the unattached GSH from a sample. It is also important to mention that a substantial portion of the initial GSH content from the alginate-GSH conjugate exited the sample through this attempt (approximately half of the total amount), meaning that the functionalization efficiency calculated above might have been an over estimation of the actual bounded amount of GSH onto the alginate backbone.

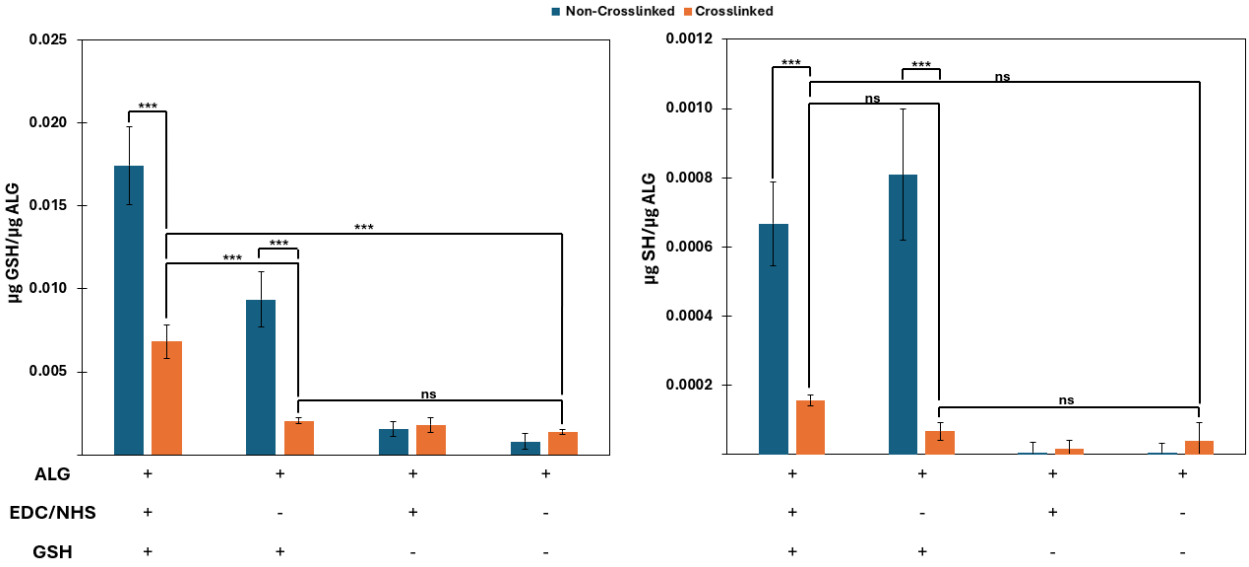

Figure 4. 12. Confirmation of GSH bonding to the alginate backbone through quantitative analysis of alginate conjugates before crosslinking and post-degradation. GSH (dark teal) & thiol group (orange) content (µg/µg alginate) in each sample and all other negative controls of reaction were measured using the BCA and Ellman's assay, respectively. (+) and (-) indicate addition or omission of the components. Error bars represent the standard deviation on the mean. Statistical significance levels are indicated as follows: $p < 0.05$ (*), $p < 0.01$ (**), $p < 0.001$ (***).

Nonetheless, the trends from this experiment accompany the ^{1}H-NMR results successfully, proving attachment of the peptide onto the alginate backbone. In relation to free thiol group content, the alginate-GSH conjugate, the blend as well as the alginate alone post-crosslinking and degradation, seem to exhibit similar concentrations as indicated by the lack of statistically significant differences between their means (alginate-GSH vs blend, p-value = 0.463; alginate-GSH vs alginate alone, p-value = 0.147; blend vs alginate alone, p-value = 0.998). This contrasts with the non-crosslinked samples, in which both the conjugate and the blend displayed significantly higher thiol group levels relative to alginate alone (section 4.6.1). These findings suggest that, once crosslinked, the presentation of thiol groups available for scavenging on the alginate-GSH conjugate becomes minimal. This outcome is expected, as a substantial portion of GSH is lost during crosslinking, reducing the number of free thiols in a nearly proportional manner between crosslinked and non-crosslinked conjugates, resulting in levels comparable to the ones of reaction negative controls.

4.7 Scavenging capability of alginate-GSH conjugate

Next, it was of interest to measure the scavenging ability of the alginate-GSH conjugates in solution. This attempt was done to confirm that alginate-GSH conjugates can reduce ROS levels in solution, a sign indicating their potential capacity to revert induced oxidative stress in biological conditions. To achieve this objective, the biomaterials, in solution and in the form of crosslinked hydrogels, were tested for their ability to scavenge H_2O_2 and DPPH, respectively.

4.7.1 Scavenging capability of Hydrogen Peroxide (H_2O_2) – non-crosslinked biomaterials

Results from the scavenging of H_2O_2 from intact alginate-GSH conjugates show H_2O_2 removal of nearly 50%, which is not significantly different from the alginate blend with GSH, that show scavenging rates of almost 60% ($p > 0.05$, Figure 4.13).

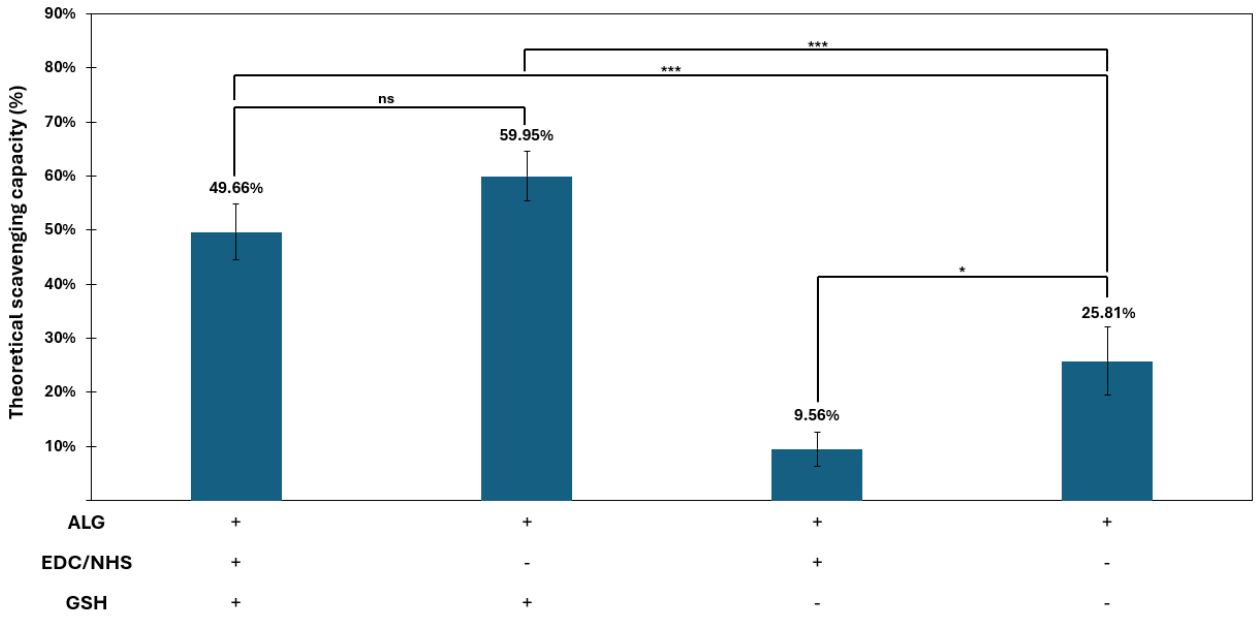

Figure 4. 13. Scavenging efficiency of H_2O_2 of non-crosslinked optimized functionalized alginate. Functionalized alginate with GSH and all negative reaction controls (blend, alginate blended with EDC/NHS and alginate alone) were dissolved with H_2O_2 (4%(w/v) alginate and 500 µM H_2O_2) and left for scavenging for 24 hours at room temperature in a light deprived environment. The scavenging capacity was calculated using Equation 2. (+) and (-) indicate addition or omission of the components. Error bars represent the standard deviation on the mean. Statistical significance levels are indicated as follows: $p < 0.05$ (*), $p < 0.01$ (**), $p < 0.001$ (***).

This result is in accordance with our quantification of free thiol contents, as free thiol group concentrations in both the alginate-GSH conjugate and blend samples showed similar trends, with slightly higher thiol group concentrations measured in blend after purification, which explains its higher scavenging capacity in comparison to alginate-GSH (section 4.6.1). Both samples showed significantly higher scavenging of H_2O_2 in comparison to the alginate alone intrinsic antioxidant capabilities[113] , with a H_2O_2 removal from the solution of nearly 26%. This proves the GSH's thiol group contribution to the removal of H_2O_2 in solution, while also showing that half this contribution is due to the alginate alone, through the action of its -OH and -COOH functional groups on its backbone[114]. Interestingly, a significant decrease in the scavenging capacity of the alginate blended with EDC/NHS in comparison to the alginate alone was quantified. This can be explained by the fact that coupling agent impurities could still be present in the alginate blended with EDC/NHS sample, mediating interactions with the -COOH functional groups on the alginate backbone and suppressing slightly its antioxidant activity. Nonetheless, alginate-GSH seems able to effectively remove H_2O_2 from aqueous mediums when dissolved as is in solution.

4.7.2 Crosslinked biomaterials - Scavenging capability of DPPH

The same experiment as before has been repeated using crosslinked functionalized alginate beads mixed and incubated the same way for two hours in 100 µM DPPH solutions, where absorbance for left over DPPH has been measured in all relevant samples. Results of the scavenging capacities of DPPH from functionalized alginate samples accompanied with all negative reaction controls are plotted in Figure 4.14.

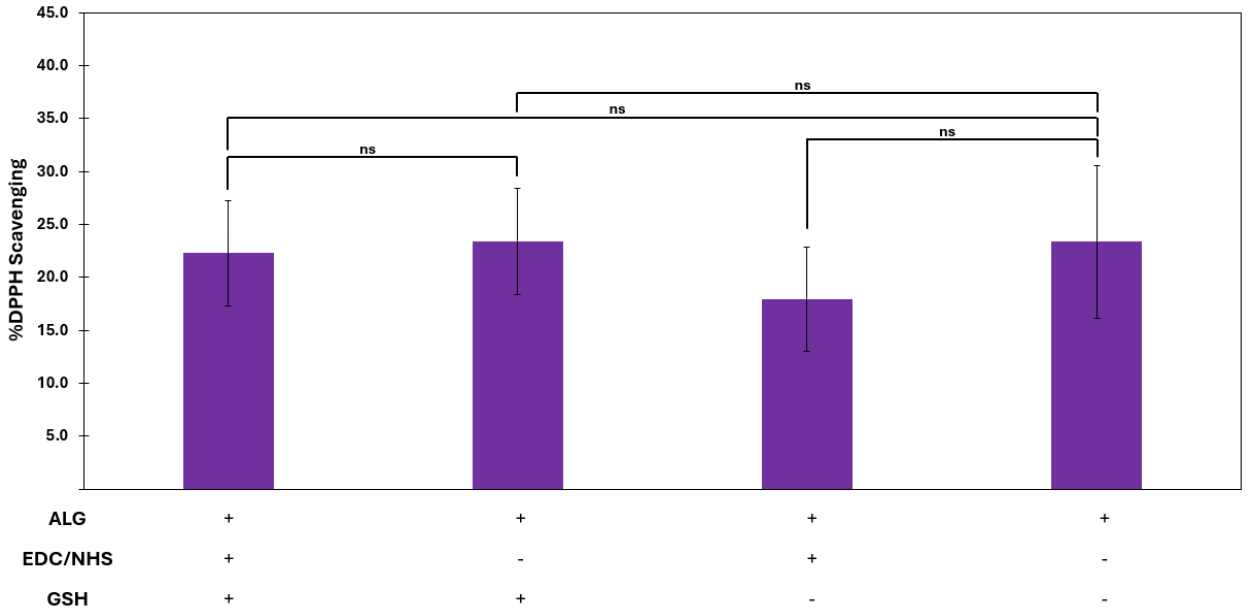

Figure 4. 14. DPPH scavenging capacities of crosslinked optimized functionalized alginate. Functionalized alginate with GSH and all negative reaction controls (blend, alginate blended with EDC/NHS and alginate alone) were ionically crosslinked and dissolved in 750 µL of 100 µM DPPH and left for scavenging for 2 hours at room temperature in a light deprived environment. Remaining DPPH proportions were quantified using a DPPH assay. The scavenging capacity was calculated using Equation 3. (+) and (-) indicate addition or omission of the components. Error bars representing the standard deviation on the mean. Statistical significance levels are indicated as follows: $p < 0.05$ (*), $p < 0.01$ (**), $p < 0.001$ (***).

Results show no apparent significant changes in scavenging contributions from the functionalized sample, in comparison to all other negative controls of reaction. This effect is logical considering the low levels of free thiol groups detected in the samples post-crosslinking like demonstrated previously (*section 4.6.3.*). In addition, the most prevalent effect on scavenging capacity would be the functionalization efficiency, lowered even more as free GSH contained in the functionalized sample left the microbead after crosslinking and washing. Finally, it could be logical to say that the DPPH molecule is unable to reach bounded GSH molecules for scavenging as per the tight network formed once the biomaterial is crosslinked, especially considering the much high DPPH molar mass (394.32 g/mol) making the molecule bulky.

From these results, it can be concluded that scavenging capability of the biomaterials is substantially decreased once the biomaterial is crosslinked, possibly because of compromised

permeability and swelling provided the tight network formed through Ca^{2+} and -COO- interactions, but mainly because of the low level of antioxidant activity conferred by the crosslinked alginate-GSH conjugate, making this test insensitive for scavenging capacity detections of the samples.

4.8 H_2O_2 exposition on cells – cytotoxicity study

In parallel to conjugate characterization, and to prepare for in vitro tests of the antioxidant potential of the conjugate in the form of a hydrogel, in the presence of fibroblasts (skin cells) in an induced oxidative stress environment, it was of interest to conduct a cytotoxicity test to identify an "optimal H_2O_2 concentration" for such experiments, one that induces stress in the cells leading to some cell death but leaving some cells viable, allowing for oxidative stress reversibility from the action of the biomaterial. In other words, we were looking into finding the IC_{50}, a concentration of H_2O_2 able to reduce by 50% the metabolic activity of fibroblast cultures. This concentration would then be used for further experiments and help determine the required amount of biomaterial to include in culture conditions to observe removal of H_2O_2 from the medium and ensure the cells' protection. To do so, NIH3T3 cells (mouse embryonic fibroblasts) were exposed to multiple H_2O_2 concentrations for 24 hours, after which their metabolic activity was measured using the alamarBlue assay. The dose response curve, indicating the relative viability of fibroblast cells in terms of the H_2O_2 concentration (μM) they are exposed to is shown in Figure 4.13.

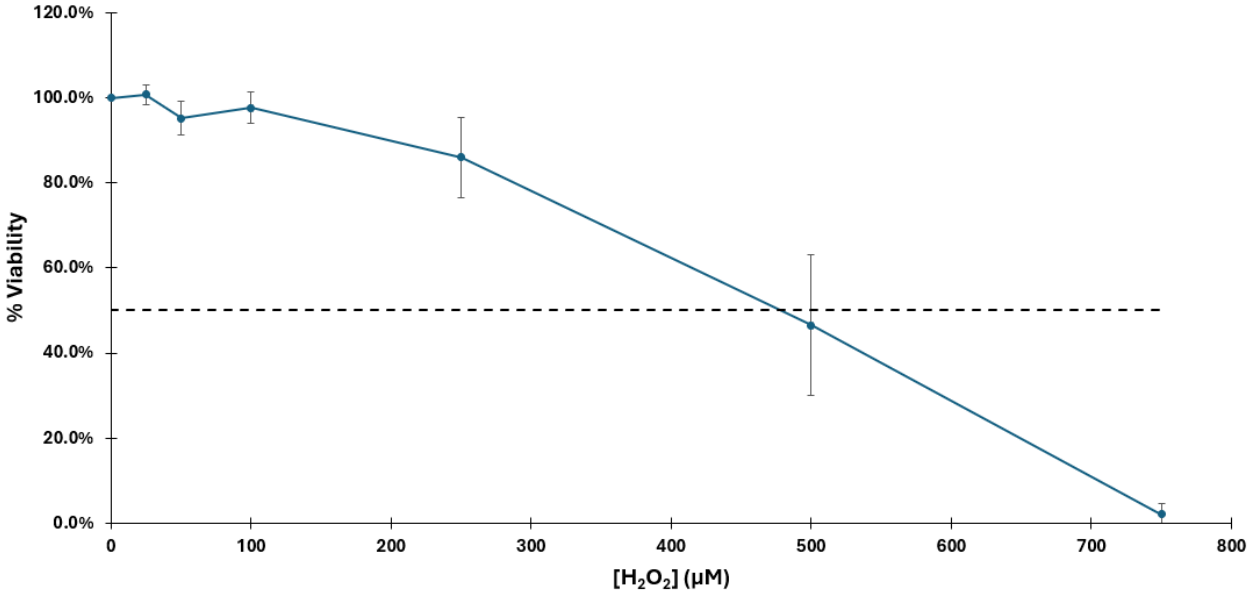

Figure 4. 15. Dose response curve of H_2O_2 on NIH3T3 cells. NIH3T3 cells were exposed to various [H_2O_2] (µM): 0, 25, 50, 100, 250, 500 and 750, for 24 hours in a cell-culture incubator (37°C, 5% CO_2, 95% humidity). Metabolic activity of cells was measured using the alamarBlue assay. Relative cell viability to the control sample (0 µM) for all culture samples was calculated such as: $\left(\frac{[F]_{sample}-[F]_{Blank}}{[F]_{Control}}\right) \times 100\%$, with error bars representing the standard deviation on their mean. The black dashed line delimits the IC_{50} cytotoxic dose.

Results show an IC_{50} around 500 µM, where 50% of cell viability is observed (black dashed line, Figure 4.13). It is complex to compare this value with theoretical outcomes, as a good number of factors such as cell density, cell line, medium composition and cell passaging can come at play influencing cell metabolic activity results. However, a publication reported that cell viability, measured with the MTT assay, decreased to 40% when exposing NIH3T3 cells to [H_2O_2] = 300 µM (incubation conditions: 3 500 cells/well in a 96 well plate, 24 hours at 37°C and 5% CO_2)[115]. The IC_{50} obtained is higher than this reported value, but it is justifiable considering the cell density used for this experiment of 60 000 cells/ml, and the high passaging number employed (between 44 and 50) that can contribute to the overall increase of the cells' metabolic activity [116], requiring a higher [H_2O_2] to observe an effect on cells' integrity. Nonetheless, this finding helps us establish

the required concentration of free thiols in solution that should be present to revert H_2O_2 effects, respecting scavenging stoichiometry of (GSH:ROS) = (2:1), which is of [-SH] = 1mM.

CHAPTER 5: CONCLUSIONS & FUTURE WORK

5.1. Conclusions

In this thesis, a GSH-alginate conjugate was successfully synthesized by carbodiimide chemistry, as confirmed with ^{1}H-NMR. Quantitative assays performed on the conjugates both as synthesized and after ionic crosslinking into hydrogels also confirm this functionalization. However, the free thiol content of the conjugates remains low despite numerous attempts to overcome this issue. Indeed, this work also highlighted the negative impact of several factors pertaining to carbodiimide chemistry on free thiol availability, such as near neutral pH, MES-based buffers, GSH–EDC interactions, and long reaction and purification times in aqueous environments, the same conditions that promoted higher amidation rates and increased peptide grafting efficiency. Attempts to preserve thiol groups, including slower peptide addition or post-functionalization treatment with TCEP of alginate-GSH and alginate-GSSG, were unsuccessful. This led to the use of a new functionalization procedure inspired by the work of Ullah Shah et al., which provided conditions protective of thiol groups and was reliably reproduced in-house. Seeking conditions that improve binding efficiency while maintaining thiol integrity, two two-level factorial experimental designs were conducted. These showed that increasing the (EDC:GSH) molar ratio, increasing pH, and the interaction between these factors enhanced GSH binding while decreasing thiol proportions, whereas reaction time showed no measurable effect. Scavenging experiments with H_2O_2 showed nearly 50% removal when the alginate-GSH conjugate was tested as synthesized, while this capacity was lost after ionic crosslinking, as confirmed in DPPH assays. Taken together, these results to characterize the synthesized alginate-GSH conjugates highlight the fact that the free thiol content of the conjugates and consequently the antioxidant activity of the material remain too low

for applications as biomaterials at this time; however, further avenues remain for the development of such materials in the group.

5.2. Future Work

After all rounds of optimization, the final conjugate, exhibiting highest GSH and free thiol contents, still showed quite low functionalization efficiency (5.15%, non-crosslinked) with 4.79% of thiol group preservation normalized to the GSH added prior to reaction. This result is an overestimation of the actual functionalization efficiency and thiol group availability present on the conjugate considering the quantitative analyses done on crosslinked and degraded alginate-GSH materials. Taking that extensive optimization has already been done on the current EDC/NHS chemistry employed for conjugation, where it is evident that a trade-off is present between grafting and thiol group integrity, it might be interesting to employ other conjugation chemistries able to ensure binding without compromising the activity of alginate-GSH materials. The use of 4-(4,6-dimethoxy-1,3,5-triazin-2-yl)-4-methylmorpholinium chloride (DMTMM) for amidation reactions as a replacement for EDC could be one avenue to improve binding efficiency while providing less of a reactive environment for thiolates to react in water[89]. Other click chemistries, such as Strain-Promoted Alkyne-Azide Cycloaddition (SPAAC) or Inverse Electron-Demand Diels-Alder reaction (IEDDA) could be useful to ensure conjugation while still avoiding the use of toxic metals, ensuring that the conjugates could be applied for biomedical applications such as wound healing. Finally, protecting thiol groups on GSH while using compounds such as acetamidomethyl (Acm), S-pyridyl, or S-thiazolidine, could also be done combined with the chemistries named previously, to widen the possibility for high binding efficiency and conjugate activity. However, conjugates must be properly purified from these compounds to prevent cytotoxic responses during cell work.

Once an enhanced synthesis strategy is identified and optimized, the next step would be to focus on ameliorating the purification to prevent thiol group losses from the alginate-GSH conjugate. Although purification rates achieved from our efforts based on the Ullah Shah procedures were between 95-96%, most assay results from peptide and thiol groups quantification to scavenging, as well as ^{1}H-NMR results, showed consistently that some free GSH was still present in the conjugates. Precipitation with ethanol 95% of freshly synthesized materials using the intact Ullah Shah and al.'s protocol has been attempted, but with no apparent purification enhancement from free GSH molecules in the gels. It could be worth employing a larger dialysate volume (1 L instead of 500 ml) and decrease the amount of material synthesized at a time (80 mg to 50 mg), achieving a dialysate to sample ratio of 20:1 instead of 6.25:1. Adding constant agitation could also aid GSH and impurities' diffusion out of the samples, as it could disturb their interactions with the alginate backbone, a possible cause of GSH impurities retention in alginate-conjugates.

The scavenging capability of the biomaterials once crosslinked into a hydrogel is another area of refinement. It could be of interest to explore other forms of the biomaterial, such as different shapes that ameliorate surface to volume contact with cells and diffusion, such as hydrogel sheets, imitating the application of a topical cream on a skin wound. Tuning the buffer environment in which the hydrogel is placed could also be an area of interest, considering the slight improvement seen on a past experiment involving the use of 4% (m/v) crosslinked beads and their incubation in PBS 1X that showed slightly improved activity of the functionalized gels, a study that could be worth repeating to confirm buffering effects on crosslinked alginate-conjugates activity. Modifying crosslinking density through lowering $CaCl_2$ bath concentration and crosslinking incubation times (from 30-40 minutes to a few minutes), could encourage a decrease in crosslinking network density, promoting diffusion and thiol release, potentially restoring the scavenging capabilities of the gels.

Finally, a recent study by Yubin et al. (2026), which functionalized alginate with alginate oligosaccharides prior to antimicrobial peptide conjugation, reported enhanced antibacterial activity in gels incorporating the oligosaccharides compared with those that did not. This approach represents an additional strategy for improving overall gel performance[117].

The addition of further characterization of the conjugates, specifically swelling and permeability tests can be important to ensure the biomaterials' capacity to retain water and wound exudates and to provide a moist environment for wound epithelialization, while confirming its capacity to reduce oxidative stress at a wound surface where ROSs can diffuse into the material for scavenging, respectively.

Finally, it could also be of interest to use other antioxidant peptides or molecules for conjugation or even blending with alginate hydrogels, with a focus on those that have a mechanism of action independent from thiol groups to ensure their antioxidant activity. Some studies have identified alternative antioxidant peptides extracted from food derivatives that contain residues such as Histidine, Tyrosine, Tryptophan, Proline, among other hydrophobic residues, whereby their activity relies on their sequence and structure rather than on one functional group[118,119]. Other non-peptidic alternatives can be used, such as phenolic acids, flavonoids, ascorbic acid derivatives, or metal-chelating molecules[120].

REFERENCES

[1] H. Yousef, M. Alhajj, A. O. Fakoya, S. Sharma, "Anatomy, Skin (Integument), Epidermis," *StatPearls*, StatPearls Publishing, Treasure Island (FL) **2025**.

[2] A. Prohic, "Skin Structure and Functions of the Skin," *Dermatovenerology Textbook*, A. Prohic, Ed., Springer Nature Switzerland, Cham **2024**, p. 3.

[3] D. D. Bikle, Z. Xie, C.-L. Tu, *Expert Review of Endocrinology & Metabolism* **2012**, *7*, 461.

[4] D. D. Bikle, M. K. Nemanic, E. Gee, P. Elias, *J Clin Invest* **1986**, *78*, 557.

[5] B. Lehmann, W. Sauter, P. Knuschke, S. Dressler, M. Meurer, *Arch Dermatol Res* **2003**, *295*, 24.

[6] D. D. Bikle, M. K. Nemanic, J. O. Whitney, P. W. Elias, *Biochemistry* **1986**, *25*, 1545.

[7] M. Cichorek, M. Wachulska, A. Stasiewicz, A. Tymińska, *Postepy Dermatol Alergol* **2013**, *30*, 30.

[8] S. Jaitley, T. Saraswathi, *J Oral Maxillofac Pathol* **2012**, *16*, 239.

[9] "Langerhans Cell - an overview | ScienceDirect Topics," accessed on May 5, 2026, https://www.sciencedirect.com/topics/veterinary-science-and-veterinary-medicine/langerhans-cell.

[10] J. Abraham, S. Mathew, *Int J Appl Basic Med Res* **2019**, *9*, 9.

[11] T. Numata, K. Harada, S. Nakae, *Front Immunol* **2022**, *13*, 923495.

[12] S. L. Sim, S. Kumari, S. Kaur, K. Khosrotehrani, *Biomolecules* **2022**, *12*, 1659.

[13] T. M. Brown, K. Krishnamurthy, "Histology, Dermis," *StatPearls*, StatPearls Publishing, Treasure Island (FL) **2026**.

[14] J. W. Streilein, *J Invest Dermatol* **1983**, *80 Suppl*, 12s.

[15] A. Herman, A. P. Herman, *Skin Research and Technology* **2019**, *25*, 111.

[16] "Integumentary System: What It Is, Function & Organs," *Cleveland Clinic*, accessed on May 5, 2026, https://my.clevelandclinic.org/health/body/22827-integumentary-system.

[17] P. M. Elias, *J Invest Dermatol* **2012**, *132*, 2131.

[18] "Office of Dietary Supplements - Vitamin D," accessed on May 5, 2026, https://ods.od.nih.gov/factsheets/VitaminD-HealthProfessional/.

[19] S. C. Freeman, A. Malik, H. Basit, "Physiology, Exocrine Gland," *StatPearls*, StatPearls Publishing, Treasure Island (FL) **2026**.

[20] W. Lopez-Ojeda, A. Pandey, M. Alhajj, A. M. Oakley, "Anatomy, Skin (Integument)," *StatPearls*, StatPearls Publishing, Treasure Island (FL) **2026**.

[21] "Causes of Wounds," accessed on May 6, 2026, http://www.woundcarecenters.org/article/wound-basics/causes-of-wounds.

[22] "Acute & Chronic Wounds : Current Management Concepts," accessed on May 6, 2026, https://elsevier-elibrary.com/contents/fullcontent/15185585/epubcontent_v2/OEBPS/xhtml/CHP0004.xhtml?utm_source=copilot.com.

[23] H. A. Wallace, B. M. Basehore, P. M. Zito, "Wound Healing Phases," *StatPearls*, StatPearls Publishing, Treasure Island (FL) **2026**.

[24] K. Raziyeva, Y. Kim, Z. Zharkinbekov, K. Kassymbek, S. Jimi, A. Saparov, *Biomolecules* **2021**, *11*, 700.

[25] M. Hunt, M. Torres, E. Bachar-Wikstrom, J. D. Wikstrom, *Commun Biol* **2024**, *7*, 1534.

[26] G. S. Schultz, G. A. Chin, L. Moldawer, R. F. Diegelmann, "Principles of Wound Healing," *Mechanisms of Vascular Disease: A Reference Book for Vascular Specialists*, R. Fitridge, M. Thompson, Eds., University of Adelaide Press, Adelaide (AU) **2011**.

[27] Y. H. Almadani, J. Vorstenbosch, P. G. Davison, A. M. Murphy, *Semin Plast Surg* **2021**, *35*, 141.

[28] S. Zhu, Y. Yu, Y. Ren, L. Xu, H. Wang, X. Ling, L. Jin, Y. Hu, H. Zhang, C. Miao, K. Guo, *Cell Death Dis* **2021**, *12*, 984.

[29] "Vasoactive Mediator - an overview | ScienceDirect Topics," accessed on May 18, 2026, https://www.sciencedirect.com/topics/immunology-and-microbiology/vasoactive-mediator.

[30] K. Ukaegbu, E. Allen, K. K. H. Svoboda, *Int Wound J* **2025**, *22*, e70330.

[31] R. J. Bodnar, *Adv Wound Care (New Rochelle)* **2015**, *4*, 641.

[32] A. Ridiandries, J. T. M. Tan, C. A. Bursill, *Int J Mol Sci* **2018**, *19*, 3217.

[33] C. Dunnill, T. Patton, J. Brennan, J. Barrett, M. Dryden, J. Cooke, D. Leaper, N. T. Georgopoulos, *Int Wound J* **2015**, *14*, 89.

[34] J. B. Johnson, D. A. Broszczak, J. S. Mani, J. Anesi, M. Naiker, *J Pharm Pharmacol* **2022**, *74*, 485.

[35] V. Oliveira-Marques, H. S. Marinho, L. Cyrne, F. Antunes, *Antioxidants & Redox Signaling* **2009**, *11*, 2223.

[36] M. Hader, B. Frey, R. Fietkau, M. Hecht, U. S. Gaipl, *Cancer Immunol Immunother* **2020**, *69*, 293.

[37] H. Li, X. Zhou, Y. Huang, B. Liao, L. Cheng, B. Ren, *Front Microbiol* **2021**, *12*, 685133.

[38] D. O. Schairer, J. S. Chouake, J. D. Nosanchuk, A. J. Friedman, *Virulence* **2012**, *3*, 271.

[39] S. M. Nagle, K. A. Stevens, S. C. Wilbraham, "Wound Assessment," *StatPearls*, StatPearls Publishing, Treasure Island (FL) **2026**.

[40] S. Guo, L. A. DiPietro, *J Dent Res* **2010**, *89*, 219.

[41] T. N. Demidova-Rice, M. R. Hamblin, I. M. Herman, *Adv Skin Wound Care* **2012**, *25*, 304.

[42] "Fetal scarless wound healing - ProQuest," accessed on May 9, 2026, https://www.proquest.com/docview/218312263?accountid=14701&parentSessionId=EzTLyogPMMSY2NabxEztukOGni2CGATYzRNh%2Fzjxiuo%3D&pq-origsite=primo&sourcetype=Scholarly%20Journals.

[43] K. Ukaegbu, E. Allen, K. K. H. Svoboda, *International Wound Journal* **2025**, *22*, e70330.

[44] "Lipid Peroxidation - an overview | ScienceDirect Topics," accessed on May 11, 2026, https://www.sciencedirect.com/topics/agricultural-and-biological-sciences/lipid-peroxidation.

[45] D. Xian, J. Song, L. Yang, X. Xiong, R. Lai, J. Zhong, *Oxidative Medicine and Cellular Longevity* **2019**, *2019*, 2304018.

[46] "Chronic wounds: Learn More – What are the treatment options for chronic wounds?," *InformedHealth.org [Internet]*, Institute for Quality and Efficiency in Health Care (IQWiG) **2025**.

[47] G. Han, R. Ceilley, *Adv Ther* **2017**, *34*, 599.

[48] Y.-F. Liu, P.-W. Ni, Y. Huang, T. Xie, *Chin J Traumatol* **2022**, *25*, 11.

[49] W. Zhang, L. Liu, H. Cheng, J. Zhu, X. Li, S. Ye, X. Li, *Materials Advances* **2024**, *5*, 1364.

[50] V. Gounden, M. Singh, *Gels* **2024**, *10*, 43.

[51] "Hydrogels with tuneable properties for accelerated wound healing," *Hydrogels for Wound Healing*, Woodhead Publishing **2026**, p. 413.

[52] M. Li, W. Xia, Y. M. Khoong, L. Huang, X. Huang, H. Liang, Y. Zhao, J. Mao, H. Yu, T. Zan, *Biomater Res* **2023**, *27*, 87.

[53] M. Downer, C. E. Berry, J. B. Parker, L. Kameni, M. Griffin, *Bioengineering (Basel)* **2023**, *10*, 1378.

[54] P. Viaña-Mendieta, M. L. Sánchez, J. Benavides, *Int Wound J* **2022**, *19*, 100.

[55] I. M. Comino-Sanz, M. D. López-Franco, B. Castro, P. L. Pancorbo-Hidalgo, *J Clin Med* **2021**, *10*, 3558.

[56] L. Maeso, P. E. Antezana, A. G. Hvozda Arana, P. A. Evelson, G. Orive, M. F. Desimone, *Pharmaceutics* **2024**, *16*, 524.

[57] "Free radicals, natural antioxidants, and their reaction mechanisms - RSC Advances (RSC Publishing) DOI:10.1039/C4RA13315C," accessed on May 12, 2026, https://pubs.rsc.org/en/content/articlehtml/2015/ra/c4ra13315c.

[58] P. Loreto Palacio, J. R. Godoy, O. Aktas, E.-M. Hanschmann, *Antioxidants* **2022**, *11*, 1181.

[59] N. R. Selvaraj, D. Nandan, B. G. Nair, V. A. Nair, P. Venugopal, R. Aradhya, *Cells* **2025**, *14*, 511.

[60] F. G. Ottaviano, D. E. Handy, J. Loscalzo, *Circ J* **2008**, *72*, 1.

[61] D. Ravi, G. P. Rajalekshmy, M. R. Rekha, R. Joseph, *Int J Biol Macromol* **2023**, *251*, 126243.

[62] B. Qian, J. Li, K. Guo, N. Guo, A. Zhong, J. Yang, J. Wang, P. Xiao, J. Sun, L. Xiong, *Regen Biomater* **2021**, *8*, rbab003.

[63] S. Zhang, Y. Pan, Z. Mao, J. Zhang, K. Zhang, J. Yin, C. Wang, *Bioeng Transl Med* **2023**, *8*, e10402.

[64] A. A. Shefa, T. Sultana, M. K. Park, S. Y. Lee, J.-G. Gwon, B.-T. Lee, *Materials & Design* **2020**, *186*, 108313.

[65] W. Liu, H. Madry, M. Cucchiarini, *Int J Mol Sci* **2022**, *23*, 1147.

[66] J. L. Drury, R. G. Dennis, D. J. Mooney, *Biomaterials* **2004**, *25*, 3187.

[67] Y. Qin, *Int Wound J* **2005**, *2*, 172.

[68] J. Jang, Y.-J. Seol, H. J. Kim, J. Kundu, S. W. Kim, D.-W. Cho, *J Mech Behav Biomed Mater* **2014**, *37*, 69.

[69] S. M. Elbayomi, H. Wang, T. M. Tamer, Y. You, *Polymers* **2021**, *13*, 2575.

[70] Z. H. Kelishomi, B. Goliaei, H. Mahdavi, A. Nikoofar, M. Rahimi, A. A. Moosavi-Movahedi, F. Mamashli, B. Bigdeli, *Food Chemistry* **2016**, *196*, 897.

[71] C. C. Winterbourn, *Redox Biol* **2019**, *22*, 101086.

[72] S. C. Lu, *Biochim Biophys Acta* **2013**, *1830*, 3143.

[73] H. J. Forman, H. Zhang, A. Rinna, *Mol Aspects Med* **2009**, *30*, 1.

[74] D. A. Averill-Bates, *Vitam Horm* **2023**, *121*, 109.

[75] K. Jomova, S. Y. Alomar, S. H. Alwasel, E. Nepovimova, K. Kuca, M. Valko, *Arch Toxicol* **2024**, *98*, 1323.

[76] H. Masaki, Y. Okano, H. Sakurai, *Arch Dermatol Res* **1998**, *290*, 113.

[77] S. K. Georgiou-Siafis, A. S. Tsiftsoglou, *Antioxidants (Basel)* **2023**, *12*, 1953.

[78] I. Sandvig, K. Karstensen, A. M. Rokstad, F. L. Aachmann, K. Formo, A. Sandvig, G. Skjåk-Bræk, B. L. Strand, *Journal of Biomedical Materials Research Part A* **2015**, *103*, 896.

[79] N. Goldberg, Y. Shmidov, O. Kryukov, D. Aranovich, S. Cohen, R. Bitton, *Materials Advances* **2021**, *2*, 440.

[80] M. Saeger, Effect of Carbodiimide Functionalization Chemistry on Alginate Structure and Hydrogel Properties. M.S., **2016**.

[81] E. A. Growney, H. R. Linder, K. Garg, J. G. Bledsoe, S. A. Sell, *Journal of Biomedical Materials Research Part B: Applied Biomaterials* **2020**, *108*, 1972.

[82] A. Golunova, N. Velychkivska, Z. Mikšovská, V. Chochola, J. Jaroš, A. Hampl, O. Pop-Georgievski, V. Proks, *International Journal of Molecular Sciences* **2021**, *22*, 5731.

[83] "Carbodiimide - an overview | ScienceDirect Topics," accessed on May 12, 2026, https://www.sciencedirect.com/topics/chemistry/carbodiimide.

[84] "Carbodiimide Crosslinker Chemistry - CA," accessed on May 12, 2026, https://www.thermofisher.com/ca/en/home/life-science/protein-biology/protein-biology-learning-center/protein-biology-resource-library/pierce-protein-methods/carbodiimide-crosslinker-chemistry.html.

[85] S. U. Shah, M. Socha, I. Fries, S. Gibaud, *Drug Delivery* **2016**, *23*, 2927.

[86] G. L. Ellman, *Archives of Biochemistry and Biophysics* **1959**, *82*, 70.

[87] M. Rubab, R. Chelliah, D.-H. Oh, "Screening for Antioxidant Activity: Diphenylpicrylhydrazine (DPPH) Assay," *Methods in Actinobacteriology*, D. Dharumadurai, Ed., Springer Protocols Handbooks, Springer US, New York, NY **2022**, p. 453.

[88] S. Baliyan, R. Mukherjee, A. Priyadarshini, A. Vibhuti, A. Gupta, R. P. Pandey, C.-M. Chang, *Molecules* **2022**, *27*, 1326.

[89] A. Golunova, N. Velychkivska, Z. Mikšovská, V. Chochola, J. Jaroš, A. Hampl, O. Pop-Georgievski, V. Proks, *IJMS* **2021**, *22*, 5731.

[90] L. Oliver-Cervelló, P. López-Gómez, H. Martin-Gómez, M. Marion, M.-P. Ginebra, C. Mas-Moruno, *Chemistry – A European Journal* **2024**, *30*, e202400855.

[91] Y. Kim, H. Park, Y. Koo, *Appl Biol Chem* **2026**, *69*, 11.

[92] I. Sandvig, K. Karstensen, A. M. Rokstad, F. L. Aachmann, K. Formo, A. Sandvig, G. Skjåk-Bræk, B. L. Strand, *J Biomedical Materials Res* **2015**, *103*, 896.

[93] "Bioconjugation and crosslinking technical handbook."

[94] BenchChem Technical Support Team, Common problems with EDC/NHS coupling reactions and solutions, **2026**.

[95] J. V. Staros, R. W. Wright, D. M. Swingle, *Analytical Biochemistry* **1986**, *156*, 220.

[96] N. E. Good, G. D. Winget, W. Winter, T. N. Connolly, S. Izawa, M. Singh, *Biochemistry* **1966**, *5*, 467.

[97] R. Timkovich, *Anal Biochem* **1977**, *79*, 135.

[98] H. Petzold, P. J. Sadler, *Chem. Commun.* **2008**, 4413.

[99] E. Falcone, A. G. Ritacca, S. Hager, H. Schueffl, B. Vileno, Y. El Khoury, P. Hellwig, C. R. Kowol, P. Heffeter, E. Sicilia, P. Faller, *J. Am. Chem. Soc.* **2022**, *144*, 14758.

[100] BenchChem Technical Support Team, **2026**.

[101] "Thioester and thioacid synthesis by acylation of thiols (thiolation)," accessed on April 1, 2026, https://www.organic-chemistry.org/synthesis/C1S/thioesters.shtm?utm_source=copilot.com.

[102] M. Schüttel, C. Heinis, *ChemBioChem* **2024**, *25*, e202300592.

[103] R. Procopio-Melino, F. W. Kotch, A. S. Prashad, J. M. Gomes, W. Wang, B. Arve, A. Dawdy, L. Chen, J. Sperry, C. Hosselet, T. He, R. Kriz, L. Lin, K. Marquette, L. Tchistiakova, W. Somers, J. C. Rouse, X. Zhong, *Sci Rep* **2022**, *12*, 7262.

[104] *Studies on Experimental Toxicology and Pharmacology*, S. M. Roberts, J. P. Kehrer, L.-O. Klotz, Eds., Oxidative Stress in Applied Basic Research and Clinical Practice, Springer International Publishing, Cham, **2015**.

[105] G. Roos, N. Foloppe, J. Messens, *Antioxidants & Redox Signaling* **2013**, *18*, 94.

[106] L. B. Poole, *Free Radical Biology and Medicine* **2015**, *80*, 148.

[107] C. E. Paulsen, K. S. Carroll, *Chem. Rev.* **2013**, *113*, 4633.

[108] I. Tahir, R. Floreani, *Foods* **2022**, *11*, 2829.

[109] D. Shukla, P. K. Mandal, L. Ersland, E. R. Grüner, M. Tripathi, P. Raghunathan, A. Sharma, G. R. Chaithya, K. Punjabi, C. Splaine, *J Alzheimers Dis 66*, 517.

[110] H. Khan, M. K. Khan, T. Ahmad, M. Haris Zaib, N. Zafar, M. A. Alghamdi, *Main Group Chemistry* **2021**, *20*, 501.

[111] D. Bustos, E. W. Hernández-Rodríguez, R. I. Castro, L. Morales-Quintana, *Biomed Res Int* **2022**, *2022*, 5576090.

[112] E. D. Carvalho, M. R. G. Morais, A. P. Pêgo, C. C. Barrias, M. Araújo, *Carbohydrate Polymers* **2024**, *323*, 121412.

[113] S. Ye, C. Xie, O. T. Agar, C. J. Barrow, F. R. Dunshea, H. A. R. Suleria, *Food Reviews International* **2024**, *40*, 2682.

[114] P. Lukova, V. Kokova, A. Baldzhieva, M. Murdjeva, P. Katsarov, C. Delattre, E. Apostolova, *Marine Drugs* **2024**, *22*, 482.

[115] G. Oktavya, Y. A. Purwestri, H. T. S. G. Saragih, A. Nuriliani, *Curr Res Nutr Food Sci* **2023**, *11*, 389.

[116] *Cell Physiol Biochem* **2022**, *56*, 50.

[117] Y. Kim, H. Park, Y. Koo, *Appl Biol Chem* **2026**, *69*, 11.

[118] J. E. Aguilar-Toalá, A. M. Liceaga, *Int J of Food Sci Tech* **2021**, *56*, 2193.

[119] B. Xu, Q. Dong, C. Yu, H. Chen, Y. Zhao, B. Zhang, P. Yu, M. Chen, *Antioxidants* **2024**, *13*, 479.

[120] K. Jomova, S. Y. Alomar, S. H. Alwasel, E. Nepovimova, K. Kuca, M. Valko, *Arch Toxicol* **2024**, *98*, 1323.

APPENDIX

Supplementary Table 1. Optimization of a conventional alginate functionalization method with GSH – Response table (DOE #1)

ID	(EDC:GSH)	(NHS:GSH)	pH	[GSH] (mM)
1	1 :1 [-]	0.35 : 1 [-]	5 [-]	0.239
2	1.2 :1 [+]	0.35 : 1 [-]	5 [-]	1.009
3	1 : 1 [-]	0.75 : 1 [+]	5 [-]	0.671
4	1.2 :1 [+]	0.75 : 1 [+]	5 [-]	1.369
5	1 :1 [-]	0.35 : 1 [-]	7 [+]	2.365
6	**1.2 :1 [+]**	**0.35 : 1 [-]**	**7 [+]**	**3.965**
7	1 : 1 [-]	0.75 : 1 [+]	7 [+]	2.374
8	1.2 : 1 [+]	0.75 : 1 [+]	7 [+]	3.560
9	1.1 :1 [0]	0.55 : 1 [0]	6 [0]	1.751
10	1.1 :1 [0]	0.55 : 1 [0]	6 [0]	2.457
11	1.1 :1 [0]	0.55 : 1 [0]	6 [0]	2.376
12	1.1 :1 [0]	0.55 : 1 [0]	6 [0]	2.415

Supplementary Table 2. Outcome of a three-way ANOVA for the results presented in Figure 4.1. Levels of significance: $p < 0.05$ (*); $p < 0.01$ (**); $p < 0.001$ (***).

Main factors	Degrees of freedom (Df)	Sum of Squares	Mean of Squares	F-value	p-value
(EDC:GSH)	2	2.511	1.256	11.271	0.0403*
(NHS:GSH)	1	0.020	0.020	0.176	0.703
pH	1	10.070	10.070	90.382	0.00247**
(EDC: GSH) x (NHS: GSH)	1	0.030	0.030	0.265	0.642
(EDC: GSH) x pH	1	0.217	0.217	1.949	0.257
(NHS: GSH) x pH	1	0.176	0.176	1.584	0.297
(EDC: GSH) x (NHS: GSH) x pH	1	0.015	0.015	0.132	0.740
Residuals	3	0.334	0.111		

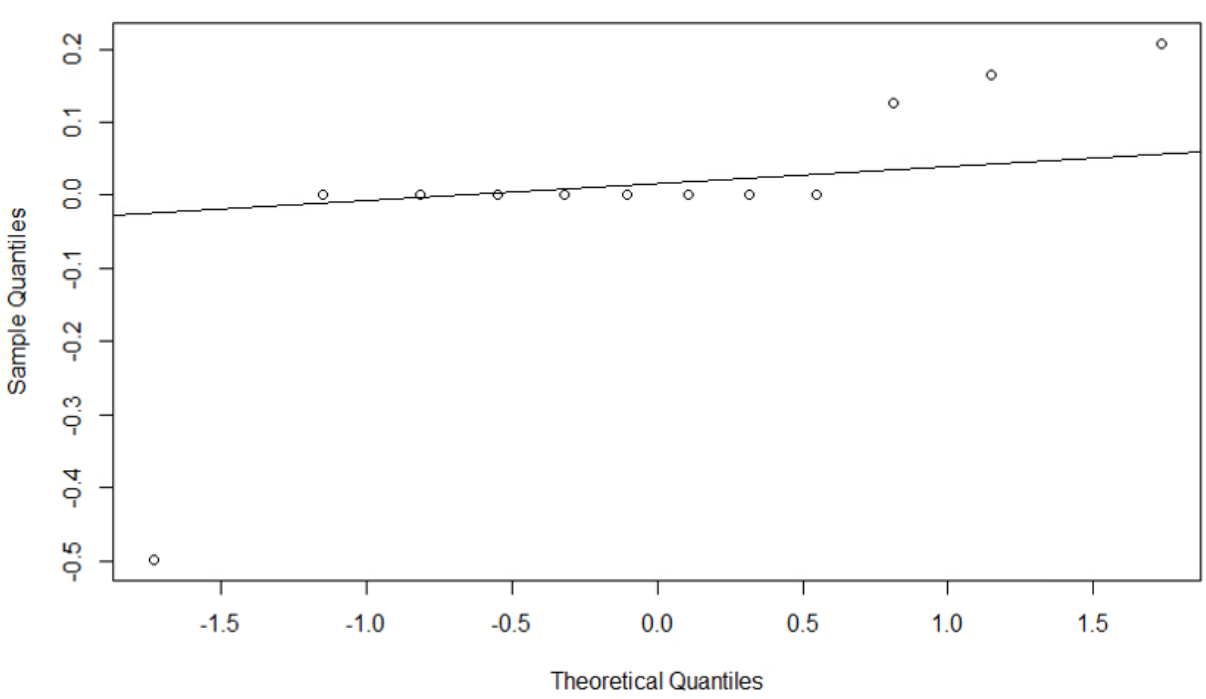

Supplementary Figure 1. Normal Q-Q plot of optimization of conventional functionalization method of alginate with GSH for highest GSH grafting ([GSH] (mM)).

Supplementary Table 3. Outcome of a curvature test for the results presented in Table 4.1. Levels of significance: $p < 0.05$ (*); $p < 0.01$ (**); $p < 0.001$ (***).

Coefficients	Factors	Estimate	Standard Error	t-value	p-value
β_0	Intercept	1.94	0.117	16.554	7.17×10^{-7}***
β_1	(EDC:GSH)	0.532	0.117	4.528	0.0027**
β_2	(NHS:GSH)	0.0495	0.117	0.422	0.686
β_3	pH	1.12	0.117	9.555	2.89×10^{-5}***
β_4	Center	0.306	0.203	1.504	**0.1763**

Supplementary Table 4. 1st Design of experiment for alginate functionalization with GSH using Ullah Shah and al.'s methodology (DOE #2) – Response table

ID	(EDC:GSH)	pH	Reaction Time (h)	[GSH] (mM)	[-SH] (mM)	$\%\left(\frac{[-SH]}{[GSH\ detected]}\right)$	$\%\left(\frac{[-SH]}{[GSH\ added]}\right)$
1	(1.5:1) [-]	4 [-]	2	0.245	0.167	68.1%	3.25%
2	(3:1) [+]	4 [-]	2	0.433	0.264	61.0%	5.13%
3	(1.5:1) [-]	8 [+]	2	0.549	0.290	52.8%	5.64%
4	(3:1) [+]	8 [+]	2	0.755	0.180	24.0%	3.51%
5	(1.5:1) [-]	4 [-]	8	0.241	0.160	66.3%	3.11%
6	(3:1) [+]	4 [-]	8	0.447	0.271	60.9%	5.28%
7	(1.5:1) [-]	8 [+]	8	0.451	0.170	37.7%	3.30%
8	(3:1) [+]	8 [+]	8	0.625	0.146	23.3%	2.83%
9	(2.25: 1) [0]	6 [0]	5 [0]	0.529	0.256	48.4%	4.98%
10	(2.25: 1) [0]	6 [0]	5 [0]	0.565	0.233	41.3%	4.53%
11	(2.25: 1) [0]	6 [0]	5 [0]	0.499	0.208	41.8%	4.05%
12	(2.25: 1) [0]	6 [0]	5 [0]	0.546	0.229	41.9%	4.45%

Supplementary Table 5. Outcome of a three-way ANOVA for the results presented in Figure 4.7. Levels of significance: $p < 0.05$ (*); $p < 0.01$ (**); $p < 0.001$ (***).

Main factors	Degrees of freedom (Df)	Sum of Squares	Mean of Squares	F-value	p-value
(EDC:GSH)	2	0.0864	0.0432	55.0	0.00432**
pH	1	0.128	0.128	163	0.00103**
Time	1	0.00603	0.00603	90.4	0.0695
(EDC:GSH) x pH	1	0.00002	0.00002	0.265	0.880
(EDC:GSH) x Time	1	0.00002	0.00002	1.95	0.871
pH x Time	1	0.00711	0.00711	1.58	0.0572
(EDC:GSH) x pH x Time	1	0.00030	0.00030	0.132	0.581
Residuals	3	0.00235	0.00078		

Supplementary Table 6. Outcome of a curvature test for the results presented in Table 4.2. Level of significance: $p < 0.001$ (***); $p < 0.01$ (**); $p < 0.05$ (*).

Coefficients	Factors	Estimate	Standard Error	t-value	p-value
β_0	Intercept	0.468	0.0132	35.379	$3.7410x^{-9}$***
β_1	(EDC:GSH)	0.0966	0.0132	7.295	0.000163***
β_2	pH	0.127	0.0132	9.566	$2.8610x^{-5}$***
β_3	Time	-0.0274	0.0132	-2.074	0.0768
β_4	Center	0.0665	0.0229	2.900	**0.0230***

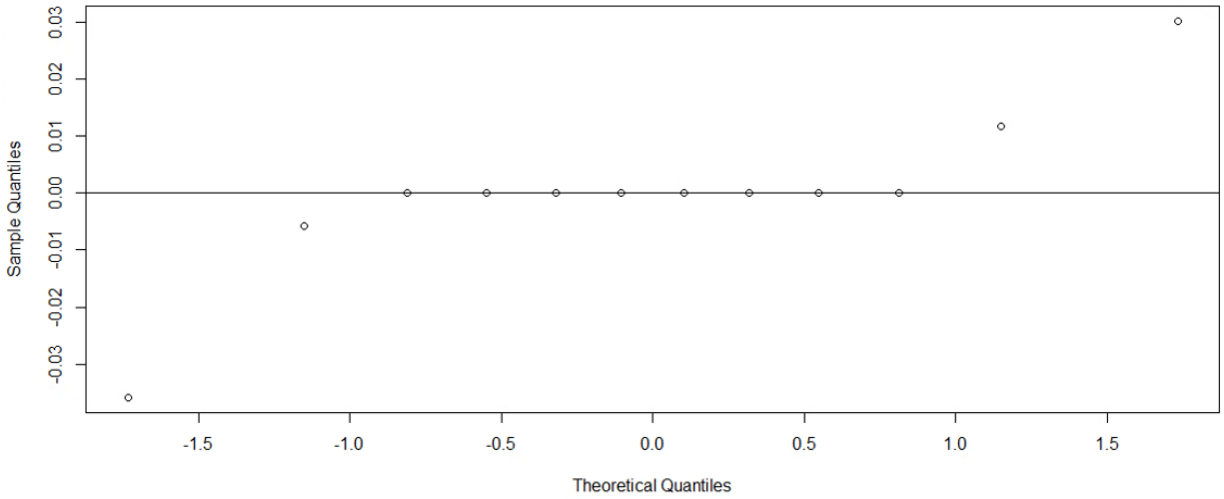

Supplementary Figure 2. Normal Q-Q plot of alginate functionalization optimization with GSH using Ullah Shah's approach for highest GSH grafting ([GSH] (mM)).

Supplementary Table 7. Outcome of a three-way ANOVA for the results presented in Figure 4.8. Levels of significance: $p < 0.05$ (*); $p < 0.01$ (**); $p < 0.001$ (***).

Main factors	Degrees of freedom (Df)	Sum of Squares	Mean of Squares	F-value	p-value
(EDC:GSH)	2	0.0481	0.0240	20.890	0.0173*
pH	1	0.175	0.175	153	0.00114**
Time	1	0.00395	0.00395	3.43	0.161
(EDC:GSH) x pH	1	0.0118	0.0118	10.2	0.0494*
(EDC:GSH) x Time	1	0.00328	0.00328	2.85	0.190
pH x Time	1	0.00238	0.00238	2.07	0.246
(EDC:GSH) x pH x Time	1	0.00207	0.00207	1.80	0.272
Residuals	3	0.00345	0.00115		

Supplementary Table 8. Outcome of a curvature test for the results presented in Table 4.3. Levels of significance: $p < 0.05$ (*); $p < 0.01$ (**); $p < 0.001$ (***).

Coefficients	Factors	Estimate	Standard Error	t-value	p-value
β_0	Intercept	0.493	0.0202	24.333	5.04×10^{-8}***
β_1	(EDC:GSH)	-0.0696	0.0202	-3.439	0.0108*
β_2	pH	-0.148	0.0202	-7.315	0.000161***
β_3	Time	-0.0222	0.0202	-1.097	0.309
β_4	Center	-0.0590	0.0351	-1.682	**0.136**

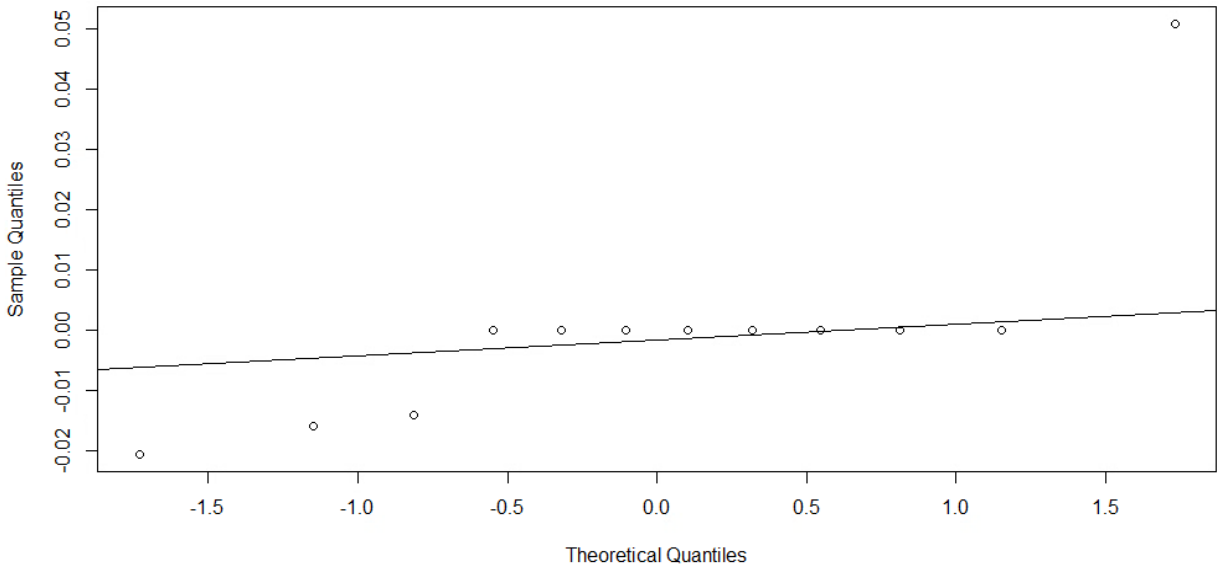

Supplementary Figure 3. Normal Q-Q plot of alginate functionalization optimization with GSH using Ullah Shah's approach for highest thiol group availability ([SH]/ [GSH grafted]).

Supplementary Table 9. Outcome of a three-way ANOVA for the results presented in Figure 4.9. Levels of significance: $p < 0.05$ (*); $p < 0.01$ (**); $p < 0.001$ (***).

Main factors	Degrees of freedom (Df)	Sum of Squares	Mean of Squares	F-value	p-value
(EDC:GSH)	2	0.0000924	0.0000462	3.19	0.181
pH	1	0.0000278	0.0000278	1.92	0.260
Time	1	0.000113	0.000113	7.83	0.0679
(EDC:GSH) x pH	1	0.000552	0.000552	38.1	0.00855**
(EDC:GSH) x Time	1	0.0000473	0.0000473	3.27	0.168
pH x Time	1	0.000115	0.000115	7.94	0.0669
(EDC:GSH) x pH x Time	1	0.0000236	0.0000236	1.627	0.292
Residuals	3	0.0000434	0.0000145		

Supplementary Table 10. Outcome of a curvature test for the results presented in Table 4.4. Levels of significance: $p < 0.05$ (*); $p < 0.01$ (**); $p < 0.001$ (***).

Coefficients	Factors	Estimate	Standard Error	t-value	p-value
β_0	Intercept	0.0401	0.00374	10.726	1.35×10^{-5}***
β_1	(EDC:GSH)	0.00184	0.00374	0.492	0.637
β_2	pH	-0.00186	0.00374	-0.499	0.633
β_3	Time	-0.00377	0.00374	-1.008	0.347
β_4	Center	-0.00495	0.00647	0.765	**0.469**

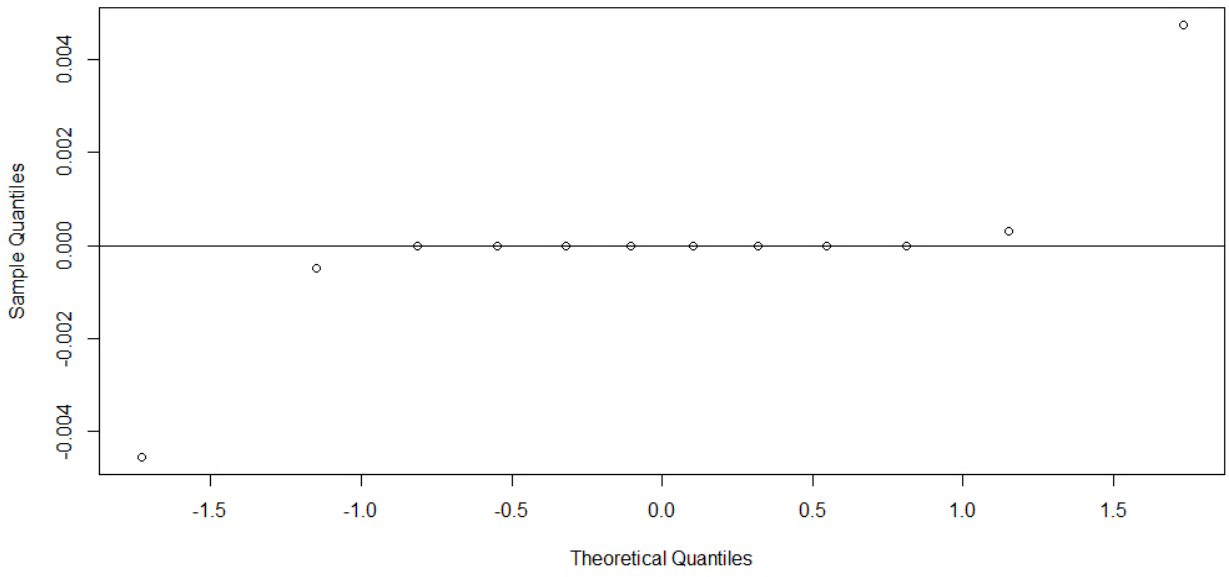

Supplementary Figure 4. Normal Q-Q plot of alginate functionalization optimization with GSH using Ullah Shah's approach for highest thiol group availability ([SH]/ [GSH added]).

Supplementary Table 11. 2nd Design of experiment for alginate functionalization with GSH using Ullah Shah and al.'s methodology (DOE #3) – Response table

ID	(EDC:GSH)	pH	[GSH] (mM)	[-SH] (mM)	$\%\left(\frac{[-\mathbf{SH}]}{[\mathbf{GSH\ detected}]}\right)$	$\%\left(\frac{[-\mathbf{SH}]}{[\mathbf{GSH\ added}]}\right)$
1	(2:1) [-]	3 [-]	0.303	0.232	76.5%	4.50%
2	(4:1) [+]	3 [-]	0.366	0.215	58.8%	4.17%
3	(2:1) [-]	5 [+]	0.317	0.216	68.2%	4.20%
4	(4:1) [+]	5 [+]	0.524	0.247	47.0%	4.79%
5	(3:1) [0]	4 [0]	0.347	0.212	61.1%	4.11%
6	(3:1) [0]	4 [0]	0.417	0.196	47.0%	3.81%
7	(3:1) [0]	4 [0]	0.346	0.210	60.7%	4.08%
8	(3:1) [0]	4 [0]	0.352	0.206	58.6%	4.00%

Supplementary Table 12. Outcome of a two-way ANOVA for DOE #3 – GSH grafting optimization using Ullah Shah and al.'s alginate functionalization method with GSH. Levels of significance: $p < 0.05$ (*); $p < 0.01$ (**); $p < 0.001$ (***).

Main factors	Degrees of freedom (Df)	Sum of Squares	Mean of Squares	F-value	p-value
(EDC:GSH)	2	0.0185	0.00926	7.663	0.0662
pH	1	0.00740	0.00740	6.128	0.0896
(EDC:GSH) x pH	1	0.00526	0.00526	4.353	0.1282
Residuals	3	0.00362	0.00121		

Supplementary Table 13. Outcome of a curvature test for the results presented in Table 4.5. Levels of significance: $p < 0.05$ (*); $p < 0.01$ (**); $p < 0.001$ (***).

Coefficients	Factors	Estimate	Standard Error	t-value	p-value
β_0	Intercept	0.377	0.0236	16.018	8.88×10^{-5}***
β_1	(EDC:GSH)	0.0675	0.0236	2.865	0.0457*
β_2	pH	0.0430	0.0236	1.826	0.1419
β_3	Center	-0.0120	0.0333	-0.036	0.737

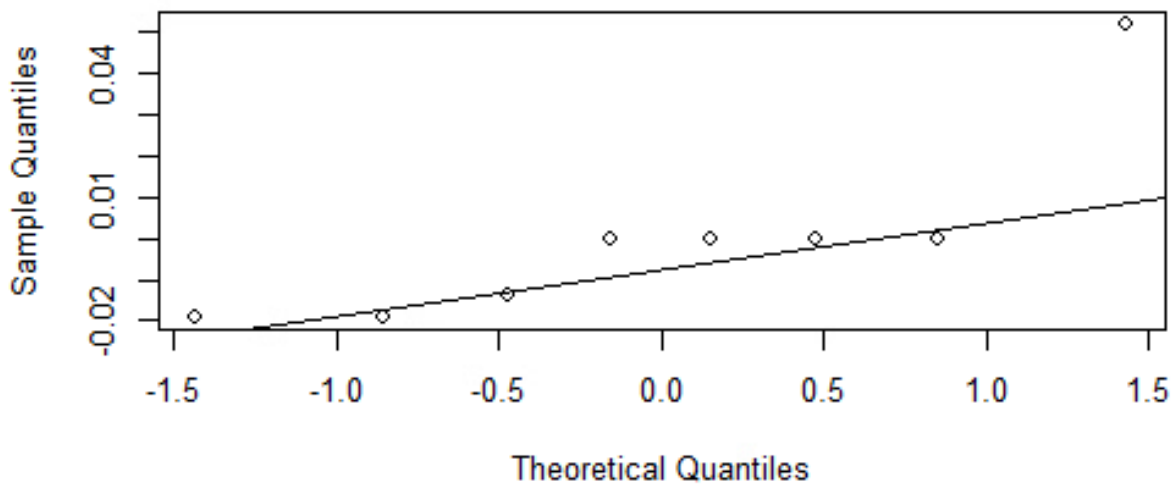

Supplementary Figure 5. Normal Q-Q plot of alginate functionalization's second optimization with GSH using Ullah Shah's approach for highest GSH grafting ([GSH] (mM)).

Supplementary Table 14. Outcome of a two-way ANOVA for % ([SH active]/ [GSH grafted]) optimization using Ullah Shah and al.'s alginate functionalization method with GSH – DOE #3. Levels of significance: $p < 0.05$ (*); $p < 0.01$ (**); $p < 0.001$ (***).

Main factors	Degrees of freedom (Df)	Sum of Squares	Mean of Squares	F-value	p-value
(EDC:GSH)	2	0.0444	0.0222	5.05	0.110
pH	1	0.0100	0.00100	2.27	0.229
(EDC:GSH) x pH	1	0.00030	0.000299	0.068	0.811
Residuals	3	0.0132	0.00440		

Supplementary Table 15. Outcome of a curvature test for the results presented in Table 4.6. Levels of significance: $p < 0.05$ (*); $p < 0.01$ (**); $p < 0.001$ (***).

Coefficients	Factors	Estimate	Standard Error	t-value	p-value
β_0	Intercept	0.626	0.0290	21.561	2.74×10^{-5}***
β_1	(EDC:GSH)	-0.097	0.0290	-3.345	0.0287*
β_2	pH	-0.0450	0.0290	-1.721	0.160
β_3	Center	-0.0577	0.0411	-1.406	0.233

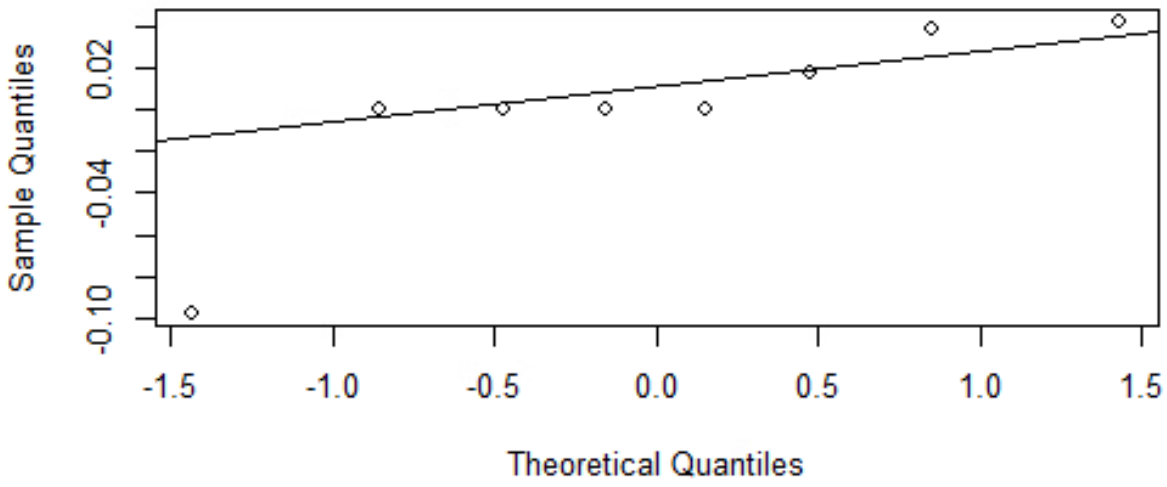

Supplementary Figure 6. Normal Q-Q plot of alginate functionalization's second optimization with GSH using Ullah Shah's approach for highest thiol group availability ([SH]/ [GSH grafted]).

Supplementary Table 16. Outcome of a two-way ANOVA for % ([SH active]/ [GSH added]) optimization using Ullah Shah and al.'s alginate functionalization method with GSH – DOE #3. Levels of significance: $p < 0.05$ (*); $p < 0.01$ (**); $p < 0.001$ (***).

Main factors	Degrees of freedom (Df)	Sum of Squares	Mean of Squares	F-value	p-value
(EDC:GSH)	2	3.60×10^{-5}	1.80×10^{-5}	10.1	0.0462*
pH	1	2.37×10^{-6}	2.37×10^{-6}	1.33	0.332
(EDC:GSH) x pH	1	2.13×10^{-5}	2.13×10^{-5}	12.0	0.0405*
Residuals	3	5.33×10^{-6}	1.77×10^{-6}		

Supplementary Table 17. Outcome of a curvature test for the results presented in Table 4.7. Levels of significance: $p < 0.05$ (*); $p < 0.01$ (**); $p < 0.001$ (***).

Coefficients	Factors	Estimate	Standard Error	t-value	p-value
β_0	Intercept	0.0442	0.00129	34.208	4.36×10^{-6}***
β_1	(EDC:GSH)	0.000664	0.00129	0.514	0.634
β_2	pH	0.000770	0.00129	0.596	0.583
β_3	Center	-0.00414	0.00183	-2.268	0.0859

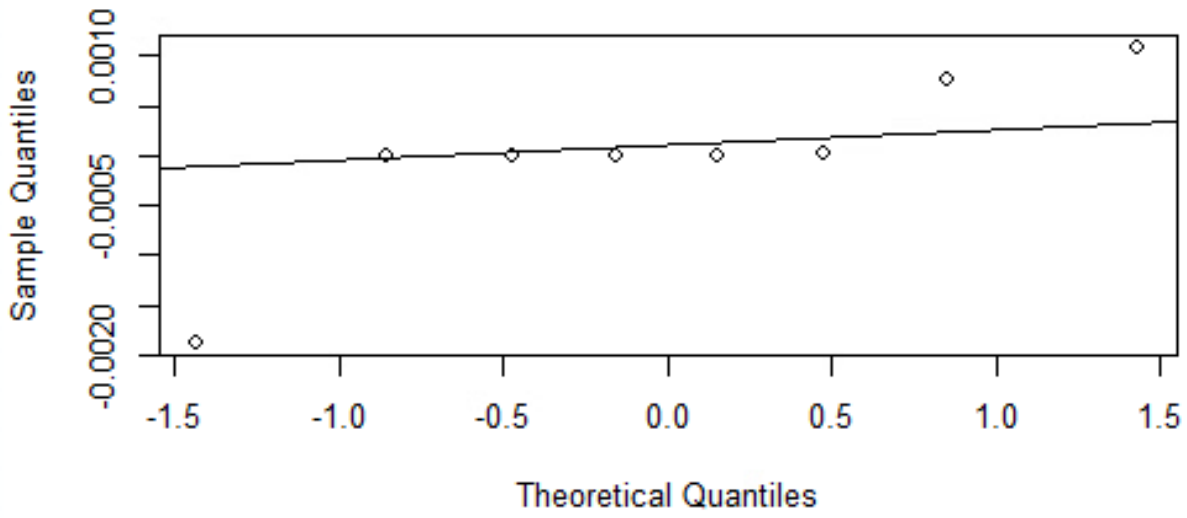

Supplementary Figure 7. Normal Q-Q plot of alginate functionalization's second optimization with GSH using Ullah Shah's approach for highest thiol group availability %([SH]/[GSH added]).